United States
Environmental Protection
Agency

Modeling and Experimental Testing of Sediment Resuspension in Water Distribution Storage Tanks

Office of Research and Development
National Homeland Security Research Center
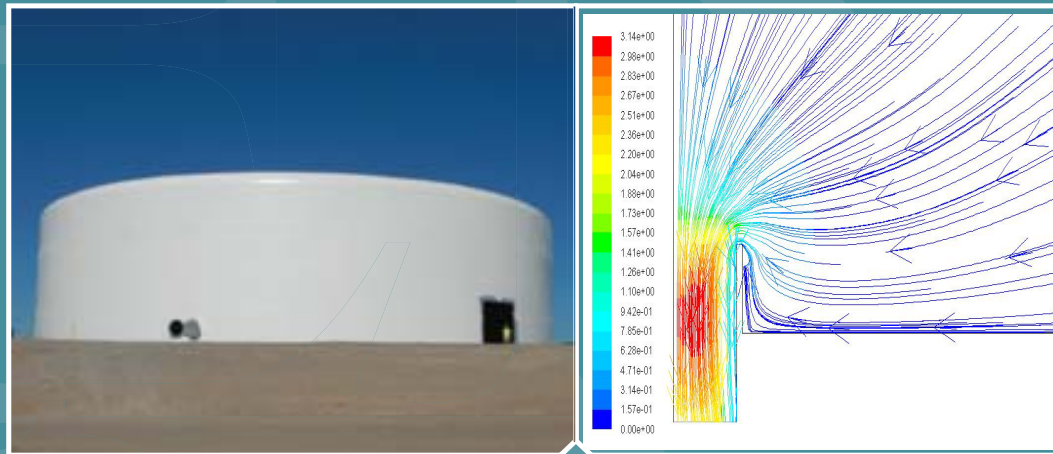
Executive Summary

Sediments in storage tanks have the potential to accumulate pathogens, metals, and other hazardous materials. This report addresses the potential for sediments in storage tanks to be transported back into water distribution systems. Computational fluid dynamics (CFD) models were developed and three simulation studies were conducted to provide insight into sediment resuspension processes in tanks. In addition, a pilot-scale experiment was conducted to validate the model predictions. The results of this study highlight tank operating conditions which might reduce resuspension and removal of sediments from tanks.

The simulation studies used a cylindrical, ground level, 11,000 m^3 (3 million gallon) tank with a single inlet/outlet as its model domain. Sediment was assumed to be distributed on the tank bottom and was made up of 0.01, 0.1, or 1 mm diameter particles. CFD models were used to calculate shear stresses on the tank bottom to predict if the particles would be resuspended from the tank bottom and then entrained in the fluid flow, removed from the tank through the drain, or deposited back on the tank bottom. Flow rates, the inlet/outlet location and diameter, filling or draining cycles were varied in order to understand the effects of these key parameters on the resulting shear stress and the potential for particle resuspension.

Key results of the simulation studies were as follows:

- Resuspension occurred under all operating conditions simulated; however less than 25% of particles were resuspended and less than 1% were drained.

- Particle resuspension only occurred within a short distance of the inlet/outlet.

- Particle resuspension generally occurred immediately following the start of either the filling or draining processes.

- Particle size, flow rate, and inlet/outlet location were found to be important factors for particle resuspension:

    o Smaller particles were more susceptible to resuspension.

    o Higher flow rates yielded greater resuspension.

    o Inlet/outlets located near the side wall yielded greater resuspension.

    o Draining yielded greater resuspension of particles than filling.

- Particle resuspension was directly correlated to the amount of momentum flow, or jet effect, through the inlet/outlet. Reducing the flow rate or increasing the diameter of the inlet/outlet reduces the momentum flow and the potential for particle resuspension.

- A raised inlet pipe extending 15 cm (6 inches) above the tank bottom substantially reduced the number of particles resuspended during filling, while a pipe height extending 30 – 61 cm (12 – 24 inches) reduced the number of particles drained from the tank.

Small-scale experimental tests were performed to validate the resuspension model. Glass beads and sand particles were placed in a 1.2 m (4 ft) diameter water-filled tank with a 2.0 cm (0.8 in) diameter inlet/outlet to study resuspension and removal. Photos and videos were recorded before and after each filling and draining event to determine where particles were resuspended from the tank bottom. Tracer tests were also performed to characterize the flow patterns and velocity fields. Finally, mitigation measures were investigated by raising the pipe inlet, which was normally flush with the tank bottom, a short distance above the tank bottom.

Key results of the experimental tests were as follows:

- Measured and simulated velocities along tank bottom matched well in the region where particles were resuspended.

- Resuspension of particles was only observed within ~1 cm from the inlet/outlet during filling and draining cycles for the flow rates used in the study.

- Smaller particles and less dense particles yielded a greater resuspension.

- Model predictions of resuspension generally matched experimental data for glass beads, and generally over predicted the amount of resuspension for silica sand. The non-spherical shape of the sand may have reduced the amount of resuspension in the tests.

- A raised inlet height of 3-8% of the head of the water above the tank bottom was able to completely mitigate particle movement near the inlet/outlet.

Based on the simulation and experimental studies conducted for this report, several strategies for reducing resuspension and removal of sediments from tank bottoms were identified:

- constructing a raised inlet pipe 30 – 60 cm (12 – 24 inches) above the tank bottom,

- placing the inlet/outlet near the center of the tank rather than near the side wall,

- reducing the inlet/outlet flow rates,, and

- increasing the diameter of the inlet/outlet pipes.

Acknowledgements

Questions concerning this document or its application should be addressed to:

    Regan Murray
    USEPA/NHSRC (NG 16)
    26 W Martin Luther King Drive
    Cincinnati OH 45268
    (513) 569-7031
    Murray.Regan@epa.gov

Disclaimer

The U.S. Environmental Protection Agency (EPA) through its Office of Research and Development funded and collaborated in the research described here under an Inter-Agency Agreement with the Department of Energy's Sandia National Laboratories. It has been subjected to the Agency's review and has been approved for publication. Note that approval does not signify that the contents necessarily reflect the views of the Agency. Mention of trade names, products, or services does not convey official EPA approval, endorsement, or recommendation.

Sandia National Laboratories is a multi-program laboratory managed and operated by Sandia Corporation, a wholly owned subsidiary of Lockheed Martin Corporation, for the U.S. Department of Energy's National Nuclear Security Administration under contract DE-AC04-94AL85000.

NOTICE: This report was prepared as an account of work sponsored by an agency of the United States Government. Neither the United States Government, nor any agency thereof, nor any of their employees, nor any of their contractors, subcontractors, or their employees, make any warranty, express or implied, or assume any legal liability or responsibility for the accuracy, completeness, or usefulness of any information, apparatus, product, or process disclosed, or represent that its use would not infringe privately owned rights. Reference herein to any specific commercial product, process, or service by trade name, trademark, manufacturer, or otherwise, does not necessarily constitute or imply its endorsement, recommendation, or favoring by the United States Government, any agency thereof, or any of their contractors or subcontractors. The views and opinions expressed herein do not necessarily state or reflect those of the United States Government, any agency thereof, or any of their contractors.

Due to the complexity of some graphs, figures, equations, and tables, some information is not amenable to screen readers. If you need assistance to access this information, please contact Kathy Nickel (nickel.kathy@epa.gov).

CONTENTS

List of Figures

List of Tables

List of Acronyms and Abbreviations

CCDF	complementary cumulative distribution function
CDF	cumulative distribution function
CFD	computational fluid dynamics
EPA	U.S. Environmental Protection Agency
gpm	gallons per minute
NHSRC	National Homeland Security Research Center
RANS	Reynolds-averaged Navier Stokes
SST	shear stress transport
UDF	user defined function
US	United States
VOF	volume of fluid

List of Parameters and Variables

d_{inlet} Diameter of the inlet pipe (m)

$d_{max,i}$ Maximum diameter of all particles in bin i (m)

$d_{min,i}$ Minimum diameter of all particles in bin i (m)

$d_{rep,i}$ Diameter of representative particle in bin i (m)

D Particle diameter (m)

D_* Dimensionless grain diameter of a particle

$D_{nominal}$ Nominal diameter of particle (m)

g Gravitational constant (m/s^2)

$m_{f,i}$ Mass fraction of particle diameter bin i (kg)

m_i Mass of all particles in bin i (kg)

$m_{min,i}$ Minimum mass of all particles in bin i (kg)

$m_{max,i}$ Maximum mass of all particles in bin i (kg)

$m_{rep,i}$ Unit mass of representative particle in bin i (kg)

m_{tot} Total mass of all particles (kg)

$m_{unit,i}$ Unit mass of representative particle in bin i (kg)

N_i Number of particles in bin i

N_{tot} Total number of all particles

$N_{f,i}$ Number fraction of bin i

Q Flow rate (m^3/s)

R_* Grain Reynolds number

r_{drain} Radius of the drain line (m)

R_{extent} Radial extent of particle emplacement (m)

S_f Corey Shape Factor

w_s Settling velocity (m/s)

u_* Shear velocity (m/s)

ν Kinematic viscosity of water (m^2/s)

ρ, ρ_p Particle density (kg/m^3)

ρ_s Solid density (kg/m^3)

ρ_{bulk} Particle bulk density (kg/m^3)

ρ_w Water density (kg/m^3)

τ_c^* Dimensionless critical shear stress

τ^* Dimensionless shear stress of tank bottom

τ Shear stress along tank bottom (Pa)

1. Introduction and Background

Storage of treated drinking water serves several important functions. Storage facilities are designed to help maintain system pressure, supply water for typical and emergency use, and improve stability in treatment processes and pumping rates. However, storage of treated water can diminish water quality and increase risks to human health. In particular, storage tanks have been implicated in several waterborne disease outbreaks [20].

This report addresses sediments in storage tanks and the potential for the transport of these sediments back into water distribution systems, possibly posing a human health risk. The objective of this study is to better understand the tank operating conditions under which sediments might be resuspended from tank bottoms and transported back into water distribution systems. To this end, several computational fluid dynamics (CFD) models were developed and three simulation studies conducted to provide insights into sediment resuspension processes in tanks. In addition, a pilot-scale experiment was conducted to validate the model predictions. The results of this study highlight tank operating conditions which might reduce resuspension and removal of sediments from tanks.

CFD models can provide detailed simulations of flow fields and hydraulic behavior in large and complex domains. CFD models are used to better understand important parameters and processes in complex systems, and to optimize performance of these systems at specific sites. Previous studies have used CFD models and experiments to investigate mixing characteristics in water tanks [1-6]. CFD models have also been used to model sediment deposition, resuspension, and/or transport in sewer systems, wastewater drainage channels, and rivers [7-16]. However, little research has been performed to model and characterize sediment resuspension and transport in water distribution storage tanks. This study begins to fill this gap.

This report is organized as follows. In the rest of this section, background information on water storage tanks, typical tank operating conditions, common water quality problems, and tank sediments is presented. In Section 2, the CFD modeling methodology and results are presented. In Section 3, the experimental study and results are presented. Finally, conclusions are summarized in Section 4.

1.1. Type and Purpose of Water Storage Tanks

There are many types of finished water storage facilities in use around the United States (US), including elevated tanks, ground level tanks, standpipes, buried tanks, and hydropneumatic tanks. The EPA 2006 Community Water System Survey of more than 1,300 US water systems estimated that more than half of drinking water systems use elevated tanks (in which the tank bottom is above ground level), about 38% of water systems use ground level tanks (in which the tank bottom is at ground level), about 20% of systems use standpipes (which are ground tanks that are taller than they are wide), 16% use buried tanks (in which some or all of the tank is below ground level), and about 9% use hydropneumatic (or pressurized) tanks [17]. The average storage capacity of a water system varies widely depending on the size of the population served, from an average of about 1,500 m^3 (0.4 million gallons) for smaller sized water systems to an average of 560,000 m^3 (149 million gallons) for systems serving more than 500,000 customers [17].

Storage facilities are used to achieve many functions in water distribution systems beyond storing water for customer use. Storage helps to provide adequate supplies for emergencies, such as fire-fighting, power outages, main breaks, or other system failures. The elevation of water levels in storage tanks helps to maintain pressures in the water distribution system and minimize fluctuations caused by changes in customer demands or system operating conditions. Filling and draining storage tanks on a regular basis throughout the day helps to equalize water flows in a distribution system, allowing water treatment processes to proceed at a steady rate while still meeting varying customer demands [18].

1.2. Typical Tank Operating Conditions

For this report, typical tank operating conditions for two US cities were determined through personal communication with staff of Albuquerque Water Authority and Greater Cincinnati Water Works. For these utilities, individual tank volumes vary from 1,900 m^3 to 11,000 m^3 (0.5 to 3 million gallons), while reservoir (i.e., very large ground level tank) volumes vary from 7,600 m^3 to 300,000 m^3 (2 to 80 million gallons). Tank diameters range from 6 to 37 m (20 to 120 feet) and reservoir diameters from 30 to 55 m (100 to 180 feet). Figure 1 shows a new ground level tank built in Albuquerque, New Mexico, in 2014.

Figure 1. Construction of an 11,000 m^3 (3 million gallon) water distribution storage tank in Albuquerque, NM.

For both utilities, tanks typically follow diurnal cycles of filling and draining, with draining occurring most often during the day and filling occurring during the night when electricity needed to pump water into tanks is less expensive. The length of fill cycles varies from 3 to 14 hours, and drain cycles from 3 to 15 hours. Water levels typically are kept within 30-95% of tank capacity in order to maintain adequate supplies of water for emergencies such as fires. Water levels in tanks are always changing; in other words, the tank is always filling or draining.

Tank inlets bring water into tanks while tank outlets are used to drain water from tanks; often, a single pipe serves as the inlet and outlet. The location of tank inlets and outlets vary significantly from being located at the center of the tank bottom to the side of tank wall. Inflow and outflow diameters and velocities are shown in Table 1.

Table 1. Range of storage facility inlet/outlet diameters and velocities (median values in parenthesis)

	Inlet diameter	Outlet diameter	Inlet velocity/ Flow Rate	Outlet velocity/ Flow Rate
Tanks	20-76 cm (61 cm) 8-30 in (24 in)	36-61 cm (41 cm) 14-24 inches (16 in)	0.03-2.7 m/s (0.24 m/s or 17 m^3/s) 0.1-9 ft/s (0.8 ft/s or 1,100 gpm)	0.03-1.2 m/s (0.27 m/s or 8.7 m^3/s) 0.1-4 ft/s (0.9 ft/s or 560 gpm)
Reservoirs	41-122 cm (69 cm) 16-48 in (27 in)	41-122 cm (69 cm) 16-48 inches (27 in)	0.03-3.0 m/s (1.2 m/s or 100 m^3/s) 0.1-10 ft/s (3.8 ft/s or 6,800 gpm)	0.15-2.4 m/s (0.79 m/s or 72 m^3/s) 0.5-8 ft/s (2.6 ft/s or 4,600 gpm)

1.3. Water Quality Problems in Storage Tanks

By storing water for periods of time, the quality of the water in finished water storage tanks can decrease. Over time, chlorine or other disinfectant residuals decrease, disinfection byproducts can form, and taste and odor issues can develop. Other potential chemical problems in tanks include an increase in pH, corrosion of tank materials, and precipitation and settling of iron and manganese [18]. Microbiological problems can include or result from bacterial regrowth, nitrification, sediment buildup, an increase in temperature, and introduction of worms, insects, bird droppings, and other materials through vents, openings, and breaches in tank covers [18, 19]. Sediments can cause water quality problems by increasing disinfectant demand, microbial growth, disinfection by-product formation, and turbidity [20].

These water quality problems can be attributed to multiple factors. Long residence times in tanks contributes to these chemical and microbiological problems. Poor mixing of water in tanks can further exacerbate water quality problems [20-22]. Moreover, inadequate maintenance and cleaning of tanks can lead to the introduction of contaminants or can facilitate the growth of microbial contaminants. EPA and industry guidance recommend comprehensive inspection and cleaning every 3 to 5 years. However, respondents to the 2006 Community Water System Survey reported that many systems meet this goal, but some systems reported long periods without comprehensive inspection and cleaning. In the survey, the average number of years reported between cleaning tanks was 6.5 [17] during which contaminants can accumulate and potentially pose human health risks.

Fortunately, steps can be taken to improve water quality in storage tanks. Water quality can be improved by increasing mixing, reducing residence time, monitoring water quality on a routine basis, inspecting, maintaining and cleaning tanks regularly, modifying inlet/outlet locations, and optimizing operations by modeling retention times and mixing characteristics. More than half of systems using at least one of these practices to maintain water quality in storage tanks [17].

1.4. Potential Human Health Impacts

Storage tanks are associated with a range of human health risks resulting from exposure to waterborne pathogens, contamination due to breaches of tank integrity or contaminants generated inside tanks from corrosion or disinfectant byproduct reactions. For example, a 1993 outbreak of

Salmonella typhurium in Gideon Missouri resulted from bird droppings in a covered storage tank; more than 600 residents became ill resulting in 7 deaths [23].

Similarly, a 2008 outbreak in Alamosa Colorado was attributed to animal waste contamination of a ground level storage tank, resulting in 442 reported illnesses and one death [24]. Significant amounts of sediment described as "black and tarry" or "sandy" were removed from Alamosa's storage tanks during cleaning and disinfection processes. The last inspection of the implicated tank had been conducted 11 years earlier; the report noted about an inch of sediment accumulated at the bottom and recommended cleaning the tank every 3-5 years. However, the utility did not appear to have a regular program for flushing, disinfecting or removing sediment from tanks.

Craun et al. [25] reported that 79 of 780 waterborne disease outbreaks recorded in the US between 1971 and 2006, about 10%, can be attributed to distribution system deficiencies. These deficiencies include contamination of storage tanks, contamination of water mains, cross-connections, and more. Of 33 waterborne disease outbreaks recorded in 2009-2010, there were 1040 related cases of illness [26]. While only a small number (12%) of the outbreaks were attributed to distribution system deficiencies, most (68%) illnesses resulted from distribution system deficiencies. In other words, the number of people who became ill was much higher for distribution system problems, including storage tank problems, than for outbreaks resulting from other types of water system deficiencies.

1.5. Sediment Accumulation in Storage Tanks

Sediments can be introduced into tanks through accidental contamination from the outside environment due to improper tank maintenance, chemical precipitation, corrosion of tank materials, or from the source water. Often, sediments accumulate on tank bottoms as a result of low velocity zones. One study of three tanks that had not been cleaned for more than 7 years found 10-71 cm (4-28 inches) of sediments on the bottom of the tanks [22].

To help expand understanding of storage tank sediments, their potential for accumulating contaminants and their risks to human health, a recent study collected sediments from 25 storage tanks at 18 drinking water systems in 12 different US states [27]. Sediment samples were collected from 3-5 locations within each tank. All of the tanks contained finished drinking water that originated from ground or surface water sources. The sediments were characterized by total organic carbon, organic matter, sand, silt, and clay content, grain size, pH, cation and anion exchange capacity, bulk and particle density, and porosity. In addition, the chemical composition of the sediments were analyzed; for example, in one sediment sample, iron, zinc, aluminum, phosphorous, magnesium, silicon, and manganese were detected [28].

As part of this study, Lu et al. [29] studied 87 sediment samples from 18 US locations and analyzed for a range of potential microbial pathogens. The study looked for both enteric pathogens present in animal excreta as well as opportunistic pathogens that are known to cause health impacts from drinking water exposure. Several opportunistic pathogens were detected: *Mycobacterium* species were found in 89.9% of samples, *Legionella* species in 66.7%, *Acanthamoeba* species in 38.9%, *Pseudomonas aeruginosa* in 22.2% and several other pathogens occurred in 5% or fewer samples. In contrast, enteric pathogens like *Escherichia coli* O157, *Salmonella*, *Giardia* and *Cryptosporidium* species were undetected, although *Campylobacter* was found in trace amounts.

This study shows that opportunistic pathogens are present within storage tank sediments and raises concerns about potential human health risks associated with tank sediments.

Another EPA study tested the adherence of several contaminants to tank sediments: nonradioactive cesium, Cs-133 (a surrogate for radioactive Cs-137), lindane, an organochlorine pesticide, *Escherichia coli*, and the attenuated strain *Bacillus anthracis Sterne* (a surrogate for pathogenic *Bacillus anthracis*) [27]). All of the contaminants adhered to sediments to some degree: cesium adherence ranged from 5-88%, lindane from 7-88%, *E. coli* from 42-100%, and *B. anthracis* from 31-100%. This study suggests that when sediments are present in tanks, both chemical and biological contaminants are likely to adhere to sediments.

1.6. Major Assumptions Used in this Report

In the rest of this report, for both the CFD modeling studies and the experimental study, the starting premise is that sediments are present at the bottom of the studied tanks. As such, this report does not address the issues of how sediments accumulate on tank bottoms or how to prevent sediment accumulation. From this assumption, this report focuses on understanding how and when sediments are resuspended from the bottom of tanks, how they are transported within the tank, and how sediments are removed from the tank back into a water distribution system.

For the CFD modeling studies, sediments are modeled as individual spherical particles of a certain size and density. Chemical and biological reactions between particles are ignored, such as adsorption or biofilm development.

A single tank configuration is studied for this report – a cylindrical ground level tank with a single inlet/outlet pipe located at the bottom center of the tank and a storage volume of 11,400 m^3 (3 million gallons). Many other tank types, shapes, configurations and sizes are used by drinking water systems around the US, and while similar sediment transport processes and behavior may be inferred from the current study, an accurate assessment would require further studies of these alternate configurations.

2. Modeling

To understand sediment resuspension in tanks and the potential for transport of sediments back into water distribution systems, three CFD modeling studies were performed: (1) an operational study to determine the temporal and spatial transport and distribution of sediment particles during both filling and draining cycles; (2) a parametric analysis to determine the impact of various parameters and processes (inlet/outlet location and diameter, flow rate, particle size, and filling vs. draining cycles) on the resulting shear stress and potential for particle resuspension along the bottom wall; and (3) a study to determine the effectiveness of a raised inlet/outlet line (just above the tank floor) in mitigating particle resuspension and removal.

2.1. Hydraulic Model

A hydraulic model for turbulent flow in a water distribution storage tank was developed using the ANSYS® Fluent® CFD^{TM} software (ANSYS, Inc., Canonsburg, PA). ANSYS® Fluent® is a CFD code that can simulate single- and multi-phase flow phenomena in complex geometries.

Fluent® has been validated in various applications relevant to water flow in tanks and used in numerous simulations across all industries [7, 11, 13, 14, 30-32]. The Fluent® software has advanced capabilities for simulating the flow paths of fluids within complex domains. The model domain for this study was assumed to be an 11,000 m³ (3 million gallon) cylindrical, ground level tank with a single inlet/outlet line at the bottom of the tank located either at the center or near the wall (Figure 2).

For this study, the hydraulic model needed to capture typical dynamics observed in tanks: the turbulent movement of water entering and exiting the tank, the complex flow patterns and eddies created in the tank, and the changing levels of the water surface. In addition, in order to capture the onset of particle movement, shear stresses along the tank bottom need to be predicted by the model.

Within the Fluent® software, there are several turbulence models that can be used. Data from the literature on tank flows and mixing tests were used to determine the most appropriate turbulence model for this study (see Appendix A for additional details). Based on these verifications, the Fluent® software's k-ω Shear-Stress Transport (SST) turbulence model was determined to be the best suited for this study. The Fluent® software solves the Reynolds-Averaged Navier-Stokes (RANS) equations to determine for time-averaged turbulent flows. The SST model uses an isotropic eddy viscosity value to solve for the Reynolds stress term in the RANS. The SST model is capable of solving turbulence equations in the near-wall region as well as in the free-stream region. The model was validated against experimental data found in the literature (see Appendix A). The shear stress along the bottom wall, which is the critical parameter in determining particle resuspension, was calculated by the hydraulic model.

The Fluent® software's two-phase Volume of Fluid (VOF) model was used to simulate the liquid flow patterns in the tank and the movement of the top surface of the water during filling and draining. The VOF model simulates two or more immiscible fluids (in this case, air and water) by solving the fluid momentum equations and tracking the volume fraction of each fluid separately in the computational domain. The VOF is often used to simulate liquid moving into a large volume of air space (e.g., water flowing from a hose, motion of liquid after a dam break).

9.9 m (32 ft) height

4.9 m (16 ft) initial water level

38.4 m (126 ft) tank
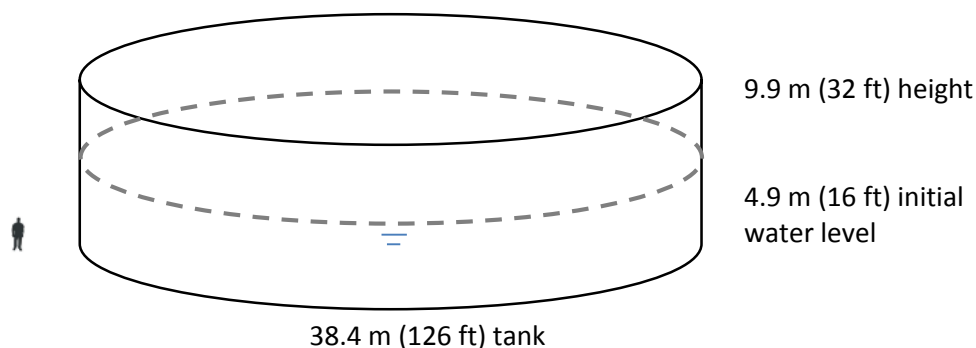
Figure 2. Schematic of the water distribution tank configuration used in the numerical simulations. The inlet/outlet line (61 cm (24") or 91 cm (36") diameter) was located flush with the bottom of the tank either in the center or near the side wall.

2.2.   Sediment Resuspension Models

With no existing mathematical model for sediment resuspension in water tanks, a literature review was conducted to evaluate models developed for other applications. Beheshti and Ataie-Ashtiani [33] summarize a number of models developed to predict sediment resuspension; they also derived their own model – referred to hereafter as the Beheshti model. This section summarizes the criteria and methods used in the Shields and Beheshti models, the two major approaches relevant to this study, and describes how these methods were applied to simulate sediment resuspension in water tanks.

2.2.1.   Shields Model

For many decades, the Shields model has been used to predict the onset of motion of sediment solids in rivers, open-water channels, and sewage systems [8-11, 15, 16, 34-37]. The model reflects the balance between the hydrodynamic forces of drag and lift that induce motion on a particle and the force of submerged weight which resists motion on a particle. If the hydrodynamic forces are greater than the forces of weight on a particle, then a critical threshold for movement has been exceeded. In the Shields model, if the calculated dimensionless shear stress of the tank bottom, τ^*, is greater than the dimensionless critical shear stress, then particle suspension will occur.

The Shields Model can be represented graphically by the Shields diagram, in which the dimensionless critical shear stress, τ_c^*, is plotted as a function of the grain Reynolds number, R_* (Figure **3**). Represented graphically, motion is induced if the dimensionless shear stress at a given grain Reynolds number is *above* the Shields curve; conversely, particles will remain stationary if the dimensionless shear stress is *below* the Shields curve. As shown in Figure 3, at low grain Reynolds numbers, the dimensionless shear stress must be high in order to induce motion of the particles. The Shields diagram is empirically based on a variety of experiments and materials (e.g., sand, minerals, glass beads, and steel shot) and should be generally applicable to flow in water storage tanks. However, the model applies to non-cohesive granular sediment and particles, not clays or muds that have electrostatic interactions. The equations do not account for armoring, in which smaller particles may be trapped and protected under a layer of larger particles or biofilm. Also, the model assumes uniformly shaped and uniformly sized particles, and does not account for the random/transient nature of incipient motion.
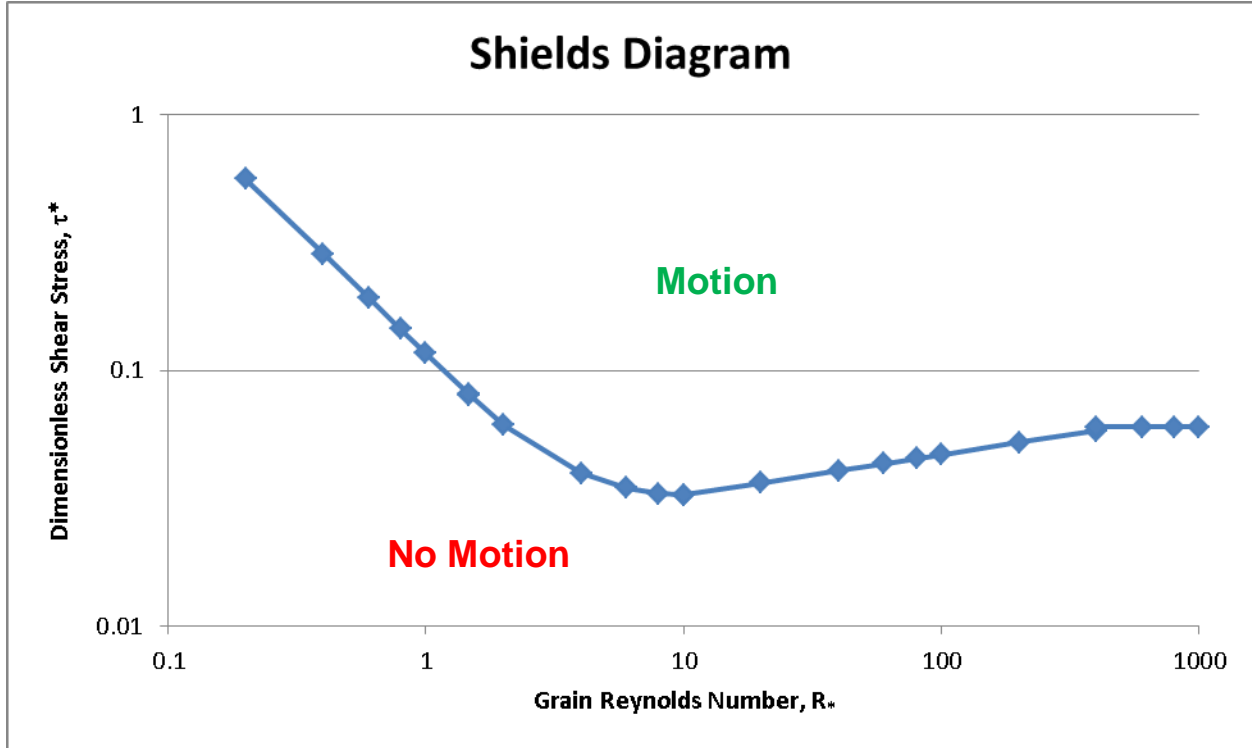
Figure 3. **Graphical representation of the Shields model in which the dimensionless critical shear stress, τ_c^* , is plotted as a function of the grain Reynolds number, R_* .**

The Shields model defines the dimensionless shear stress, τ^*, the dimensionless grain Reynolds number, R_*, and the shear velocity, u_*, (in units of m/s) as follows:

$$\tau^* = \frac{\tau}{(\rho_s - \rho_w)gD} \qquad (1)$$

$$R_* = \frac{u_* D}{\nu} \qquad (2)$$

$$u_* = \sqrt{\frac{\tau}{\rho_w}} \qquad (3)$$

where τ is the shear stress on the bottom wall (Pa), ρ_s and ρ_w are the solid and liquid densities (kg/m^3), g is acceleration due to gravity (9.81 m/s^2), D is the particle diameter (m), and ν is the kinematic viscosity of the liquid (m^2/s). The shear stress at the tank bottom, τ, is used to find the grain Reynolds number, R_*, and the dimensionless shear stress of the tank bottom, τ^*. The dimensionless critical shear stress, τ_c^*, plotted in Figure **3** is a function of the grain Reynolds number, R_*. Typically, in drinking water storage tanks, particle diameters would vary from 0.01 – 1 mm (see Appendix B), shear stresses from 0.1 to 10 Pa, and grain Reynolds numbers from 0.1 to 100.

The dimensionless critical shear stress, τ_c^*, is represented by the piecewise function in Figure 3 according to the following equation for different values of the grain Reynolds number [38]:

21

$$\text{For } R_* \leq 1.47, \quad \tau_c^* = .1166 \cdot R_*^{-.977482} \tag{4}$$

For $1.47 < R_* \leq 10, \quad y = -.9078950 - 1.2326090 \cdot x + .7298640 \cdot x^2 - .0772426 \cdot x^3$
where $y = \log(\tau_c^*)$ and $x = \log(R_*)$

For $10 < R_* \leq 400, \quad \tau_c^* = .0227 \cdot R_*^{.1568}$

For $R_* > 400, \quad \tau_c^* = .06$

2.2.2. Beheshti Model

Beheshti and Ataie-Ashtiani [33] performed more recent studies with new data sets and concluded that the Shields method led to discrepancies because of the inability to address particle shape, randomness of entrainment, and the difficult with defining criteria for incipient motion. In the Beheshti model, the use of a dimensionless movability number as a function of dimensionless grain diameter was found to provide better matches to the data. They state that the movability number, which includes the settling velocity, provides an implicit inclusion of shape effects in the threshold determination. The dimensionless grain diameter of a particle, D_*, is defined as

$$D_* = D \left[\frac{\rho_p - \rho_w}{\rho_w \left(\frac{g}{v^2} \right)} \right]^{1/3} \tag{5}$$

where ρ_p is the particle density (kg/m^3). The critical movability number of a particle is a function of D_* and represents the threshold of particle resuspension. It can be represented by the following piecewise function:

$$\begin{cases} 9.6674 D_*^{-1.57}, & D_* \leq 10 \\ 0.4738 D_*^{-.226}, & D_* > 10 \end{cases} \tag{6}$$

Determining the actual movability number of a particle to compare with the critical movability number requires first finding the particle's shear velocity, u_*, and settling velocity, w_s, by

$$u_* = \sqrt{\frac{\tau}{\rho_w}} \tag{7}$$

$$w_s = \frac{Av}{BD} \left[\sqrt{\frac{1}{4} + \left(\frac{4B}{3A^2} D_*^3 \right)^{\frac{1}{a}}} - \frac{1}{2} \right]^a \tag{8}$$

where
$$A = 53.5e^{-0.65 S_f}, \quad B = 5.65e^{-2.5 * S_f}, \quad a = 0.7 + 0.9 S_f$$

The coefficients A and B are derived empirically and represent the effect of particle shape on settling. Known as the Corey Shape Factor, S_f is 0.7 in this study, which is typical of naturally

occurring sediment particles. The actual movability number can then be determined by dividing the shear velocity by the settling velocity, or u_*/w_s.

Figure 4 shows a plot of the critical movability number as a function of the dimensionless grain diameter, D_*. Similar to the Shields curve, if the actual movability number of a given particle is greater than the critical movability number, then particle suspension will occur. In drinking water storage tanks, typical dimensionless grain range from 0.25 – 25.
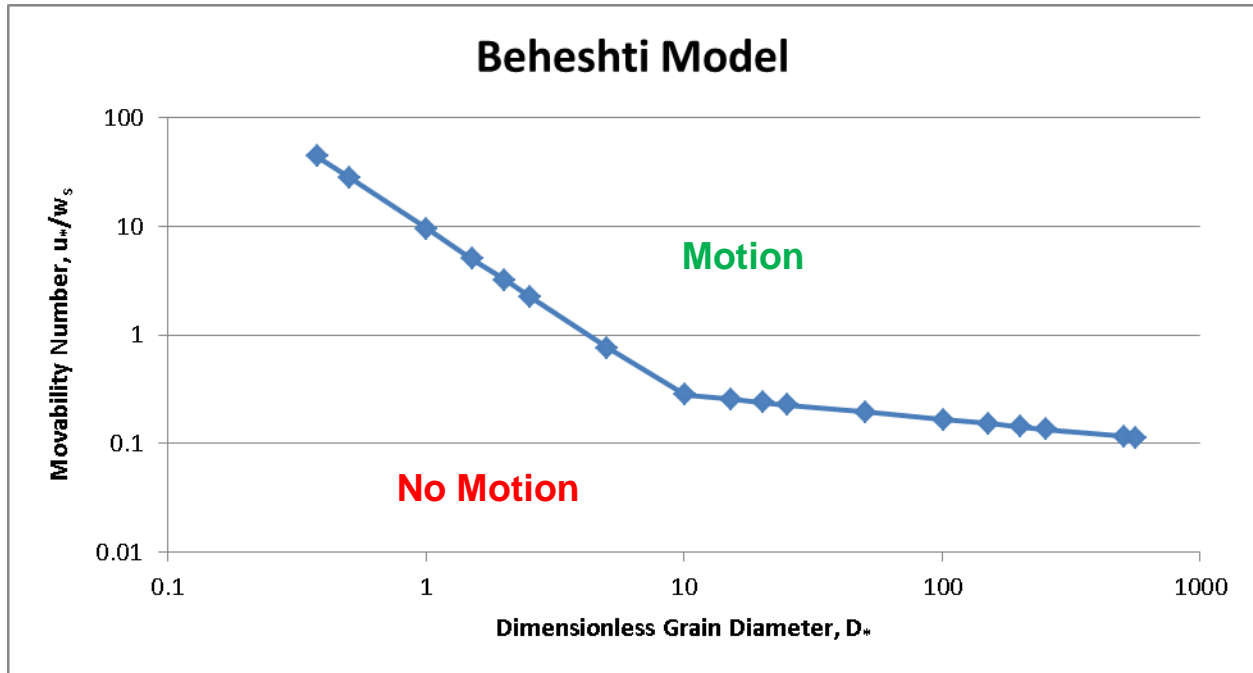
Figure 4. Graphical representation of the Beheshti model (adapted from [33]) in which the critical movability number is plotted as a function of the dimensionless grain diameter.

2.2.3. *Implementation of Sediment Suspension Models in CFD Model*

For the CFD simulations conducted as part of this study, both the Shields and Beheshti sediment transport models were implemented using C code consisting of user-defined functions (UDFs). A UDF is defined by macros provided by the Fluent® software that allows the user to enhance normal features and perform advanced tasks. For instance, UDFs can customize flow parameters, control time step size during a transient simulation, alter material properties, obtain information about specified grid mesh faces and cells, and modify boundary conditions, among other features.

In the operational simulation study (Section 2.3), UDFs were used to model particle movement during a transient simulation of a representative fill/drain cycle. Particles were initially distributed along the bottom wall of the tank (see Appendix B). Three different representative particle sizes (0.01, 0.1, and 1 mm) were included in the simulations based on sediment samples collected from several water distribution storage tanks (Appendix B). The size distribution of particles collected from water tanks ranged from ~0.01 – 1 mm. The density of the particles was assumed to be 2,650

kg/m^3 (silica sand). The UDF "injects" 6,000 particles consisting of equal numbers of 0.01, 0.1, and 1 mm diameter particles on the tank bottom at the start of a simulation. Each size of particles was distributed across the bottom face of the tank in the same locations, resulting in 2,000 different initial positions and 3 different-sized particles at each position. The initial particle positions were scaled towards the tank center since the particles further away from the inlet/outlet line were less likely to experience resuspension and were thus of less interest (see Appendix B for more information).

At each subsequent time step of the calculation, wall shear stresses were recorded at locations of all particles touching the bottom wall. If the sediment suspension model predicted that particle suspension would occur (e.g., the wall shear stress at the particle location was greater than the critical shear stress), the particle was injected (allowed to move) into the fluid domain at that location. Once injected, the motion of the particles was simulated in the Fluent® software using a Lagrangian reference frame governed by a force balance on the particle. The force balance includes a drag force that accounts for the velocity of the particle, velocity of the surrounding fluid, particle size, and fluid properties [39]. If, on the other hand, a particle was in contact with the bottom wall of the tank and the suspension model predicted a deposition (e.g., the wall shear stress at the particle location was less than the critical shear stress), the particle would be recorded as deposited in the UDF with an associated time stamp and particle identification number. Thus, the number of particles deposited on the tank bottom, entrained in the flow and moving through the tank, or drained from the outlet line were tracked and recorded at each time step.

To increase accuracy, the sediment suspension UDFs interpolated wall shear stresses between centroids of the domain grid mesh faces comprising the bottom wall. In addition, critical particle information for every particle that was either removed (drained) from the system or deposited along the bottom wall, such as particle diameter, time of drain/deposition, time of preceding resuspension, and particle position, were written to a text file for post-processing.

At the air-water interface, the Fluent® software does not by default include forces due to surface tension. Therefore, a surface-tension model was created and implemented in a UDF to correctly account for surface-tension forces on particles at the air-water interface, which prevented particles from moving into the air phase from the liquid phase unrealistically. Appendix C describes the surface tension model in detail.

In the parametric study (Section 2.4) and the small-scale validation study (Section 3), where particles were not injected into the domain, UDFs were only used for post-processing after the simulations were completed. The UDFs determined whether the wall shear stress at each bottom wall mesh face exceeded the critical shear stress according to the Beheshti and Shields models, i.e. particles would be resuspended at that face. The total area of particle resuspension was determined by summing the individual areas of each face whose wall shear stress exceeded the critical shear stress. In addition, the radial extent of resuspension was determined by dividing the bottom wall into twenty individual regions of equal angular (azimuthal) span and averaging the radial extents of resuspension over all regions. The averaging procedure accounted for small but noticeable radial asymmetries in the bottom wall shear stresses.

2.3. Operational Study of Particle Movement during Filling and Draining Cycles

The purpose of the operational study was to determine the temporal and spatial transport and distribution of particles during typical tank operating conditions, which includes continuous filling and draining cycles. Typical tank operating conditions were assumed to follow those described in Section 1.2. The following sections describe the model development for the operational study and the modeling results.

2.3.1. Geometric Configuration and Flow Parameters

In the operational study, two separate representative fill/drain cycles for a 38.4 m (126 ft) diameter, 9.75 m (32 ft) high Albuquerque Water Authority tank (11,300 m^3 or 3 million gallons) were simulated in the Fluent® software (Figure 2). Although tanks can have an inlet/outlet transmission line located near the side walls, only the center-line tanks were modeled in the operational study, allowing for a simpler and computationally efficient 2D axisymmetric domain. The axisymmetric domain assumes that the flow is symmetric about the vertical centerline of the tank. Figure 5 shows the 2D domain and computational mesh used in the operational study simulations. The mesh cells near the inlet/outlet and bottom wall are noticeably finer, which is necessary in order to provide accurate flows and bottom wall shear stresses required to predict resuspension and deposition of particles. The 2D axisymmetric mesh consists of 24,133 cells and 24,444 nodes. Appendix D documents the validity of the 2D axisymmetric solution when compared to 3D simulations. Grid convergence studies were also performed to ensure the adequacy of the grid resolution. For this operational study, the 2D simulations of a single fill or drain cycle took several weeks to complete. Full 3D simulations would take considerably longer (an order of magnitude or more).

The flow parameters for the operational study are listed in Table 2. Two cases – a high flow rate and a low flow rate – were simulated based on values provided by the two water utilities. Both cases began with the fill stage, immediately followed by draining after 5,400 seconds (1.5 hours). This time was sufficient to allow the particles to become suspended and recirculate through the tank. The high flow case represents roughly the highest inlet/outlet velocity reported by the Albuquerque Water Authority, while the low flow case represents the lower velocities.

Table 2. Tank and flow parameters used in operational study.

Both Cases	Tank Diameter (ft / m)	Tank Height (ft / m)	Inlet/Oulet Diameter (in / m)	Fill Time (s)	Drain Time (s)	Initial Water Level
	126 / 38.4	32 / 9.75	24 / 0.61	5400	5400	50%

Case	Flow Rate (gpm) / (m^3/s)	Flow Velocity at Line (ft/s) / (m/s)
High Flow	10,000 / 0.631	7.09 / 2.16
Low Flow	3,400 / 0.215	2.42 / 0.738
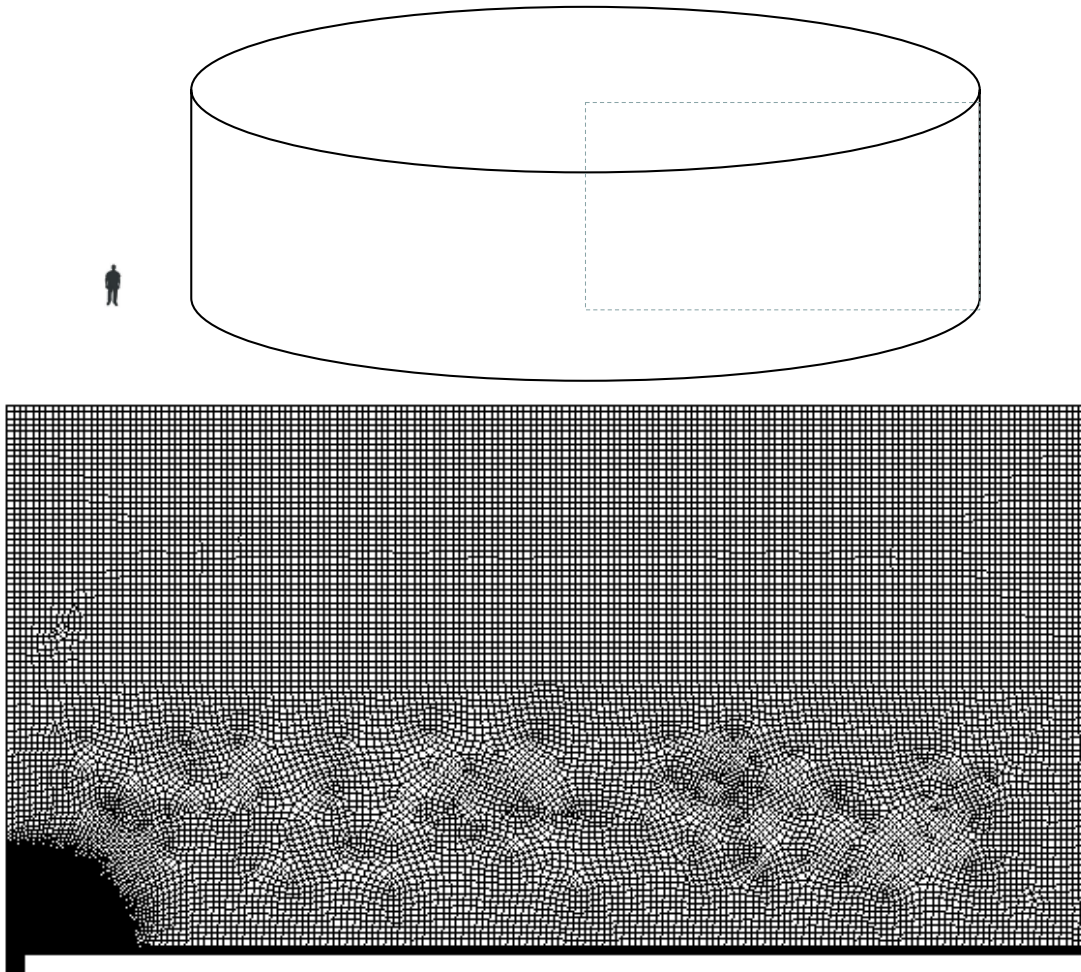
Figure 5. Mesh of 2D axisymmetric model used in operational study. The dashed outline in the schematic on top shows the location of the computational domain.

2.3.2. *Results of Operational Study*

Simulated flow pathlines – the trajectories that individual fluid particles follow – are displayed in Figure 6 (high flow case) and Figure 7 (low flow case) at selected times (10, 5400, 5410, and 10,800 seconds). The pathlines are colored by the velocity of the fluid particles: red indicates higher velocities and blue indicates lower velocities. During the filling stage, a circulation zone forms early and grows in size until it occupies nearly the entire water-filled region of the tank. Other, smaller, circulation zones can be seen as well. Once draining begins, much of the circulation zone formed during filling is still present; however, flow near the inlet/outlet begins to split into two directions: downward toward the outlet and upward in accordance with the circulation zone. As the drain stage progresses, the circulation zone breaks down and the flow becomes highly irregular far away from the inlet/outlet, characterized by rapid changes in direction and turns. Chaotic flow was also observed in the 3D model during a drain-only run (see Appendix D).
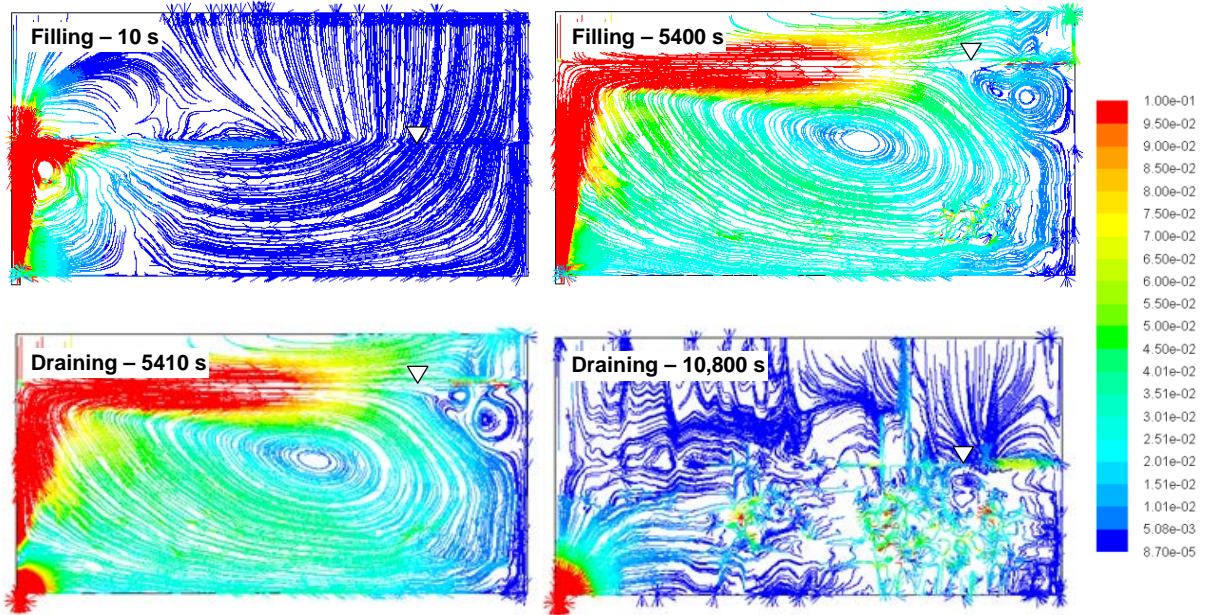
Figure 6. Flow pathlines colored by velocity magnitude (m/s) during filling and draining cycles in high flow rate case (0.631 m³/s or 10,000 gpm). Upside-down triangle denotes water level. Flow pathlines above the water level denote velocity of the air phase.
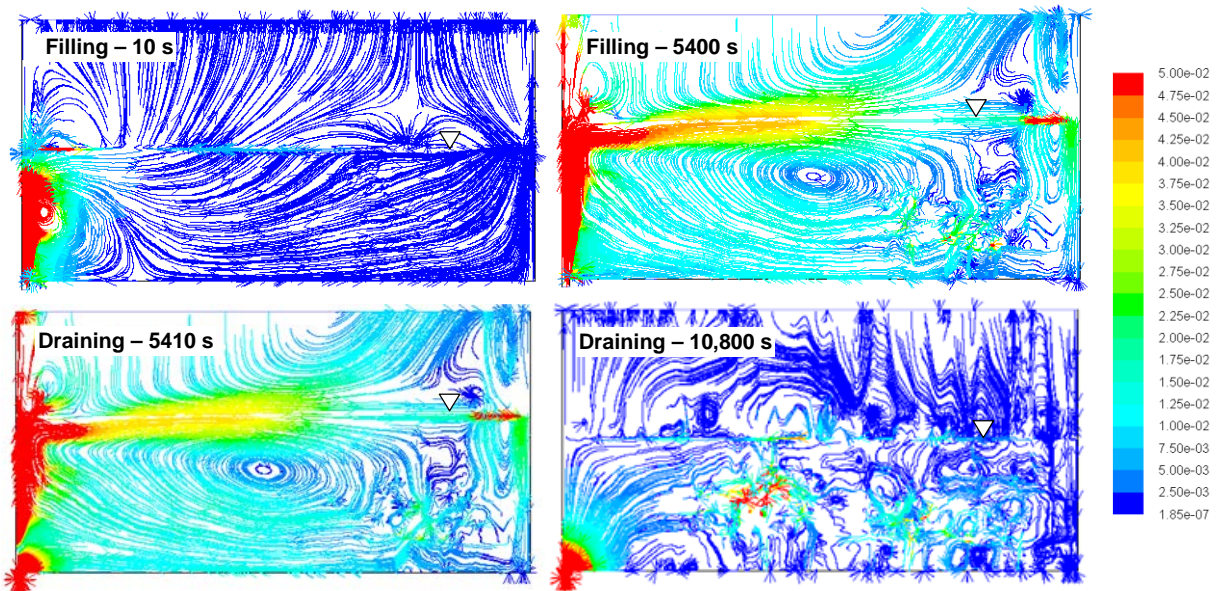
Figure 7. Flow pathlines colored by velocity magnitude (m/s) during filling and draining cycles in low flow rate case (0.215 m³/s or 3,400 gpm). Upside-down triangle denotes water level. Flow pathlines above the water level denote velocity of the air phase.

The pathlines in the filling stage of the high flow case (Figure 6) are slightly more stable and orderly than in the low flow case (Figure 7). The primary circulation zone is also larger in the high

flow case. However, both cases in the drain stage exhibit significantly high instabilities in the fluid flow.

Figure 8 and Figure 9 display the particle traces of resuspended particles at selected times (every 2,000 seconds in addition to 10, 5400, and 10,800 seconds) for the high flow and low flow cases, respectively. The red, green, and blue particles represent particle diameters of 1.0, 0.1, and 0.01 mm, respectively. The light blue mesh outline represents water, while the white space represents air; any other colors in the mesh (near the water surface) represent cells in the process of switching between the air phase and the water phase. When describing particle movement, particles are categorized as resuspended (scoured from the tank bottom and entrained in the fluid flow), drained (removed from the tank through the outlet pipe), or deposited back on the tank bottom. The percentage of resuspended, drained, and deposited particles are summarized in Table 3.

Table 3. Summary of operational study results

Particle Size* (diameter)	0.01 mm		0.1 mm		1 mm		All particle diameters	
Flow Rate**	High Flow	Low Flow	High Flow	Low Flow	High Flow	Low Flow	High Flow	Low Flow
% of particles resuspended	11.98%	8.70%	8.05%	4.27%	4.40%	1.45%	24.43%	14.42%
% of particles deposited	7.97%	6.02%	5.72%	2.48%	2.62%	0.70%	16.30%	9.20%
% of particles drained	0.15%	0.32%	0.13%	0.25%	0.05%	0.28%	0.33%	0.85%
% of particles drained whose preceding resuspension occurred during filling stage	0.15%	0.00%	0.00%	0.00%	0.00%	0.00%	0.15%	0.00%
% of particles entrained in flow at end of filling (5400 s)	0.65%	0.38%	0.38%	0.07%	0.37%	0.00%	1.40%	0.45%
% of particles entrained in flow at end of draining (10800 s)	3.87%	2.37%	2.20%	1.53%	1.73%	0.47%	7.80%	4.37%
% of particles in upper stagnation region	3.15%	1.68%	1.80%	1.15%	0.92%	0.47%	5.87%	3.30%
% of particles in lower recirculation region	0.23%	0.30%	0.20%	0.32%	0.47%	0.00%	0.90%	0.62%
Maximum radial position at which resuspension occurred (m)	2.55	2.25	1.32	0.79	0.79	0.49	2.55	2.25

*6,000 particles were initially in the tank (2,000 each of 0.01, 0.1, and 1 mm diameter)

**High flow = 10,000 gpm (0.631 m^3/s), Low flow = 3400 gpm (0.215 m^3/s)

Filling – 10 s

Filling – 2000 s

Filling – 4000 s

Filling – 5400 s

Draining – 6000 s

Draining – 8000 s

Draining – 10,000 s

Draining – 10,800 s
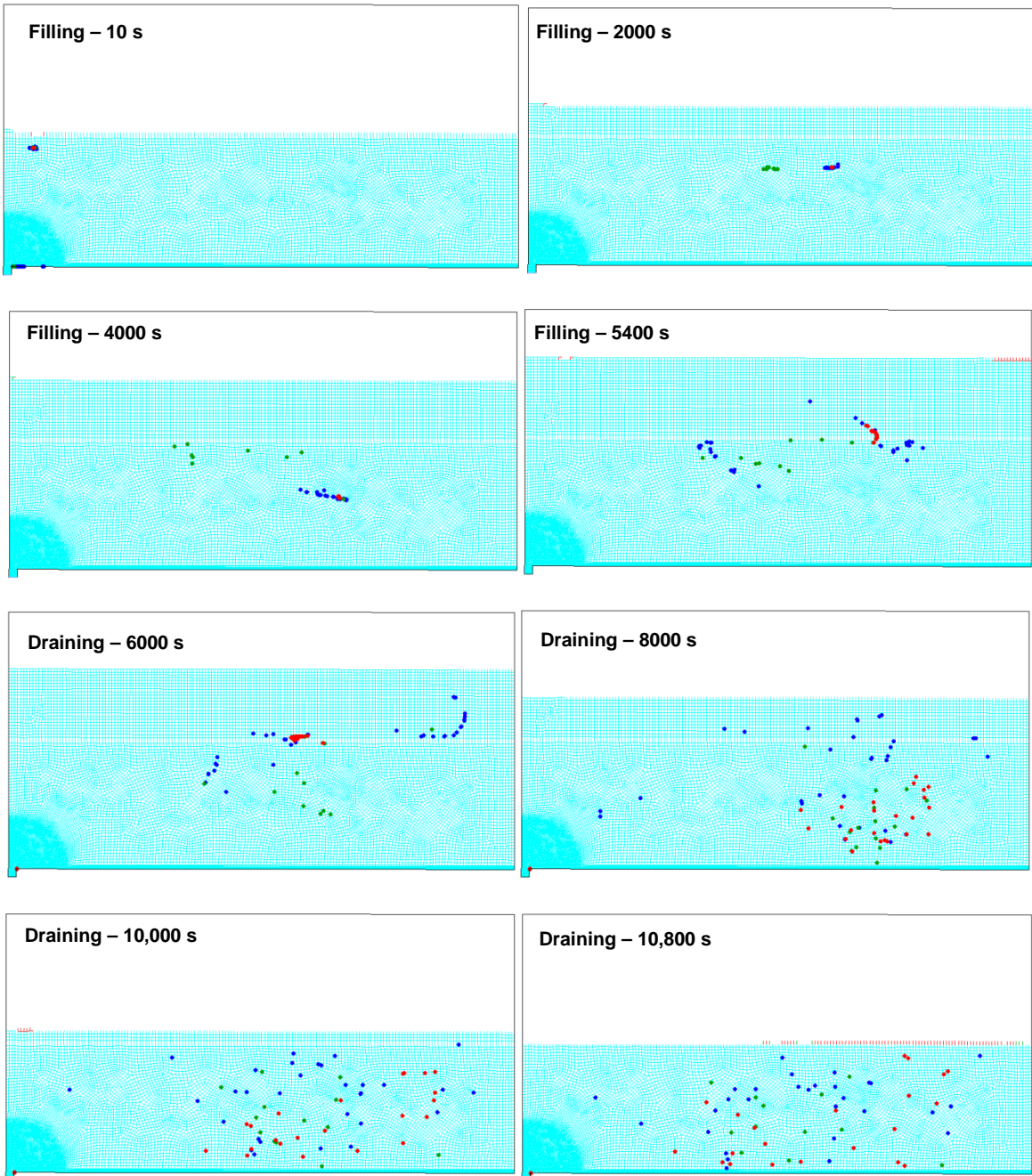
Figure 8. Particle traces during filling and draining cycles in high flow rate case (0.631 m³/s or 10,000 gpm).   Particles colored by particle diameter (red = 1 mm, green = 0.1 mm, dark blue = 0.01 mm). Light blue mesh denotes the water domain.
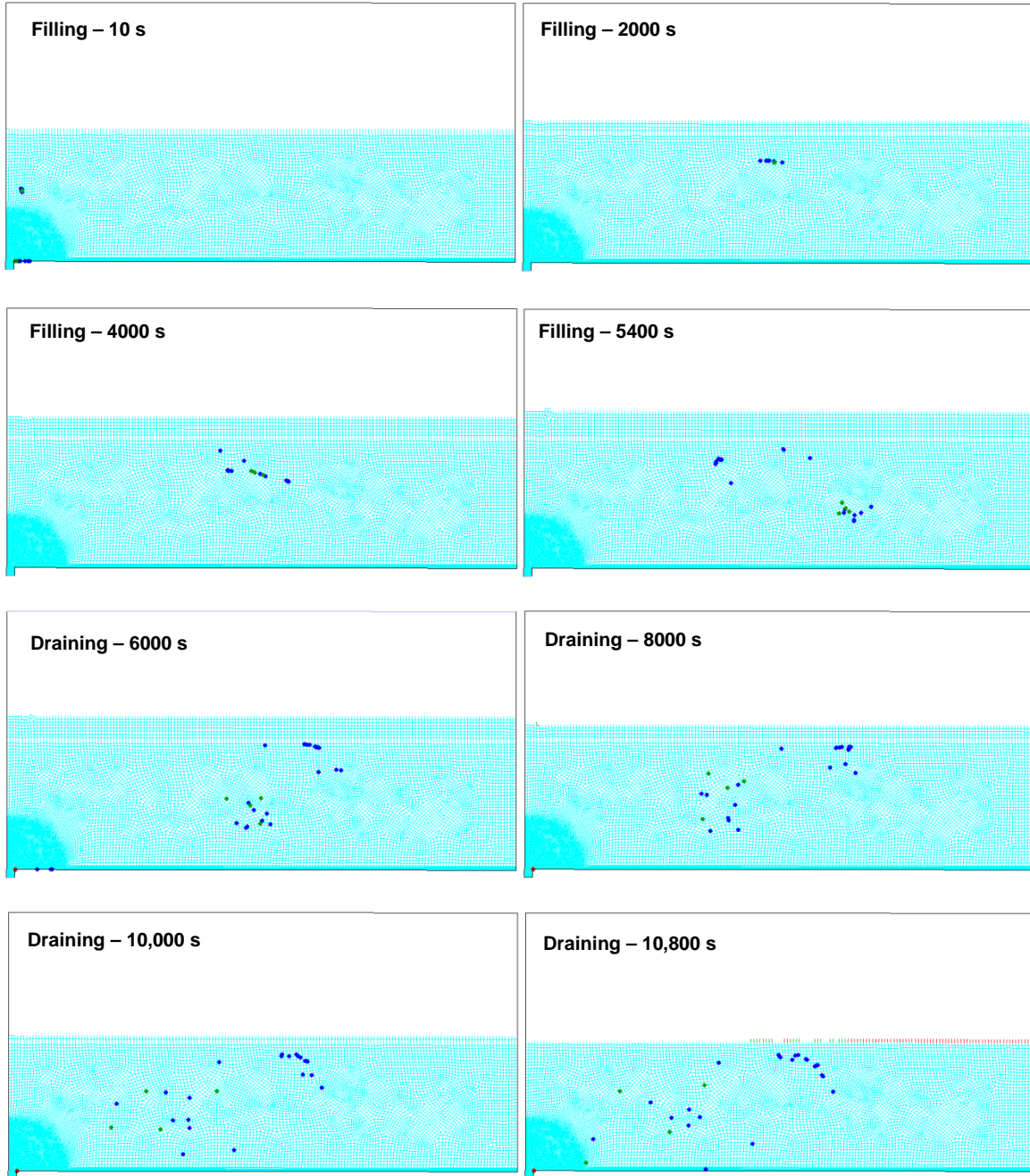
Figure 9. Particle traces during filling and draining cycles in low flow rate case (0.215 m³/s or 3,400 gpm). Particles colored by particle diameter (red = 1 mm, green = 0.1 mm, dark blue = 0.01 mm). Light blue mesh denotes the water domain.

In both the high- and low-flow cases, the particles are clumped together in the beginning of the cycle and then steadily disperse, particularly during the draining cycle. The particles circulate around the tank in the filling stage but begin to scatter less predictably in the drain stage, consistent with the pathline patterns. Another common feature is the high proportion of 0.01-mm-diameter particles entrained in the fluid flow. During the drain stage, both cases also show an increase in the number of particles entrained in the flow compared to the fill stage.

Due to its higher velocities and thus higher shear stresses, the high flow case exhibits a larger number of resuspended particles and significantly more scatter in the particle traces. In addition, a sizeable number of 1-mm-diameter particles become resuspended in the high flow case, compared to only a few in the low flow case, which did not produce shear stresses along the bottom wall sufficient to suspend the larger particles.

During the drain stage in both cases, a seemingly stationary particle trace can be seen near the bottom of the tank connecting the inlet/outlet to the bottom wall. In fact, two tightly packed clusters of particles are located in this region. One cluster is caught in a circulation zone within the inlet/outlet; these particles are considered drained or removed from the tank. The other cluster of particles remains stagnant on the bottom wall near the transmission line and is thus considered deposited. These two recirculation patterns result from relatively sharp bends in the flow path near the transmission line (Figure 10).
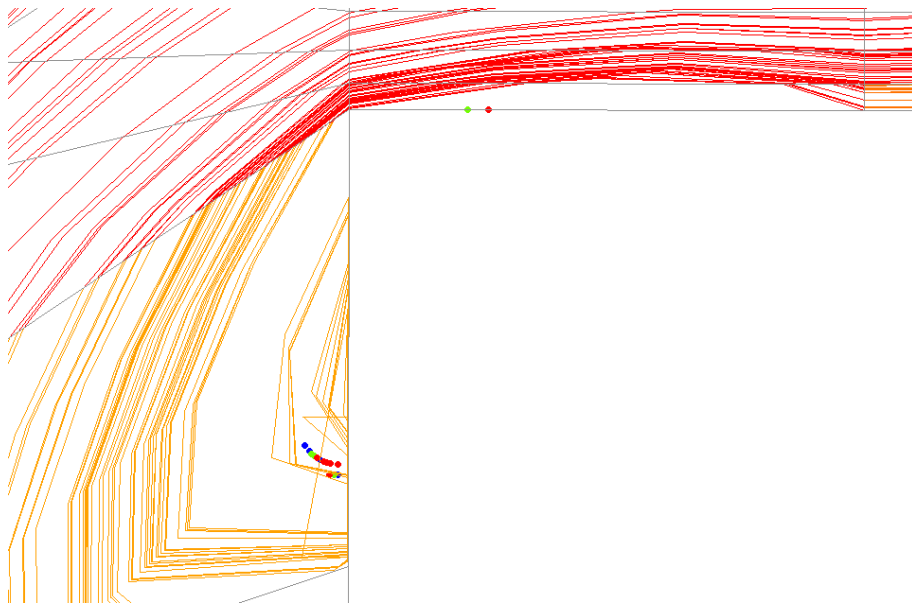
Figure 10. Pathlines and particle traces near the transmission line during draining. The mesh is outlined in gray, the pathlines are red and orange, and the particles are red (1 mm), green (0.1 mm), and blue (0.01 mm). Two "stagnant" particle clusters are shown here: one within the transmission line and one on the bottom wall. The pathlines can be seen making relatively sharp bends in order to enter the transmission line, yielding recirculation zones where the particles get trapped.

Figure 11 to Figure 18 illustrate additional results of the high- and low-flow cases, respectively. Figure 11, Figure 16, and Figure 17 demonstrate that particles closer to the inlet/outlet are more likely to experience resuspension. Figure 12 shows that the initial positions of particles that were eventually drained during the simulation were close to the inlet/outlet (within one meter). Similarly, Figure 13 shows the initial positions of particles that were entrained in the flow at the end of the simulation; smaller particles close to the inlet are more likely to be entrained. Figure 12 shows that the smallest particles (0.01 mm) were drained closest to the tank center in the high flow case, whereas the largest particles (1 mm) were drained closest to the tank center in the low

flow case. In the high flow case, particles close to the tank center (including the largest particles) were entrained in the flow during filling. While the larger particles were more prone to dropping out of the entrainment at a location further from the inlet, the smaller particles tended to remain entrained until the draining cycle, at which time they were more readily drained. In the low flow case, the larger particles near the tank center were not entrained during the filling cycle, but during the draining cycles, the shear stress near the inlet/outlet was greater, and the larger particles that remained could be drained.

Figure 14 shows a high degree of scatter observed in the particles that were still entrained at the conclusion of the cycle. The horizontal strip of symbols in both plots of Figure 14 represents the particles stuck in the recirculation/stagnation zones referred to in Figure 10. This is a result of low axial velocities (compared to the radial component) along the bottom wall away from the transmission line (as seen in the velocity pathline figures), causing such particles to be "dragged" along the bottom wall and toward the recirculation/stagnation zones. Furthermore, according to Figure **15**, among the particles that were resuspended at least once but ended up deposited on the bottom wall at the end of the cycle, the majority were deposited close to their initial positions, suggesting that most of these particles were deposited soon after being resuspended. This notion is supported by Figure 16 and Figure 17, which show that the bulk of resuspensions *and* depositions occurred during the same general times (shortly after the starts of filling at 0 s and draining at 5,400 s). Figure 17 also indicates high shear stresses during draining due to the surge of resuspensions immediately after the beginning of the drain stage.

Regarding the impact of different flow rates, the low-flow case resulted in a smaller number of resuspensions than in the high flow case (Figure 17). Additionally, unlike in the high flow case where depositions still occurred even after the drain stage was well underway (after about 6400 seconds in Figure 16), the low flow case exhibited no such depositions. This helps explain the qualitative differences between the high- and low-flow cases in Figure **15**. The former shows that a modest fraction of the particles at rest on the bottom wall at the end of the cycle end up considerably further away from the tank center relative to their initial positions; the latter displays no such particles. Since a separate analysis revealed that no particles that were resuspended during the low-flow fill stage were deposited during the drain stage, the above observations establish that all particles that were deposited during the low-flow cycle were only briefly resuspended beforehand. Despite the large number of resuspensions, the lower velocities and shorter periods of entrainment prevented the particles from being transported large distances in the low-flow case. Also, the total number of particles drained in the low-flow case was less than that of the high-flow case. More particles were resuspended and redistributed away from the inlet/outlet in the high-flow case, and fewer particles were available near the inlet/outlet when draining commenced.

Regarding the impact of different particle sizes, Figure 17 shows that the smallest particles (0.01 mm) were more prone to resuspensions than the larger particles (0.1 and 1 mm). However, the number of particles eventually drained from the system was not largely dependent on particle size in the low-flow case. Figure 18 shows that in the low-flow case, roughly the same number of particles of each size were drained.   This is caused by the resuspension of smaller particles near the inlet line during filling. When draining commences, fewer smaller particles are near the drain line. In contrast, fewer large particles (1 mm) are resuspended during filling in the low-flow case. When draining commences, the larger shear stresses along the tank bottom enable resuspension and draining of the larger particles that were previously immobile during filling, along with smaller

particles located in regions outside the previously scoured region during filling. In the high-flow case, fewer large particles are observed to drain (Figure 18). As shown in Figure 14, Figure **15**, and Figure 17, because of the larger momentum and shear stresses of the high-flow case, more large particles are resuspended during filling and subsequently entrained or deposited to locations further from the transmission line. Thus, fewer large particles are drained in the high-flow case. In general, fewer particles were drained in the high-flow case due to more particles being entrained and redistributed during filling.
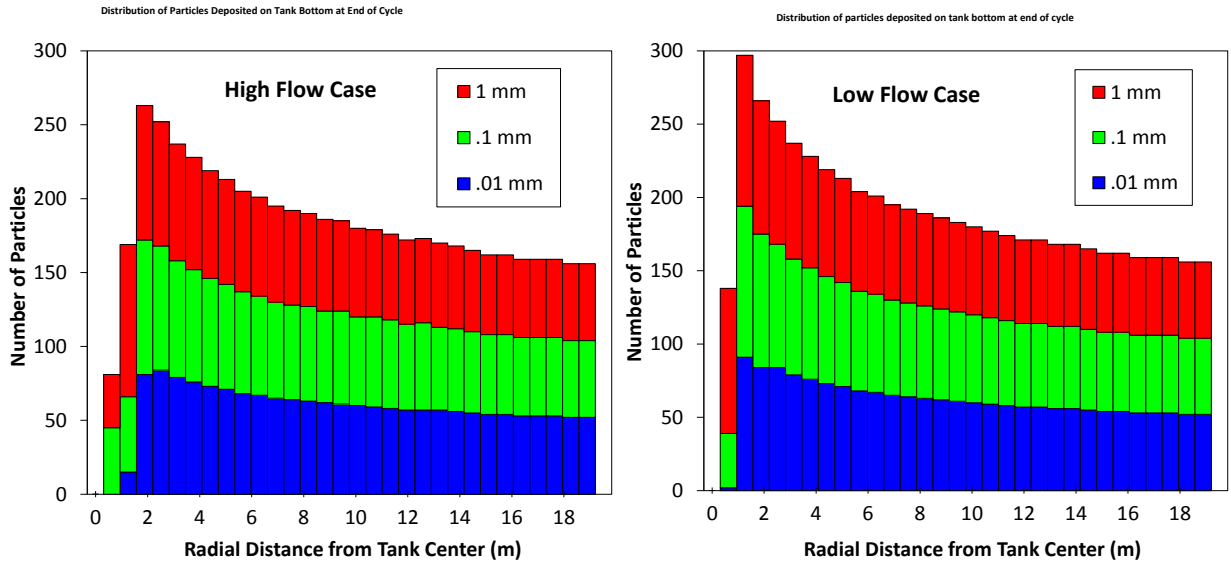
Figure 11. Distribution of particles deposited on tank bottom at end of fill/drain cycle.
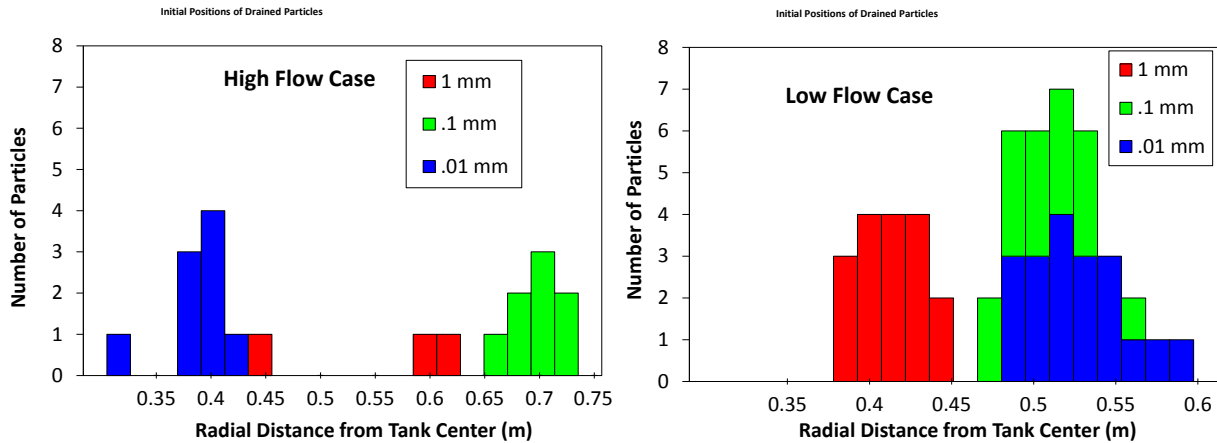
Figure 12. Initial positions of drained particles.
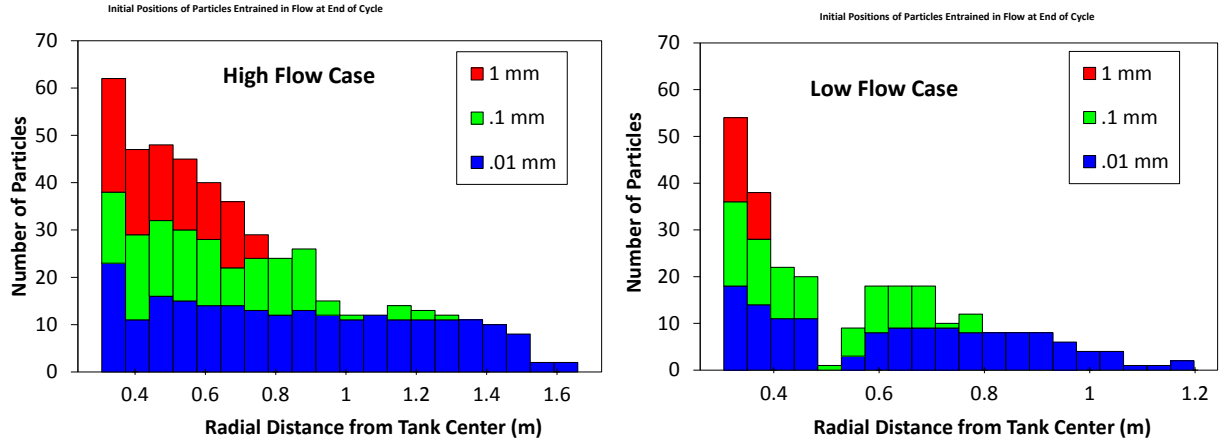
Figure 13. Initial positions of particles entrained in flow at end of cycle
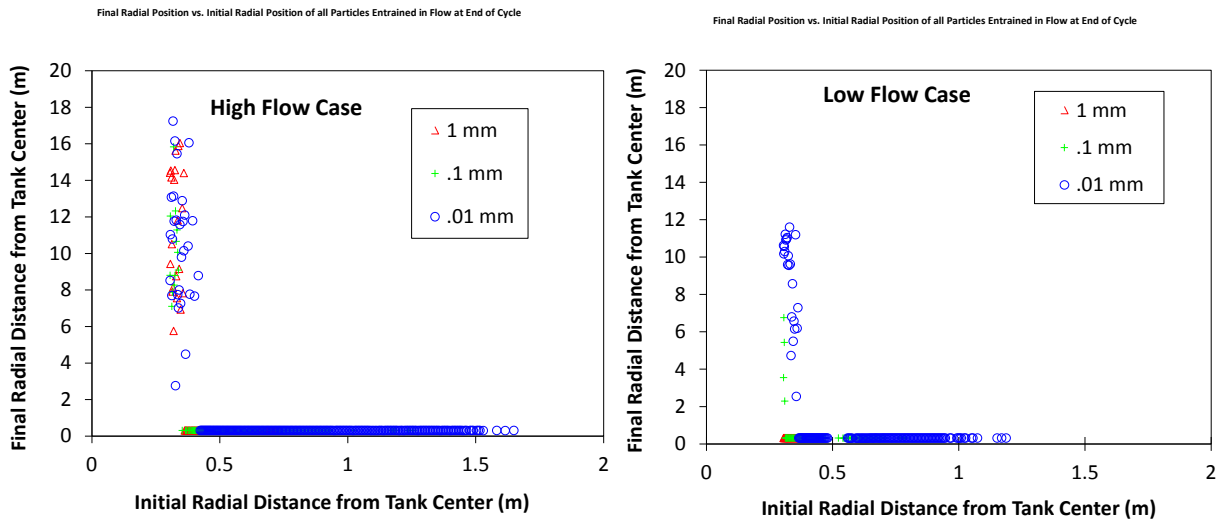
Figure 14. Final radial position vs. initial radial position of all particles entrained in flow at end of cycle.
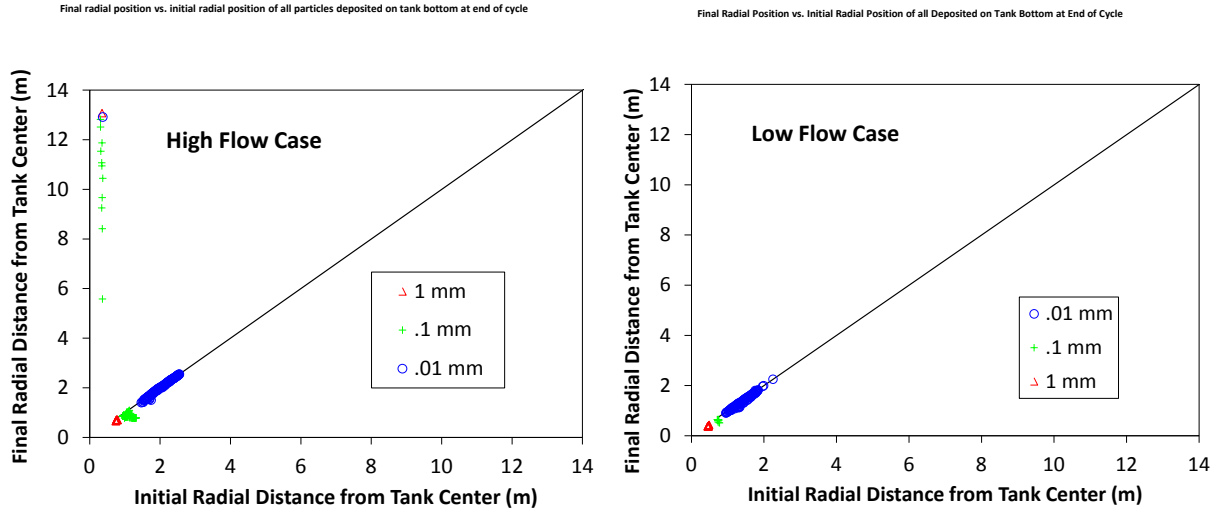
Figure 15**. Final radial position vs. initial radial position of all particles deposited on tank bottom at end of cycle. The black line represents particles that remained deposited throughout the entire cycle.**
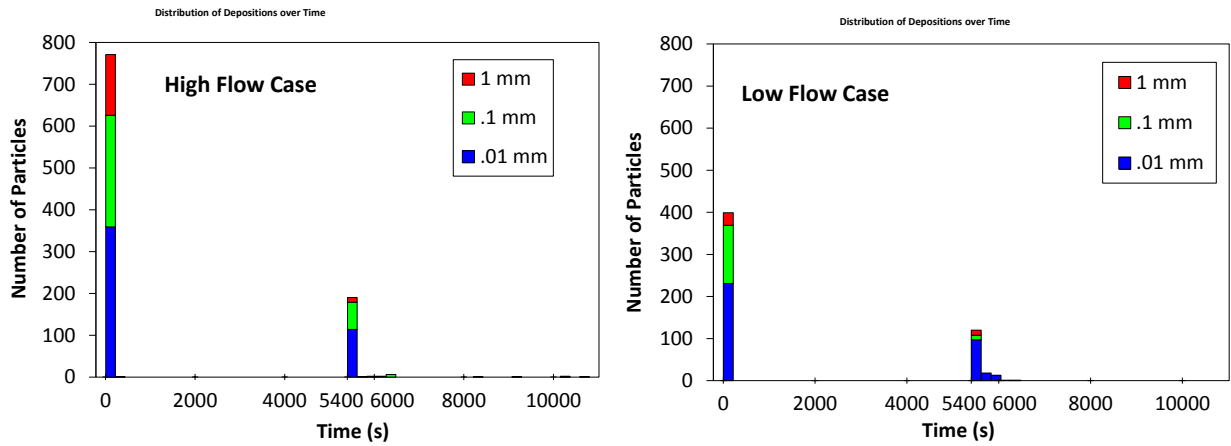
Figure 16. Distribution of depositions over time.

35
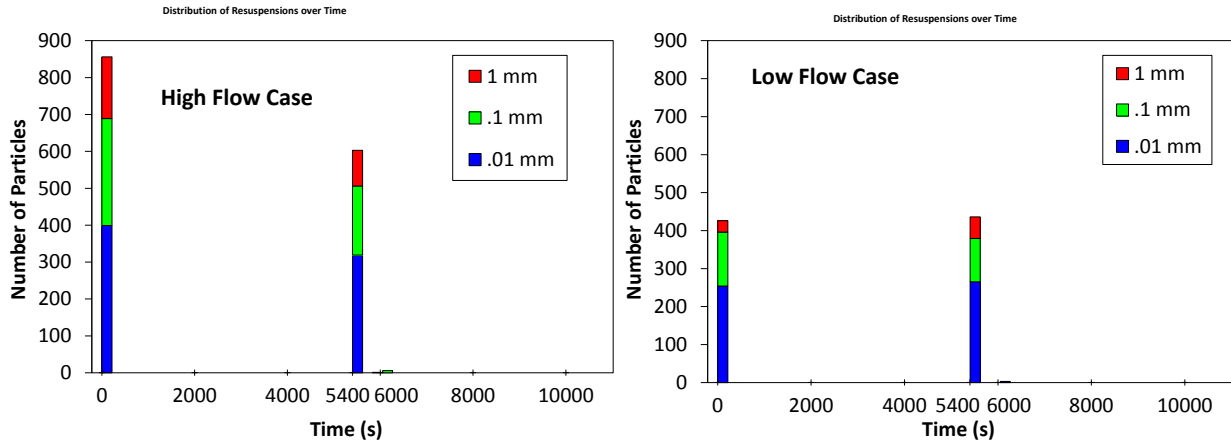
Figure 17. Distribution of particle resuspensions over time.
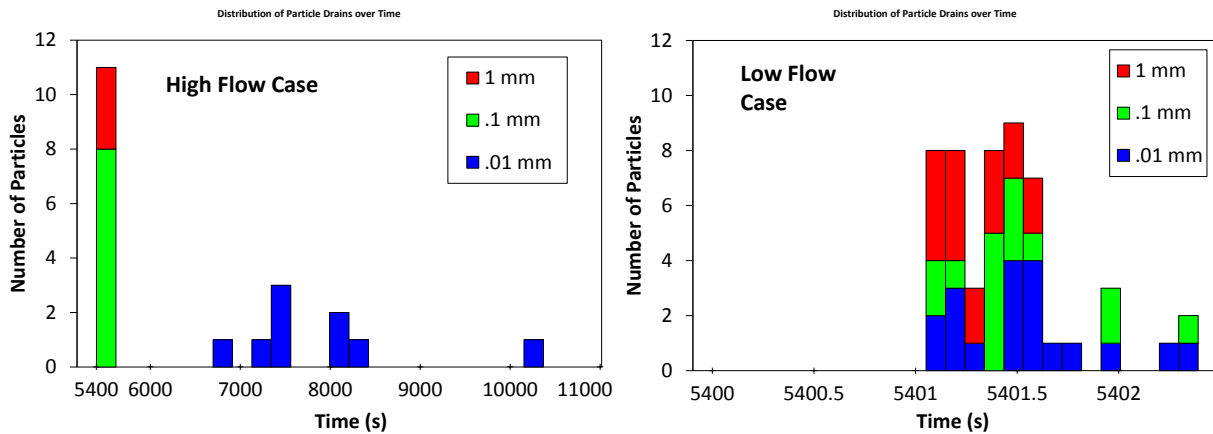
Figure 18. Distribution of particle drains over time.

2.4. Parametric Study

The purpose of the parametric study was to determine the relative importance of various parameters and processes, such as inlet/outlet location and diameter, flow rate, particle size, and filling vs. draining cycles, on the resulting shear stress and potential for particle resuspension along the bottom wall. When describing particle movement, particles are categorized as resuspended (scoured from the tank bottom and entrained in the fluid flow), drained (removed from the tank through the outlet pipe), or deposited back on the tank bottom.

2.4.1. Parametric Study Approach

The parametric study utilized a 3D half-symmetry model of a cylindrical water tank with a diameter of 126 feet and height of 32 feet (see Figure 19). A 3D half-symmetry model (as opposed to an axisymmetric model used in the operational study) was needed for the parametric study because of the inclusion of a near-wall nozzle condition. The model had an initial water height of 16 feet (half full) for all studies. The two-phase volume-of-fluid model in the Fluent® software

36

was used to simulate the two-phase water and air interactions at the water surface, and the k-ω-SST turbulence model was used to simulate turbulent flows in the tank. Approximately 670,000 model domain grid elements were used for this study. A grid-convergence study was performed to ensure that that this was a sufficiently resolved mesh. Models were evaluated with different element sizes, and each successive study refined elements around critical flow regions (regions with distinct flow characteristics such as those near the nozzle location). Performance metrics (particle velocity, nozzle velocity, flow patterns) were compared between studies to determine if results changed between different mesh sizes. A sufficient grid was determined as the smallest number of elements to produce an identical solution independent of the mesh size.

The transient modeling Courant number was kept as close to one as possible to ensure that an accurate transient solution was being achieved. The transient model was run until the maximum bottom-wall shear stresses were recorded (typically before 700 seconds of flow time), and the recorded shear stresses were used in the sediment suspension models to determine where particle resuspensions could occur in each scenario.

Figure 19. Half-symmetry tank domain used for the parametric study. The tank is 9.8 m (32 ft) high with a diameter of 38 m (126 ft) and an initial water height of 4.9 m (16 ft).

An experimental design simulation matrix was created to define the parameter combinations investigated in this study (see Table 4). Three two-level (low vs. high) factors were analyzed in the CFD simulations for both filling and draining scenarios: inlet/outlet flow rate, diameter, and location. The values chosen for each of the parameters were representative of the possible minimum and maximum values during operation of similar sized water tank in Albuquerque, NM.

Table 4. Experimental design matrix for cases simulated in the parametric study.

Filling			
Design Study	**Flow Rate (gpm) / (m³/s)**	**Inlet Line Diameter (in) / (m)**	**Line Location**
1	10,000 / 0.631	36 / 0.91	Near Side Wall
2	3,400 / 0.215	24 / 0.61	Center
3	10,000 / 0.631	24 / 0.61	Near Side Wall
4	10,000 / 0.631	36 / 0.91	Center
5	3,400 / 0.215	36 / 0.91	Center
6	3,400 / 0.215	24 / 0.61	Near Side Wall
7	3,400 / 0.215	36 / 0.91	Near Side Wall
8	10,000 / 0.631	24 / 0.61	Center
Draining			
Design Study	**Flow Rate (gpm) / (m³/s)**	**Inlet Line Diameter (in) / (m)**	**Line Location**
1	10,000 / 0.631	36 / 0.91	Center
2	10,000 / 0.631	36 / 0.91	Near Side Wall
3	500 / 0.0315	24 / 0.61	Near Side Wall
4	10,000 / 0.631	24 / 0.61	Center
5	500 / 0.0315	24 / 0.61	Center
6	500 / 0.0315	36 / 0.91	Near Side Wall
7	10,000 / 0.631	24 / 0.61	Near Side Wall
8	500 / 0.0315	36 / 0.91	Center

2.4.2. Results of Parametric Study

The simulated shear stresses on the bottom of the water tank were analyzed to determine regions that were susceptible to particle resuspension. Any shear stress (and particle size) resulting in a movability number above the critical movability number in the Beheshti model was reported as a susceptible region for particle resuspension. The results were reported as a contour plot in Figure 20 (red denotes regions susceptible to resuspension). Figure 20 shows the contours of the small inlet/outlet diameter, high flow rate, and center location for three particle sizes. The results show that smaller particles were more susceptible to resuspension for a given shear stress. Additional contour plots similar to Figure 20 for all of the cases simulated in the parametric studies can be found in Appendix E. The filling cases generally did not yield large shear stresses near the transmission line, except for the cases where the line was near the wall during high flow rates. The simulated shear stress near the transmission line was generally greater during draining, yielding a greater region of potential resuspension.
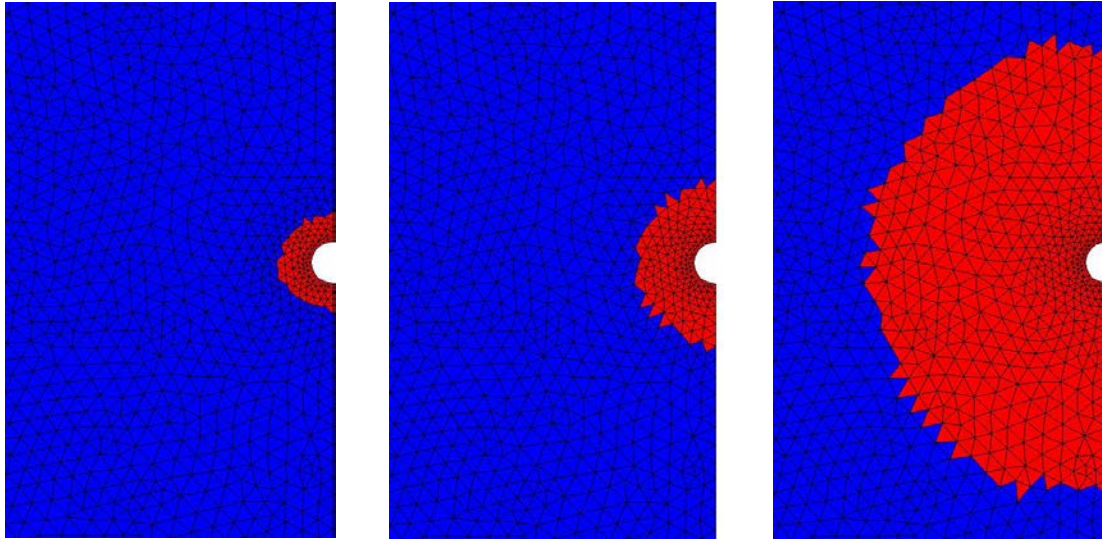
Figure 20. Plan view of the tank bottom showing area around inlet/outlet line susceptible to particle resuspension (shown in red) for the 24 inch line, center location, high flow rate case during draining for different particle diameters of 1 mm (left), 0.1 mm (center), and 0.01 mm (right).

Figure 21 and Figure 22 show the fraction of the tank bottom-wall area susceptible to resuspension as a function of flow rate, inlet/outlet diameter, inlet/outlet location, and particle size. Results of the tank filling scenario reveal that the high flow rate scenarios are most effective at inducing particle resuspension, but only when the inlet/outlet is located near the tank wall. The case with highest particle resuspension (>10%) for 0.01mm particles is the 24 inch line diameter, near wall location, and high flow rate. The other particle sizes were only affected slightly during filling. The draining scenarios were affected mostly by the high flow rate cases for all particle sizes regardless of line location. The area susceptible to particle resuspension was also sensitive to the particle size, with smaller particle sizes yielding larger areas of potential resuspension. These charts include the entire area of the bottom of the tank for each particle size. Multiple particle sizes can be resuspended in the same area of the tank. This chart does not explain the spatial locations of resuspension – only the total amount of particles resuspended.
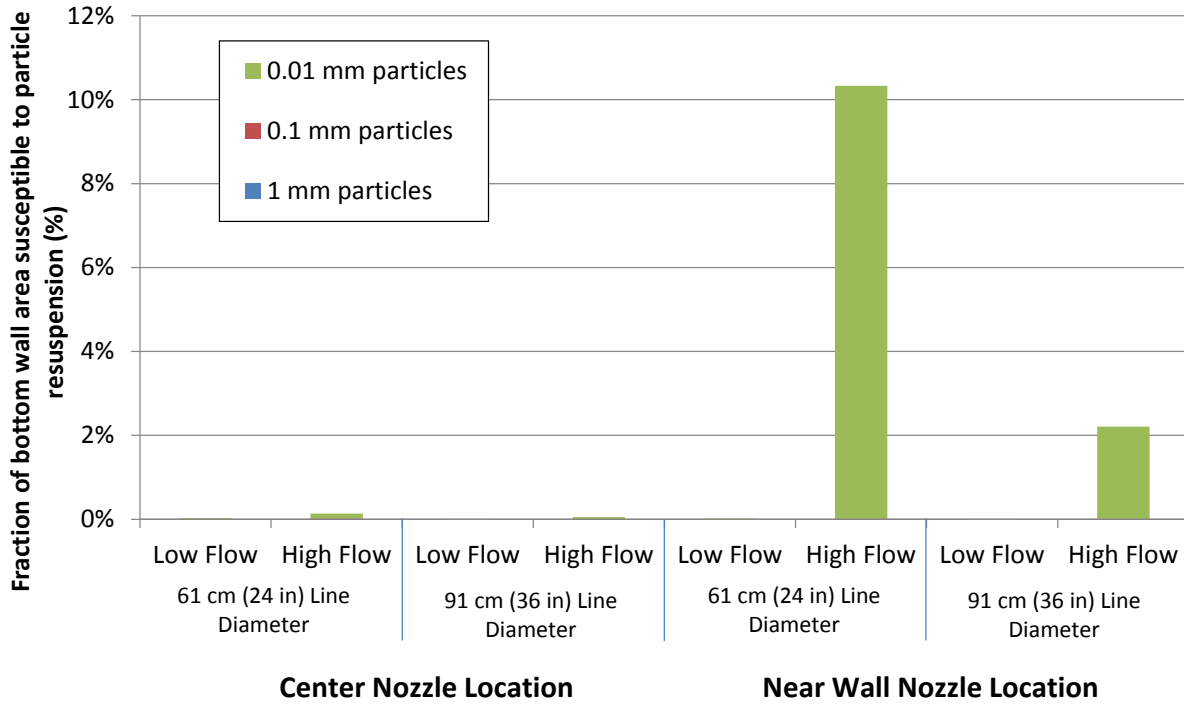
Figure 21. Fraction of bottom wall area susceptible to particle resuspension as a function of various parameters _during filling_.
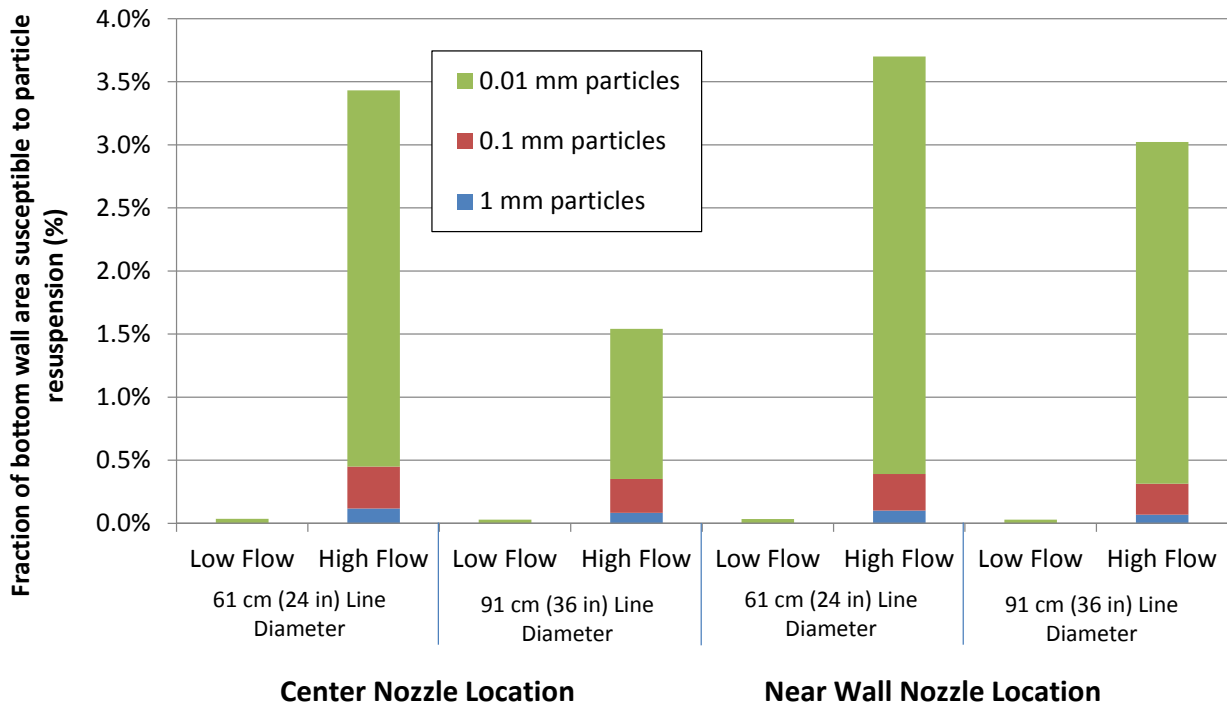
Figure 22. Fraction of bottom wall area susceptible to particle resuspension as a function of various parameters _during draining_.

40

A statistical analysis was performed on the filling and draining cases to determine the relative importance of each of the parameters on the fraction of area on the bottom of the tank that results in particle resuspension. An analysis of variance (ANOVA) was performed to evaluate the impact of input parameters (flow rate, inlet diameter, inlet location, and particle size) on the particle resuspension. The ANOVA method evaluates the mean of the dependent variable (percentage of area susceptible to particle resuspension) for all cases when a particular independent variable (e.g., flow rate, inlet diameter, inlet location, particle size) is set to its high or low value. If the means are statistically different between these two settings based on the variance of the dependent variable, the independent variable is considered statistically important. The interactions of independent variables, say A and B, can also be evaluated by evaluating the mean of the dependent variable at the high levels of both A and B.

Figure 23 shows a Pareto chart describing the relative importance of the input parameters on the filling and draining cases.[1] Particle size, flow rate, and the interaction between particle size and flow rate were found to be significant factors during both the filling and draining scenarios. The inlet diameter, inlet location, and interactions among those parameters were not found to be statistically significant in impacting the amount of particles resuspended.
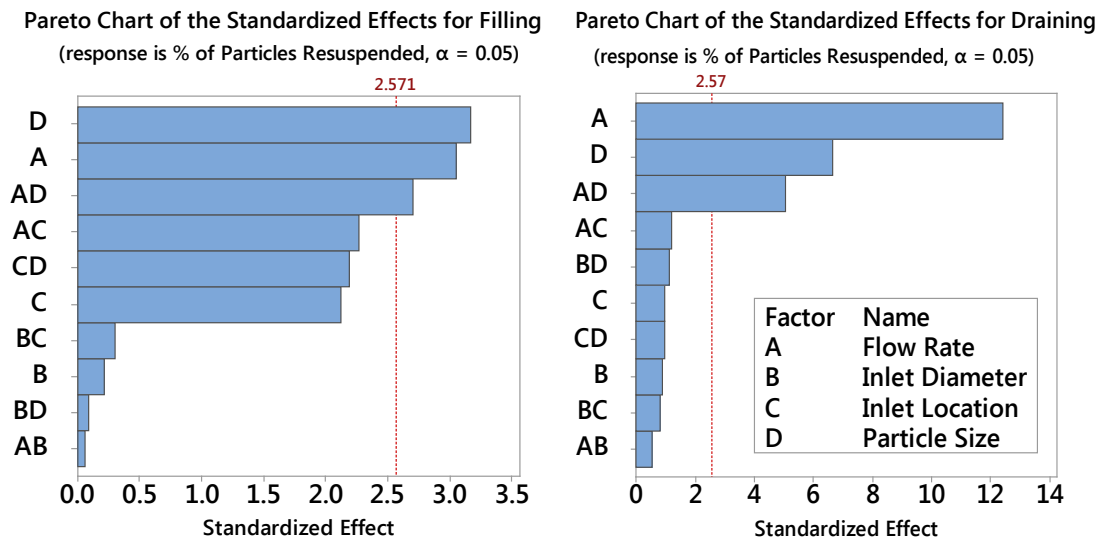
Figure 23. Pareto charts of the standardized effects showing the relative importance of each factor (and interactions) on particle resuspension during filling (left) and draining (right).

Figure 24 – Figure 27 show the fraction of bottom wall area susceptible to particle resuspension as a function of momentum flow (jet effect) through the transmission line for different particles

---

[1] The standardized effect of the independent parameters (A=Flow Rate, B=Inlet Diameter, C=Inlet Location, D=Particle Size) is the absolute value of the t-statistic, which is equal to the coefficient (b1, b2, b3, b4) divided by the standard error of the coefficient in the linear regression model: $y = b0 + b1*A + b2*B + b3*C + b4*D + b5*AB + b6*AC + b7*AD + b8*BC + b9*BD + b10*CD$. The value of the threshold for the standardized effect to determine significance corresponds to the cutoff in the t-distribution for an α of 0.05, where t is the $(1 - \alpha / 2)$ quantile of a t-distribution with degrees of freedom equal to the degrees of freedom for the error term.

sizes, line location, and filling vs. draining. The momentum flow (measured in Newtons, N) is defined as the product of the mass flow rate and the momentum per unit mass:

$$\text{Momentum Flow (N)} = \dot{m}v = \rho_w v^2 A = \frac{4\rho_w}{\pi}\left(\frac{Q}{d_{inlet}}\right)^2$$

where ρ_w is the water density (1,000 kg/m^3), Q is the flow rate of the water through the transmission line (m^3/s), and d_{inlet} is the diameter of the transmission line (m). Results show that particle resuspension is directly correlated with momentum flow through the transmission line. Smaller particles are more susceptible to resuspension in all cases, and, during filling, the near-wall inlet/outlet yielded greater particle resuspension than the center inlet/outlet. During draining, both the near-wall and center inlet/outlet scenarios yielded similar particle resuspension trends, with significantly greater particle resuspension occurring for the smallest (0.01 mm) particles. These results indicate that reducing the momentum flow, or jet effect, through the orifice of the inlet/outlet can reduce the potential for particle resuspension. The momentum flow can be lowered by reducing the flow rate or increasing the inlet/outlet diameter. Particle resuspension may also be reduced during filling by placing the inlet/outlet near the center of the tank rather than near the side wall.
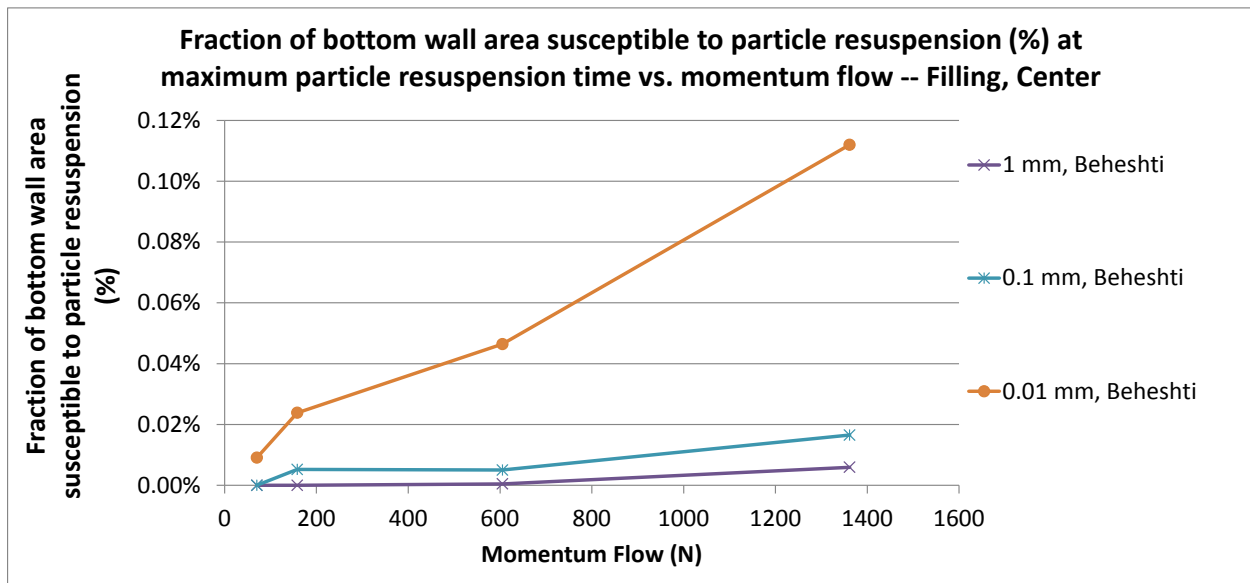
Figure 24. Fraction of wall area susceptible to particle resuspension vs. momentum flux for filling at the center line location for three particle diameters.
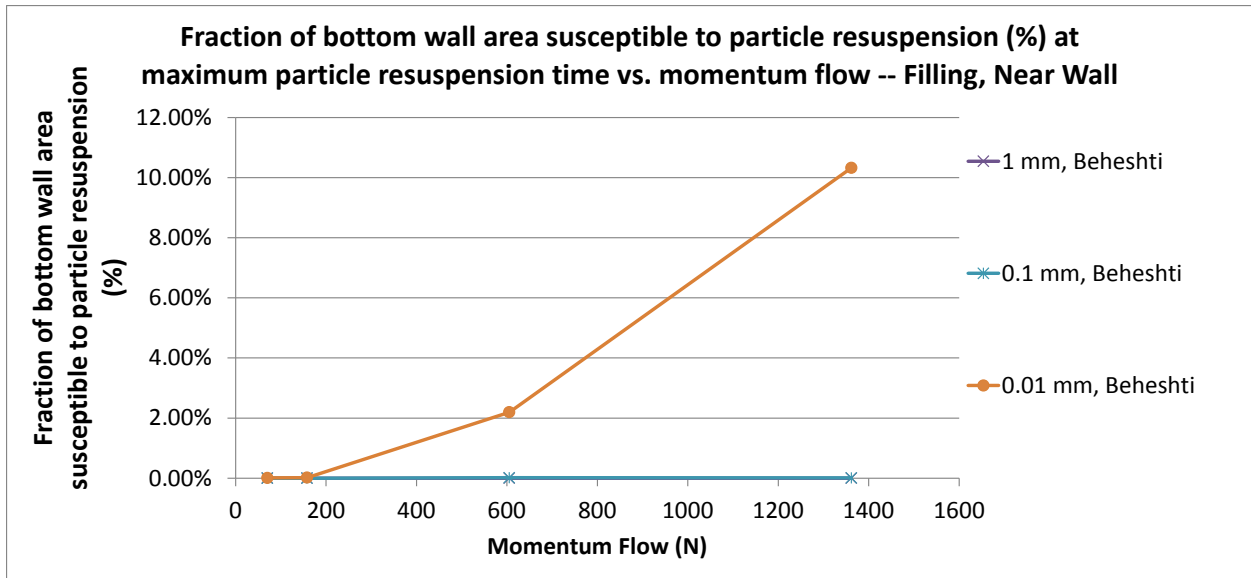
Figure 25. Fraction of wall area susceptible to particle resuspension vs. momentum flux for filling at the near wall line location for three particle diameters.
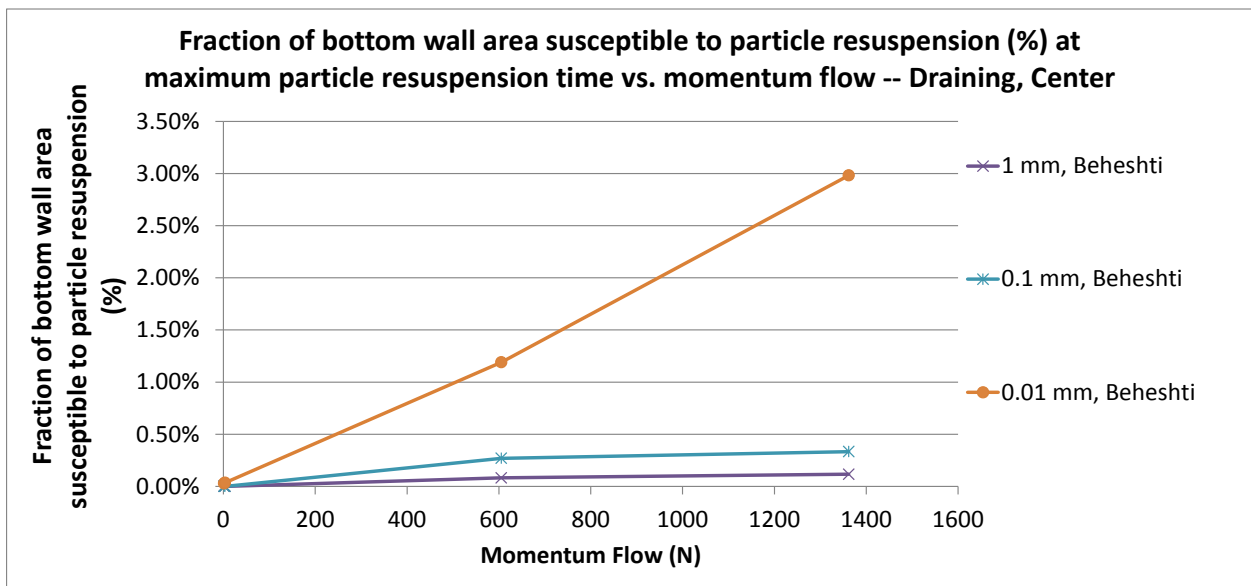
Figure 26. Fraction of wall area susceptible to particle resuspension vs. momentum flux for draining at the center line location for three particle diameters.
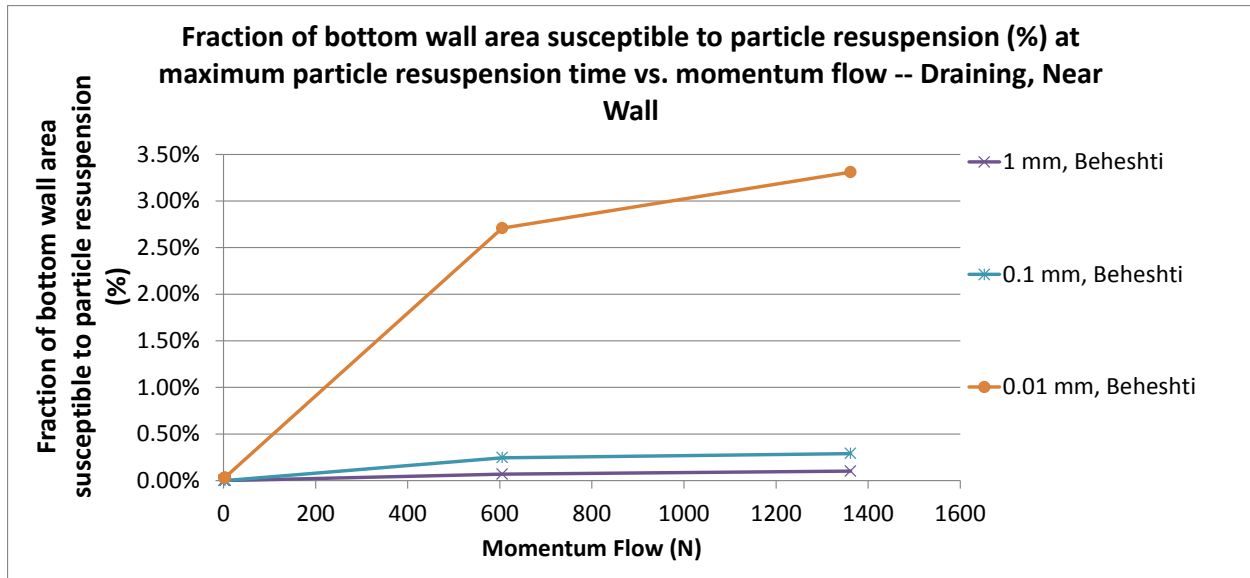
Figure 27. Fraction of wall area susceptible to particle resuspension vs. momentum flux for draining at the near wall line location for three particle diameters.

2.5. Mitigation Measures

In order to mitigate the potential for particle resuspension and drainage near the inlet/outlet, the use of a raised inlet was evaluated in this modeling study. Raised inlet/outlet lines, sometimes called silt rings, have been used in the construction of commercial water storage tanks. Figure 28 shows an example of a 3 ft (0.91 m) diameter silt ring installed by Bohannan Huston Inc. civil engineering firm (Albuquerque, NM) in a 3 million gallon (11,000 m^3) water storage tank in Albuqeurque, NM (tank walk-through courtesy of Todd Burt, VP Water Systems, Bohannan Huston). The silt ring extends about one foot (0.3 m) above the tank floor. The hypothesis is that the raised inlet/outline line would reduce the shear stresses near the inlet/outlet and reduce the potential for particle resuspension and drainage.

Figure 28. Raised inlet/outlet line (silt ring) installed by Bohannan Huston in an 11,000 m^3 (3 million gallon) water tank installed in Albuquerque, NM. The cover on top of the ring would be removed during normal operation. The small hole on the side allows for complete tank drainage.

44

For this study, a raised inlet configuration was added to the 2D axisymmetric tank model used in the operational study to analyze its effects on particle resuspension. Extension height was varied, while wall thickness was kept constant at 1 inch (2.54 cm) since it did not significantly affect resuspension. The various cases are outlined in Table **5**. As previously, in each case, 2,000 particles of each of three different particle sizes (0.01, 0.1, and 1 mm) were included in the simulations. The UDFs employed in the operational study were used in these simulations.

Table 5**. Raised inlet line cases run in the Fluent® software. In all cases, the flow duration was 200 seconds and the inlet/outlet line velocity was 2.162 m/s, yielding a flow rate of 0.631 m³/s (10,000 gpm).**

Filling/Draining	Extension Height Above Bottom Wall
Filling	0.61 m (24 in)
Filling	0.30 m (12 in)
Filling	0.15 m (6 in)
Filling	0
Draining	0.61 m (24 in)
Draining	0.30 m (12 in)
Draining	0.15 m (6 in)
Draining	0.61 m (24 in)

Filling and draining pathlines near a 0.30 m (12-inch) high raised inlet are displayed in Figure 29 and Figure 30, respectively. The raised inlet line forces the pathlines to make wide turns a moderate distance away from the line, producing lower wall shear stresses adjacent to the line (Figure 31 and Figure 32). As a result, many resuspended particles were transported along the bottom wall and were deposited immediately outside the raised inlet. Figure 33 illustrates that in the filling cases, a line height of at least 0.15 m (6 inches) above the bottom wall prevented all of the 0.1 mm and 1 mm particles from being suspended in the flow at the end of the run. A line height of 0.61 m (24 in) also prevented the 0.01 mm particles from being suspended. In the draining cases, increasing the extension line height to 0.61 m (24 in) prevented the 0.1 and 1 mm particles from being drained, but the smallest 0.01 mm particles continued to be susceptible to suspension and subsequent drainage (Figure 34). In general, increasing the raised inlet line height above the base of the tank appears to reduce the likelihood of suspending and draining particles, especially if they are ~0.1 mm or larger.
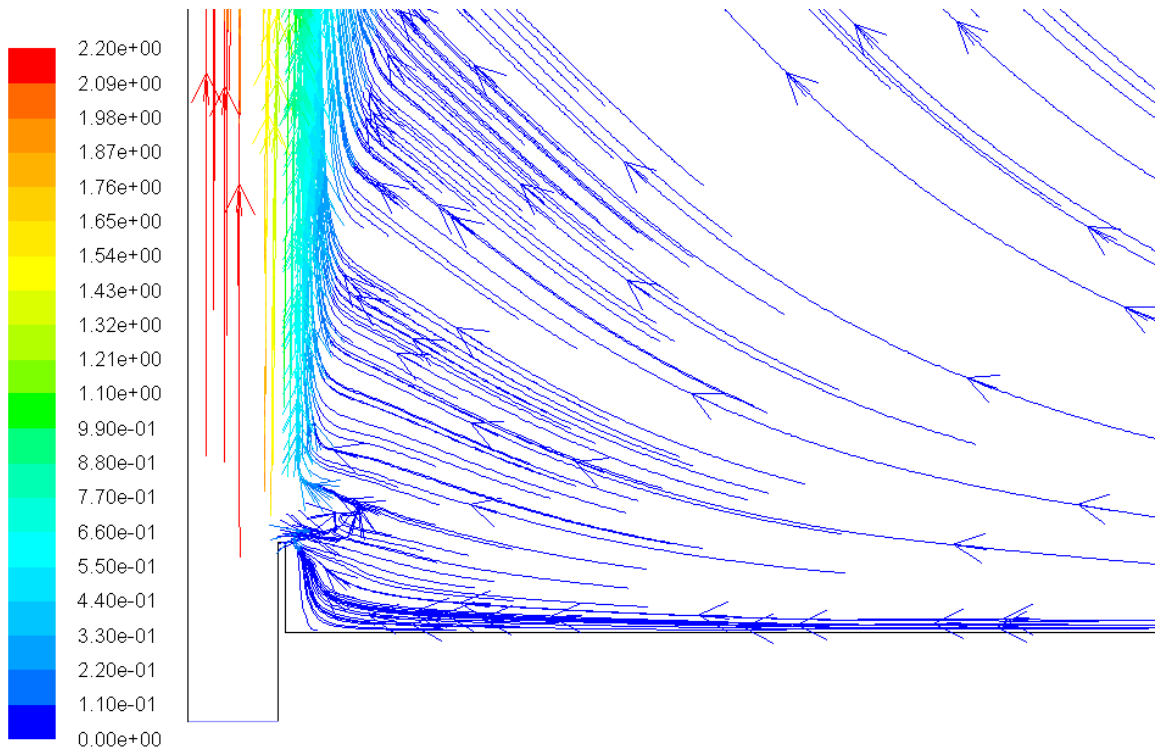
Figure 29. Filling at 200 seconds – pathlines colored by velocity magnitude
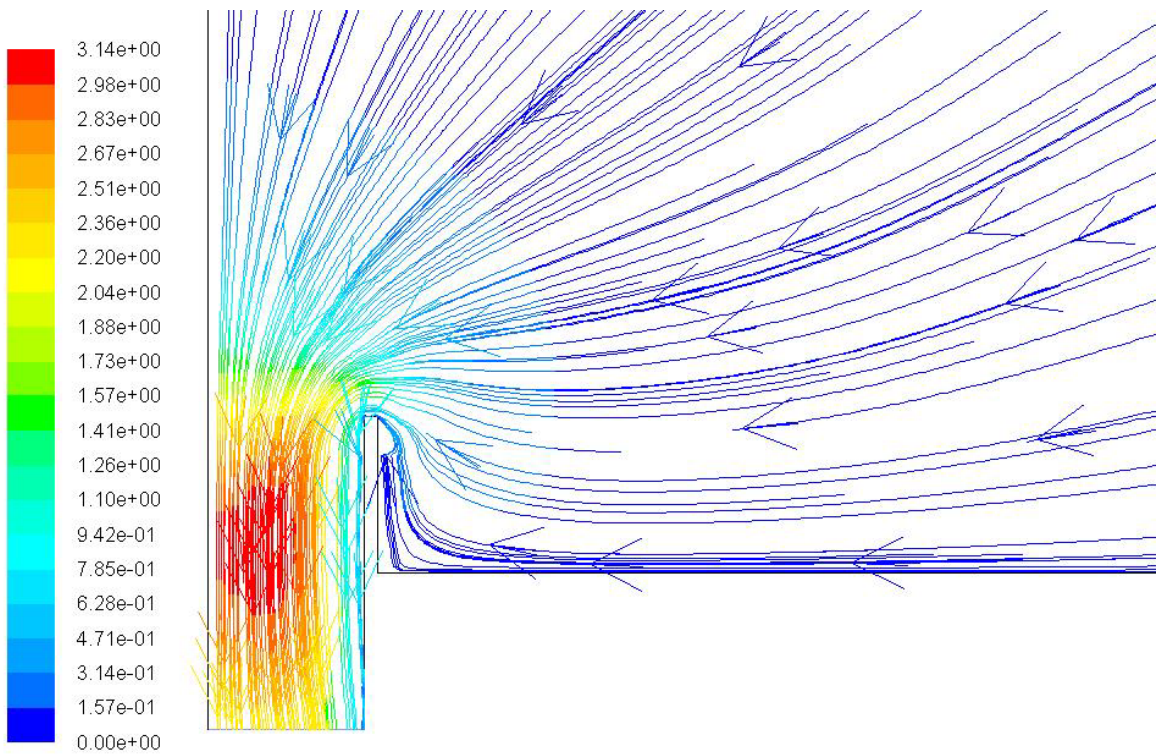
Figure 30. Draining at 200 seconds – pathlines colored by velocity magnitude

46
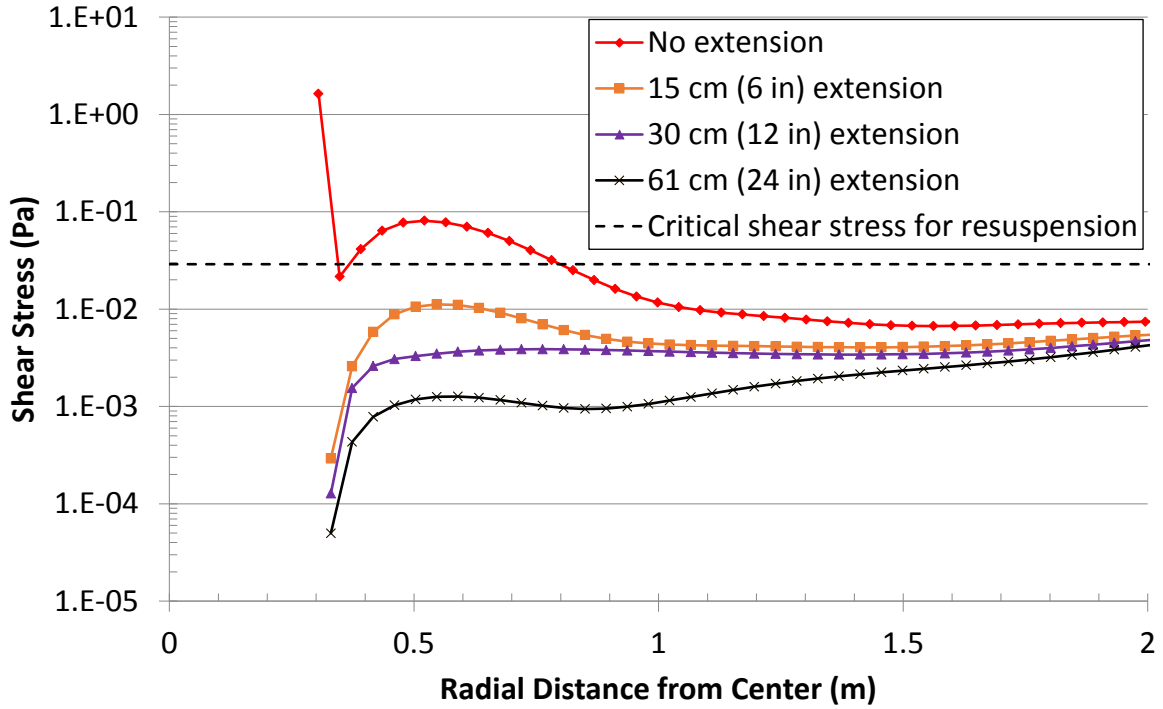
Figure 31. Filling at 200 seconds – variation of bottom wall shear stress with radial distance from inlet line
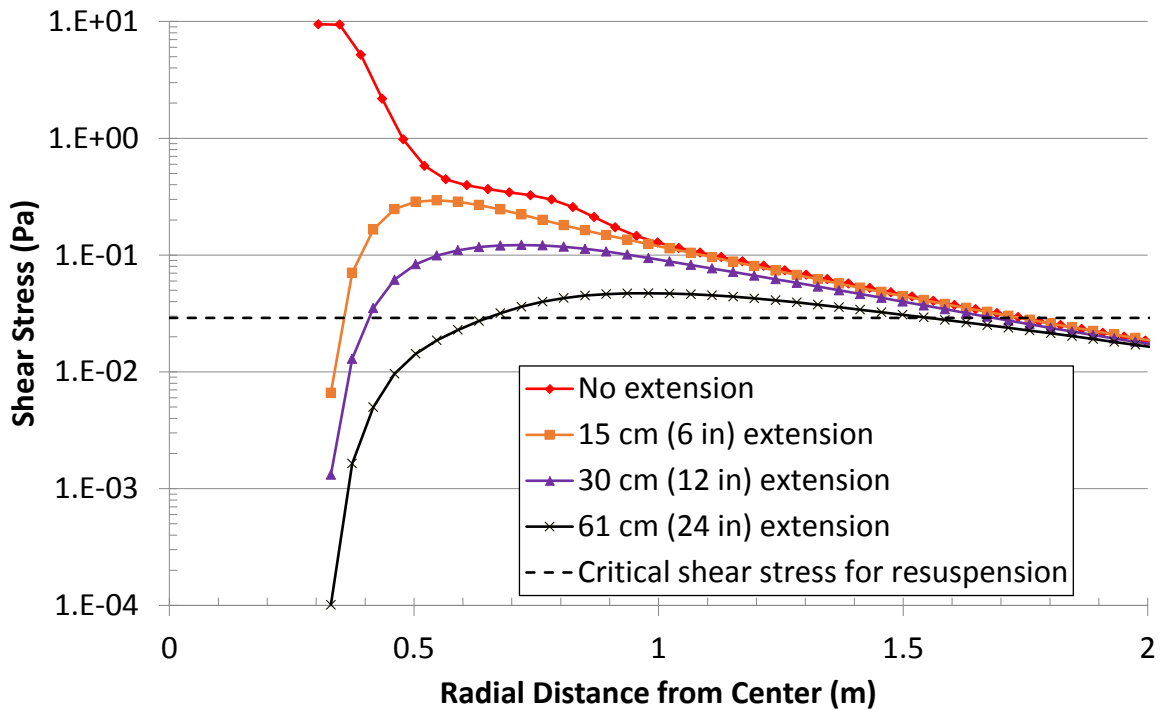
Figure 32. Draining at 200 seconds – variation of bottom wall shear stress with radial distance from inlet line
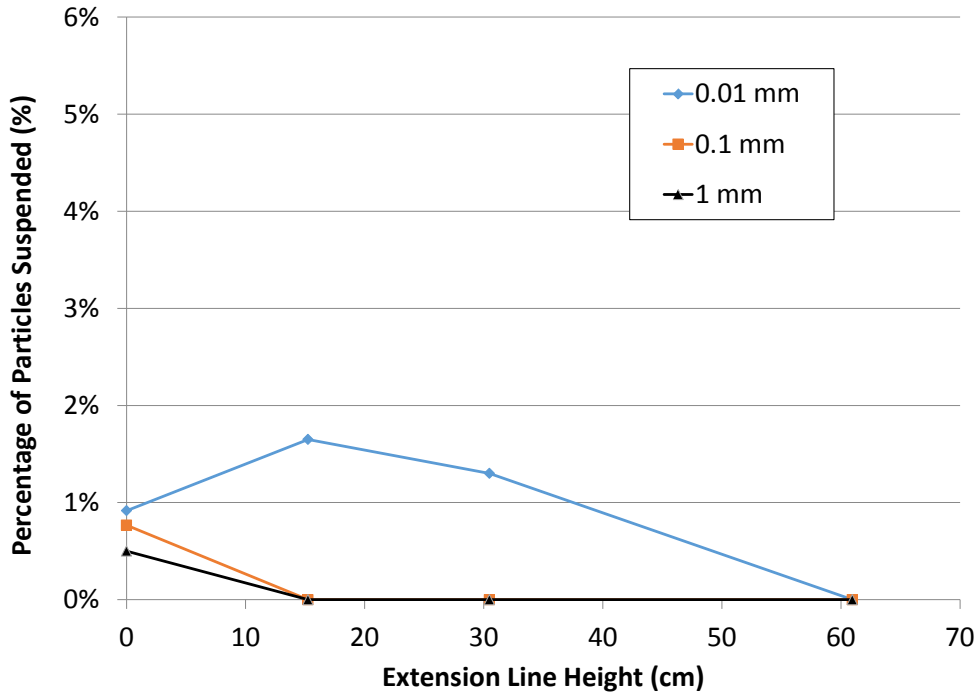
Figure 33. Percentage of resuspended particles as a function of raised inlet line height after 200 seconds of filling.
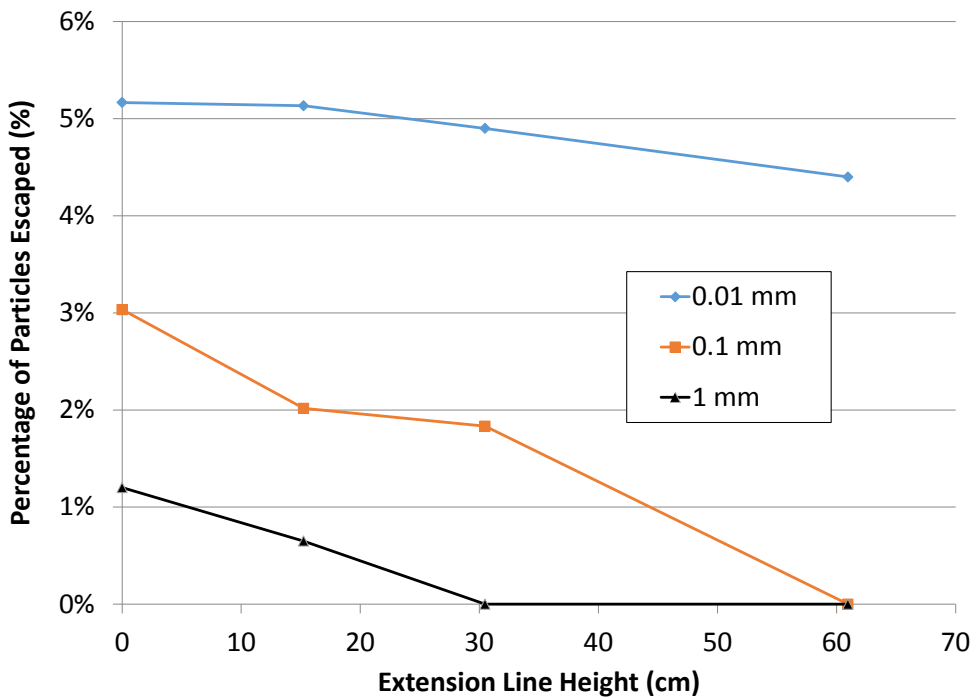
Figure 34. Percentage of particles drained as a function of raised inlet line height after 200 seconds of draining.

3. Experimental Testing

Small-scale physical tests were performed to investigate particle resuspension during filling and draining in a 1.2 m (4 ft) diameter water-filled plastic tank with a 0.02 m (0.8) diameter inlet located in the center of the tank (see Figure 35). Two different particles (silica sand and glass beads) with different densities were used in separate tests. During filling, different pumping flow rates were investigated, but during draining, only gravity-induced draining was examined. Initially for each test, the particles were distributed uniformly around the inlet line. Photos and videos were recorded before and after each filling and draining event to determine where particles were resuspended from the tank bottom. Tracer tests were also performed to characterize the flow patterns and velocity fields. Finally, mitigation measures were investigated by raising the pipe inlet, which was normally flush with the tank bottom, a short distance above the tank bottom. In addition, a simulation study was conducted to compare CFD model predictions with the physical test results.
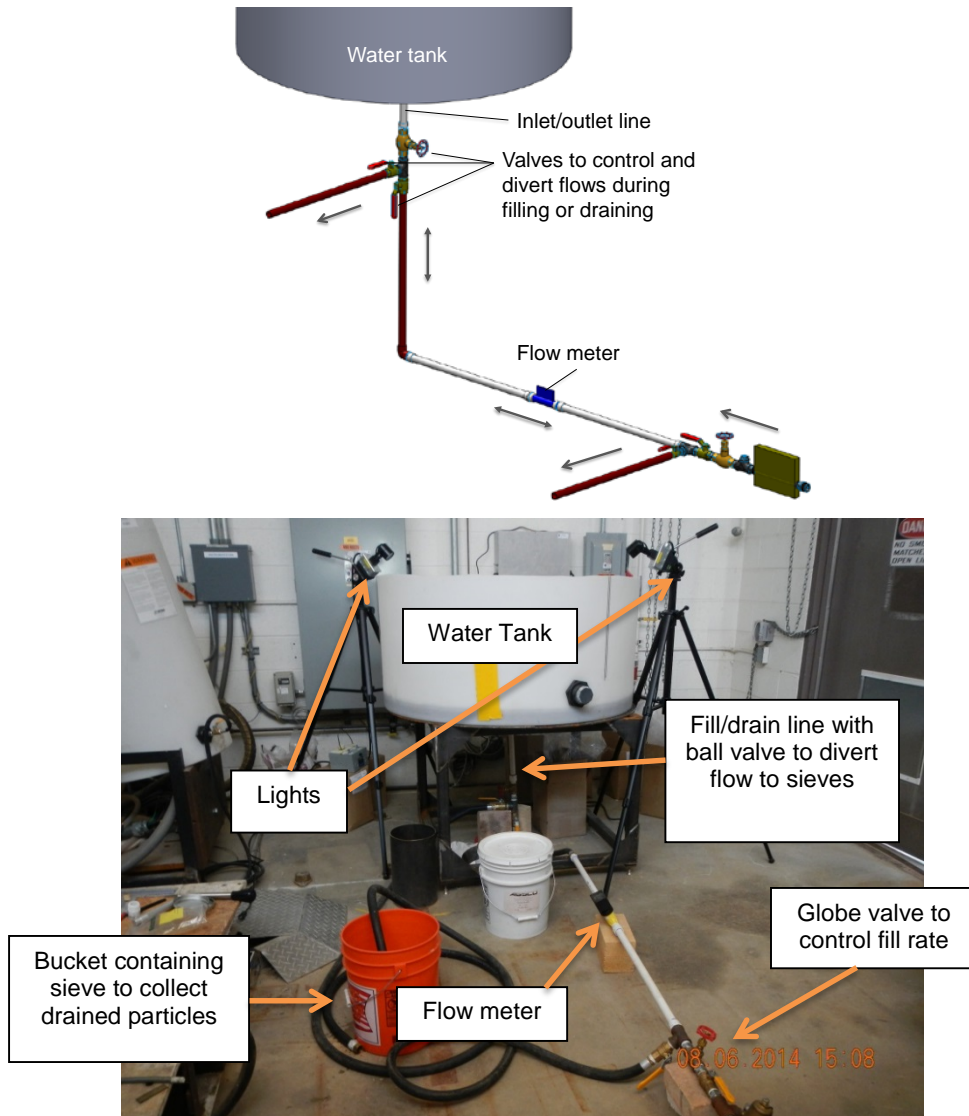
Figure 35. Schematic (top) and photograph (bottom) of test apparatus.

3.1. Physical Test Description

Figure 35 shows the general configuration of the test apparatus. A globe valve was used to control the flow rate during filling, and a flow meter used to measure the flow rate during both filling and draining. Beneath the water tank are two ball valves, which were used to divert water either up into the tank during filling, or out of the tank and to the drain during draining. The orange bucket contained a sieve which would capture particles during draining; the bucket also had a hole in the bottom, allowing water to drain out. The lights were used to illuminate the particles before and after a test in order to take pictures of the initial and final distribution of particles, respectively. A view of the bottom of the water tank is shown in Figure 36.

Figure 36. Top view of the bottom of the experimental tank. The inlet/drain line can be seen in the middle, surrounded by concentric circles. The circles were drawn 1 cm apart from each other for spatial reference during the particle resuspension tests.

In order to test particle resuspension, three scenarios were identified: draining, filling, and a series of filling and draining cycles (the draining scenarios only considered gravity drainage).   For a draining test, the tank was initially filled to a head of 0.3 m (12 inches), which was representative of a full tank assuming a height/diameter aspect ratio of 1:4. Next, a monolayer of particles was evenly distributed around the drain. To obtain the monolayer of particles, a prescribed mass of particles was initially measured to theoretically cover a given area around the drain based on the particle mass per unit area. This calculation was conducted as follows:

To find mass per area:

$$\frac{mass}{area} = \rho_{bulk} \times D_{nominal} \tag{9}$$

where ρ_{bulk} is the particle bulk density (2650 kg/m^3 x 0.6 = 1590 kg/m^3, assuming a porosity of 0.4) and $D_{nominal}$ is the nominal diameter of the particle (m).

To obtain the desired area:

$$area = A = \pi R_{extent}^2 - \pi r_{drain}^2 \tag{10}$$

where R_{extent} is the radial extent of the particle emplacement and r_{drain} is the radius of the drain line. The desired radial extent was determined from preliminary tests. Finally, the necessary mass of particles can be obtained as follows:

$$mass = \frac{mass}{area} \times A \qquad (11)$$

The calculated mass of particles was then weighed and evenly distributed as a monolayer in the water-filled tank around the drain using a cylindrical shell. Figure 37 shows the steel cylinder and aluminum plug used to restrict the particles only to the desired area surrounding the drain. The steel cylinder had a radius of about 10 centimeters, which covered a sufficiently large region around the drain for the particle resuspension tests. After particle emplacement, the cylinder and aluminum plug were removed (the particles remained stationary during this process).

Figure 37. Cylinder used to restrict particles during particle emplacement.

Figure 38 shows the position of the valves required for each test. During a draining test, the lower ball valve was closed and the upper ball valve was open, diverting the draining water towards the sieve contained within the drain bucket.

Open during draining,
closed during filling.

Open during filling,
closed during draining.

07.08.2014 14:12
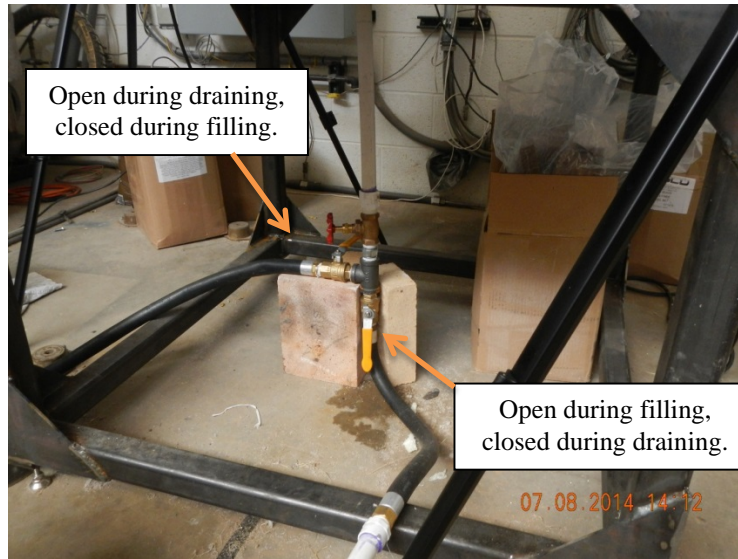
Figure 38. Valves used to control filling and draining.

During draining, drained particles were collected in a set of sieves for particle-size and mass analysis (Figure 39). Once the test had run to completion (when the water level reached six inches (15 cm), or half the initial water height), the scoured region was measured radially from the drain, at five to eight different locations. The drained particles were dried, distributed by diameter with a sieve shaker, and weighed (Figure 40 and Figure 41).

07.08.2014 14:40

Figure 39. Drained particles collected in sieve.

Figure 40. Dried particles were sorted by size using a sieve shaker (Dual H-4325).

Figure 41. Dried particles from sieve were poured into containers (left) and weighed using a Scientech ZSA 210 scale (right).

For the water-filling tests, the water tank was initially filled to a head of 0.15 m (6 inches), and a monolayer of particles was distributed around the drain, as discussed before. The fill rate was measured with the flow meter shown in Figure 42. The flow meter was a Blue-White Industries F-1000 flow meter. Two flow rates were selected to use during fill tests, a low fill rate and a high fill rate. The low fill rate was around 1.89×10^{-4} m^3/s (about three gallons per minute) and the high flow rate was 3.79×10^{-4} m^3/s (about six gallons per minute).

Figure 42. Flow meter used to measure fill rate during filling.

The tank was then filled to a head of nine inches. A final head of 0.225 m (9 inches) was sufficient to observe the particle resuspension behavior during the filling test. Once a filling test had run to completion, the scoured radial extent of the tank bottom was measured at five to eight radial locations around the drain.

For a fill-drain-fill-drain test, the tank was initially filled to a head of 22.5 m (9 inches) and a monolayer of particles was evenly distributed around the drain. The tank was then filled to 30 cm (12 inches), drained to 22.5 cm, filled to 30 cm again, and finally drained to 22.5 cm. The range from 22.5 to 30 cm (9 to 12 inches) was selected in order to keep the test time short, but still provide maximum shear stresses and velocities during draining. Once the test had been run to completion, the drained particles were dried, distributed by diameter with the sieve shaker, and weighed. The radial extent of resuspension from the drain was also measured at five to eight radial locations around the drain.

Tracer tests were also performed for both filling and draining scenarios prior to the particle resuspension tests to evaluate the flow fields and fluid velocities near the tank bottom. Blue dye (food coloring) was injected using a commercial baster at various positions along the bottom of the tank (Figure 43). For draining tests, the dye was video recorded to obtain fluid velocities near the bottom of the tank. Windows Movie Maker was used to analyze the velocity of the tracer as it moved past the concentric rings spaced 1 cm apart. The time in Movie Maker is reported in milliseconds, allowing for a precision within 0.03 seconds.

Figure 43. Tracer testing during draining. Note: Each ring is one centimeter apart.

Tracer tests were also performed to evaluate the velocity near the inlet during filling. Results showed that flow along the bottom wall within 1 – 2 millimeters from the edge of the drain exhibited high velocities, but were low elsewhere along the bottom wall. Figure 44 shows an example of a tracer test performed during filling, which revealed velocity distributions around the inlet. In Figure 44, blue dye resting on the bottom moved very little as compared to the dye that had entered the region directly above the drain. The fluid velocities outside the region within one or two millimeters of the drain were very small, as compared to the fluid velocity directly next to and above the drain. Resuspension tests conducted later confirmed this behavior.
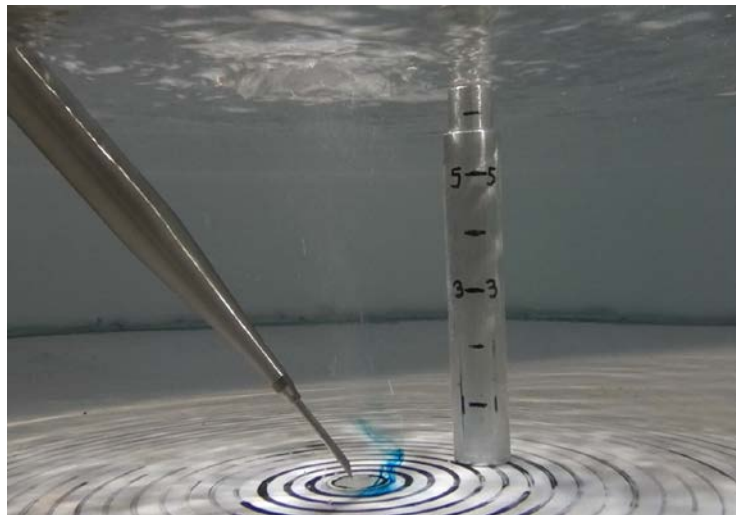
Figure 44. Example of tracer testing during filling. Numbers on the vertical plug are in inches.

3.2. Test Results

3.2.1. *Tracer Tests*

Figure 45 shows the velocities measured along the tank bottom during draining with an initial water head of 0.3 m (12 inches). The velocities were measured during the tracer tests described in Section 3.1. Figure 45 shows that far away from the drain, fluid velocities were very low (<0.01 m/s). However, within about three centimeters from the center of the drain, fluid velocity increases exponentially to greater than 0.1 m/s.

Solidworks^{TM} Flow Simulation software and ANSYS® Fluent® CFD^{TM} software were used to simulate fluid velocities at varying radial distances from the drain. Results of simulated velocities 5 mm above the tank bottom using the Fluent® software and Solidworks^{TM} software are also shown in Figure 45. The Fluent® model used a two-phase volume-of-fluid model described in Section 2.1. The Solidworks^{TM} model assumed a single-phase system with a constant fluid pressure boundary condition at the top of the domain (no air-water interface as in the Fluent® model). The results show that for draining conditions, both models match the data well within approximately 0.05 m from the drain. Thus, during draining, modeling flow and particle resuspension near the drain with a single-phase constant-head model may be adequate at discrete points in time. For filling, the two-phase model is necessary to accurately capture the changing water level at the air-water interface and the resulting recirculating flow patterns.
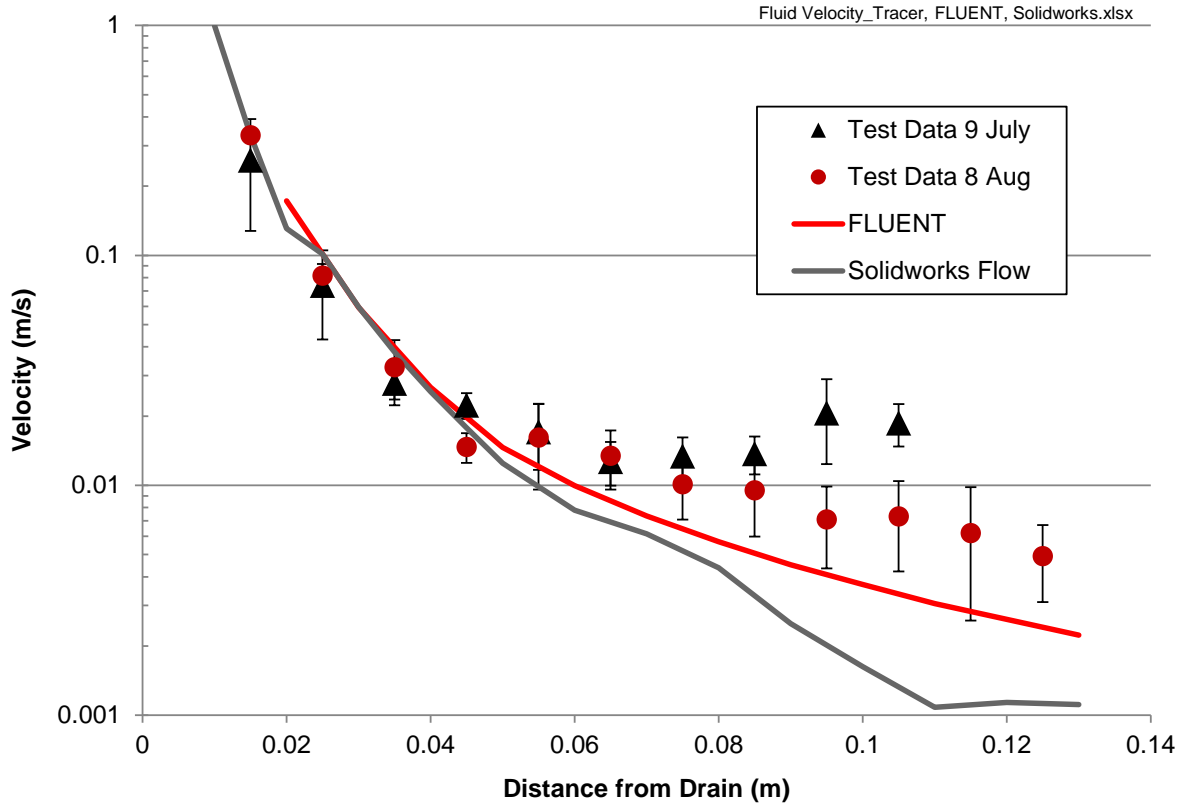
Figure 45. Measured and simulated velocity along the tank bottom during draining as a function of radial distance from the center of the drain. Error bars represent plus/minus one standard deviation.

For comparison with the experimental results, a 0.3 to 0.15 m (12 to 6 inch) drainage simulation was run with 3D reflection symmetry in the Fluent® software. To account for the continuous decrease in the drain rate in the experimental tests, the velocity boundary condition at the outlet was modified at every 0.0254 m (1 inch) change in the water level. The flow velocity in the Fluent® simulation was linearly interpolated between the measured drain rate at the equivalent water level and the measured drain rate after a 0.0254 m (1 inch) decrease in the equivalent water level. The flow parameters are outlined in Table 6.

Table 6. Flow parameters for simulation draining from 0.3 to 0.15 m (12 to 6 inches)

Water Height (m - in)	Measured Drain Velocity (m/s)	Drain Velocity Input in Fluent® (m/s)	Flow Time (s)
0.3 m (12 in)	0.804	0.7977	0.000
0.28 m (11 in)	0.791	0.7860	108.046
0.25 m (10 in)	0.781	0.7757	217.699
0.23 m (9 in)	0.771	0.7636	328.811
0.2 m (8 in)	0.756	0.7510	441.690
0.18 m (7 in)	0.745	0.7413	556.464
0.15 m (6 in)	0.737	n/a	672.729

3.2.2. Particle Resuspension Tests

During particle resuspension tests, all three scenarios described in Section 3.1 were conducted: (1) draining, (2) filling, (3) fill-drain-fill-drain. For draining and fill-drain-fill-drain tests, the mass drained and radial extents of resuspension were the two measured quantities. For filling, the radial extent of resuspension was the only measured and recorded quantity. Table 7 - Table 9 summarize the results of the particle resuspension testing. After each test, the mass of particles drained was recorded using the methods described in Section 3.1. The radial extent of resuspension was determined by measuring the radial distance of the scoured region around the drain. Several radial measurements were taken and then averaged. In between tests, the tank was drained and any remaining particles on the bottom of the tank were wiped toward the drain for removal before filling the tank again with water.

The draining tests for the silica sand were consistent with the modeling studies that predicted smaller particles were more likely to be resuspended as compared to larger particles of the same density. As shown in Table 7, small silica sand particles (on the order of 0.05 to 0.1 mm diameter) experienced more resuspension than the 0.853 to 1.68 mm silica sand as evidenced by a greater mass fraction collected during draining and a larger scoured region around the drain.

Table 7. Draining test results.*

Particle Type	Particle Density (kg/m³)	Particle Diameter (mm)	Number of Tests Run	Particles Collected During Draining (% by mass)	Average Radial Extent of Resuspension from Drain Edge (cm)**
Silica Sand	2650	0.053 – 0.104	5	4.17 ± 2.46	1.28 ± 0.06
Silica Sand	2650	0.853 – 1.68	3	2.79 ± 0.08	0.92 ± 0.07
Glass Beads	2450	1	1	4.20	1.51 ± 0.25
Glass Beads	2450	2	1	2.72	1.74 ± 0.26

* Uncertainty in measurements represented by plus/minus one standard deviation
** 5 -8 radial measurements per test

The radial extent of the resuspended/drained particles was greater for the smaller sized silica sand, but statistically similar for the glass beads. Additionally, the draining tests show that particles with a lower density were more likely to be resuspended. The 1 mm glass beads experienced a greater

amount of resuspension when compared to the 0.853 – 1.68 mm silica sand. Additionally, the scoured region was greater for the less dense glass beads as compared to the more dense silica sand. Figure 46 and Figure 47 show examples of the radial extent of resuspension for silica sand and glass beads during draining-only tests.
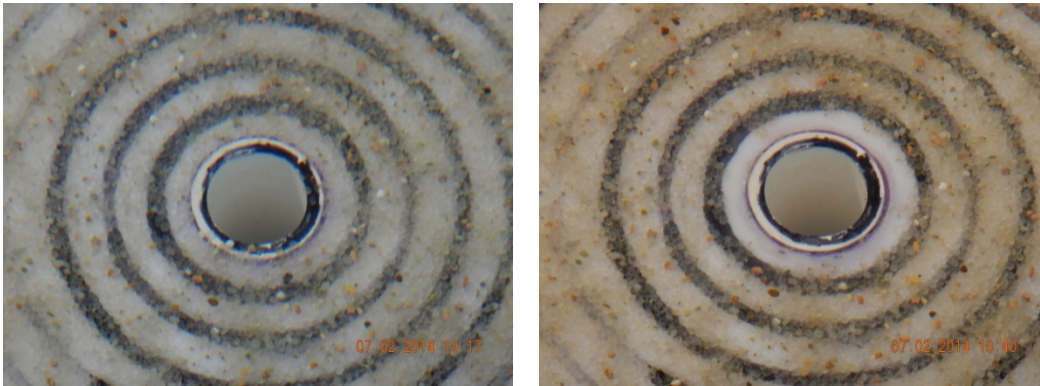
Figure 46. Example of photos of 0.853 – 1.68 mm silica sand particles on the tank bottom near the inlet/drain before (left) and after the draining-only test (right). Concentric rings are 1 cm apart.
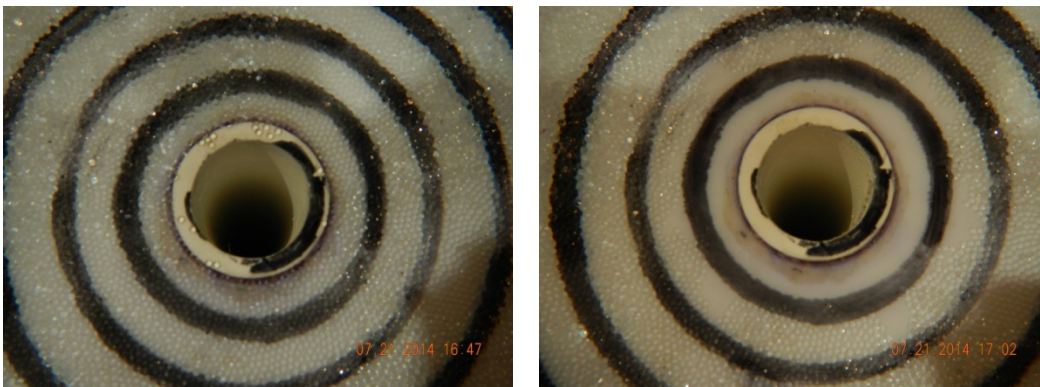
Figure 47. Example of photos of 1 mm glass bead particles on the tank bottom near the inlet/drain before (left) and after the draining-only test (right). Concentric rings are 1 cm apart.

Filling tests revealed that particle resuspension generally occurred within a 0.2 – 0.5 cm radius around the drain for all cases (Table 8). In this region, shear stresses were sufficiently high to cause particle resuspension. Often this meant that particles were resuspended but quickly settled outside the affected region. This region was consistent across the range of particle size and particle density. Glass beads had a greater radial extent, but these values fall within one standard deviation of silica sand values.

Table 8. Filling test results.*

Particle	Particle Density (kg/m^3)	Particle Diameter (mm)	Fill Rate (m^3/s)	Number of Tests Run	Average Radial Extent of Resuspension from Drain Edge (cm)**
Silica Sand	2650	0.053 – 0.104	1.96E-04	1	0.15 ± 0.05
Silica Sand	2650	0.053 – 0.104	4.01E-04	1	0.15 ± 0.05
Silica Sand	2650	0.853 – 1.68	1.92E-04	1	0.22 ± 0.11
Silica Sand	2650	0.853 – 1.68	3.65E-04	1	0.30
Glass Beads	2450	1	1.91E-04	1	0.44 ± 0.12
Glass Beads	2450	1	3.81E-04	1	0.50
Glass Beads	2450	2	1.92E-04	1	0.30
Glass Beads	2450	2	3.84E-04	1	0.30

* Uncertainty in measurements represented by plus/minus one standard deviation
** 5 -8 radial measurements per test

The fill-drain-fill-drain cycle tests yielded variable results when compared to the pure draining and filling tests (Table 9). The larger silica particles experienced less resuspension than when the tank was purely draining. One possible explanation is that the larger particles were resuspended by the inflow during filling, but quickly fell outside the area that would be drained. Videos from the filling test and cycle test support the initial hypothesis that the larger particles were kicked up and quickly settled outside the area of action. Results of the fill-drain-fill-drain tests show that a larger mass fraction of glass beads was drained when compared to the drain-only tests, but the radial extents were statistically similar. It is possible that a small amount of particles were left over from previous tests such that the mass collected from one test included particles from a previous test. The radial extent of resuspension for all the tests are summarized in Figure 48.

Table 9. Fill, drain, fill, drain results.*

Particle	Particle Density (kg/m^3)	Particle Diameter (mm)	Fill Rate (m^3/s)	Number of Tests Run	Particles Collected during Draining (% by mass)	Average Radial Extent of Resuspension from Drain Edge (cm)**
Silica Sand	2650	0.053 – 0.104	1.91E-04	2	3.91 ± 0.51	1.36 ± 0.04
Silica Sand	2650	0.053 – 0.104	3.79E-04	2	5.53 ± 0.46	1.45 ± 0.13
Silica Sand	2650	0.853 – 1.68	1.89E-04	1	1.57	0.72 ± 0.15
Silica Sand	2650	0.853 – 1.68	3.66E-04	1	1.54	0.90 ± 0.19
Glass Beads	2450	1	1.89E-04	1	5.11	1.63 ± 0.30
Glass Beads	2450	1	3.85E-04	1	4.87	1.94 ± 0.29
Glass Beads	2450	2	1.93E-4	2	7.32 ± 0.19	1.83 ± 0.29
Glass Beads	2450	2	3.83E-04	1	5.76	1.90 ± 0.54

* Uncertainty in measurements represented by plus/minus one standard deviation
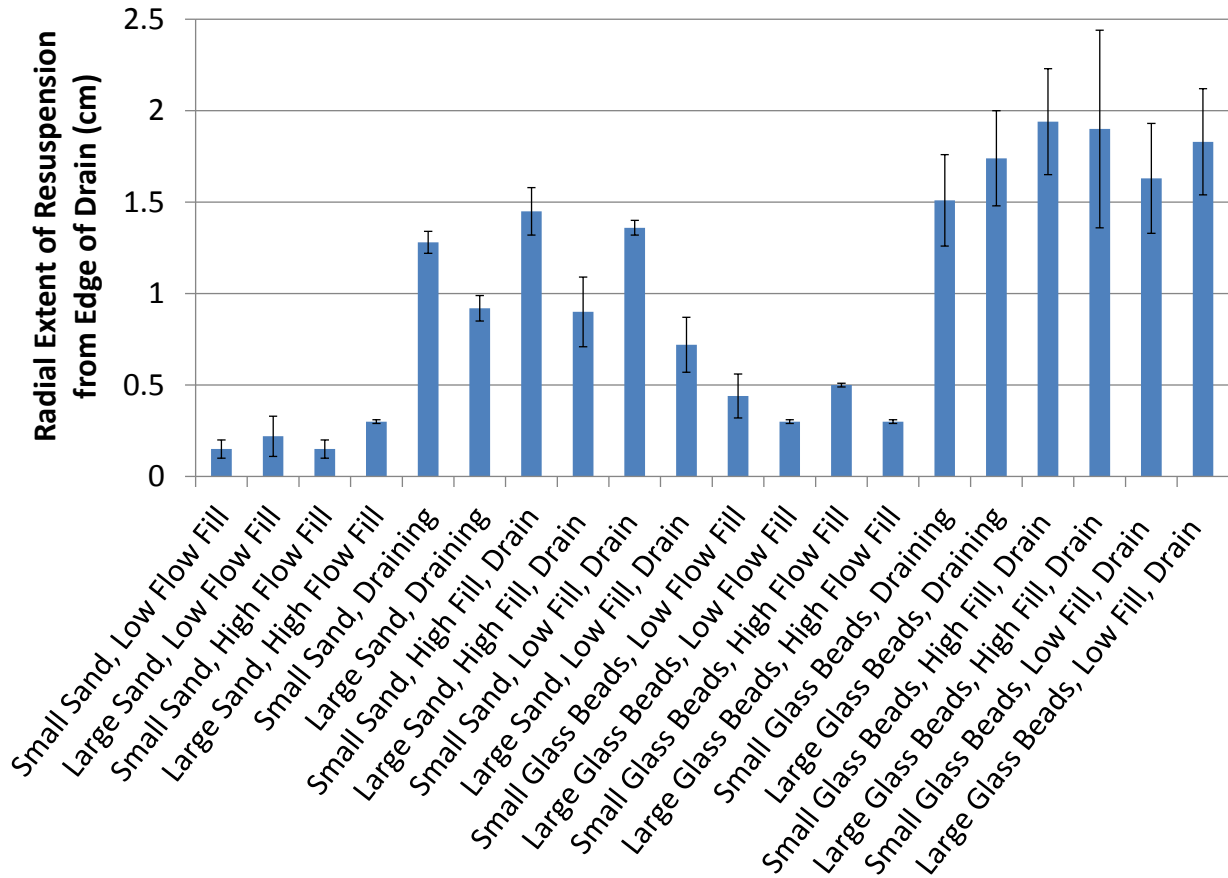** 5 -8 radial measurements per test

Figure 48. Average radial extent of resuspension from the edge of the drain for all tests. Error bars represent one standard deviation about the mean.

or draining tests and fill-drain-fill-drain cycle tests, the drained particles were weighed and a mass distribution was obtained. These mass fraction histogram and cumulative distribution function (CDF) can then be compared to the mass fraction histogram and CDF for particle from the manufacturer.   Figure 49 and Figure 50 show some representative histograms and CDF plots for the 12 – 20 mesh (0.853 – 1.68 mm) silica sand. Results show that the size distribution of particles collected after draining was nearly identical to the initial size distribution from the manufacturer, indicating that the resuspension and drainage behavior for all particles within a given size range was similar for each test.
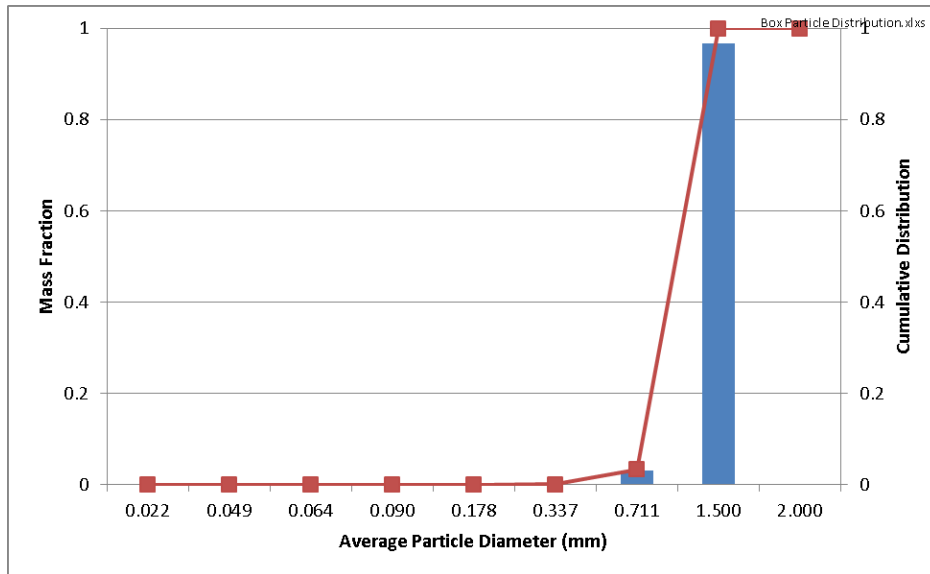
Figure 49. Mass fraction histogram and cumulative distribution (CDF) for #12 - #20 silica sand from manufacturer.
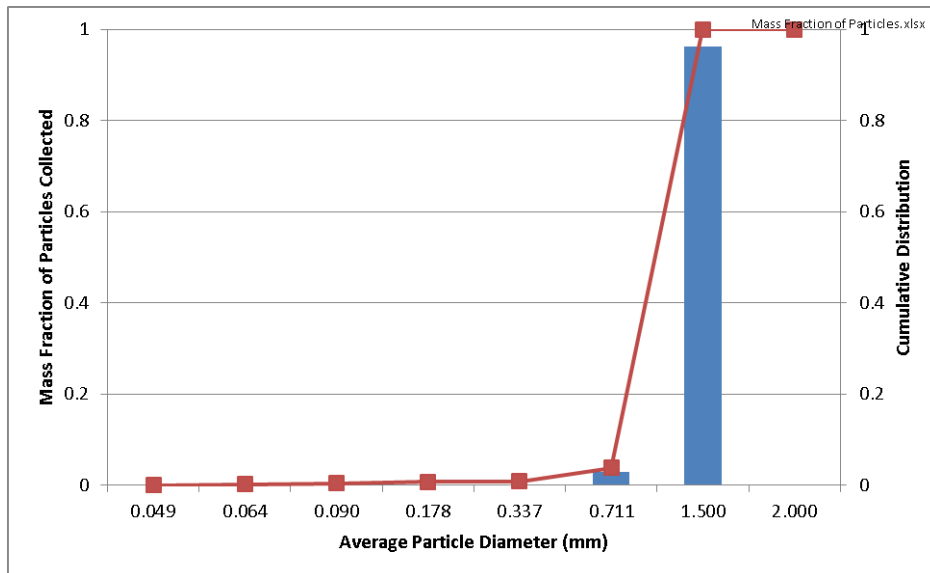

Figure 50. Histogram and cumulative distribution function (CDF) for the mass fraction of #12 - #20 silica sand collected after draining test.

Simulations of the particle resuspension tests were performed using the Solidworks^{TM} software and the ANSYS® Fluent® CFD^{TM} software. Both programs simulate shear stresses at various radial locations from the drain, which can be used to predict particle resuspension based on the Shields or Beheshti models. The simulated shear stresses were used to determine the radial extent of particle resuspension, which was compared against experimental data. The results have been compiled below, using both the Shields and Beheshti models for particle resuspension. Table 10 and Table 11 show the simulated radial extent of particle resuspension from draining scenarios

using the Solidworks™ software and the Fluent® software, respectively. Figure 51 – Figure 52 provide bar charts that illustrate the data presented in Table 10 and Table 11. Table 12 shows the simulated radial extent of particle resuspension during filling-only scenarios using the Fluent® software.

Table 10. Draining scenarios: experimental radial extent of resuspension compared with modeled radial extent of resuspension. Shear stresses for modeled results obtained using the Solidworks™ software.

Particle	Particle Diameter (mm)	Test Type	Modeled Radial Extent of Particle Resuspension from Edge of Inlet/Drain (cm)		Experimental Radial Extent of Particle Resuspension from Edge of Inlet/Drain (cm)
			Shields Model	Beheshti Model	
Silica Sand	0.053-0.104	Draining	2.48 - 3.70	1.95 - 2.48	1.28 ± 0.06
Silica Sand	0.853-1.68	Draining	1.34 - 1.60	1. 34 - 1.60	0.92 ± 0.07
Glass Beads	1	Draining	1.34-1.60	1.34-1.60	1.51 ± 0.25
Glass Beads	2	Draining	1.08-1.34	1.08-1.34	1.74 ± 0.26

Table 11. Draining scenarios: experimental radial extent of resuspension compared with modeled radial extent of resuspension. Shear stresses for modeled results obtained using the ANSYS® Fluent® CFD™ software.

Particle	Particle Diameter (mm)	Test Type	Modeled Radial Extent of Particle Resuspension from Edge of Inlet/Drain (cm)		Experimental Radial Extent of Particle Resuspension from Edge of Inlet/Drain (cm)
			Shields Model	Beheshti Model	
Silica Sand	0.053-0.104	Draining	5 -6	4 -5	1.28 ± 0.06
Silica Sand	0.853-1.68	Draining	2 – 3	2 – 3	0.92 ± 0.07
Silica Sand	0.053-0.104	High Fill, Drain	5 -6	4 -5	1.45 ± 0.13
Silica Sand	0.853-1.68	High Fill, Drain	2 – 3	2 – 3	0.90 ± 0.19
Silica Sand	0.053-0.104	Low Fill, Drain	5 -6	4 -5	1.36 ± 0.04
Silica Sand	0.853-1.68	Low Fill, Drain	2 – 3	2 – 3	0.72 ± 0.15
Glass Beads	1	Draining	2 – 3	2 – 3	1.51 ± 0.25
Glass Beads	2	Draining	1 – 2	1 – 2	1.74 ± 0.26
Glass Beads	1	High Fill, Drain	2 – 3	2 – 3	1.94 ± 0.29
Glass Beads	2	High Fill, Drain	1 – 2	1 – 2	1.90 ± 0.54
Glass Beads	1	Low Fill, Drain	2 – 3	2 – 3	1.63 ± 0.30
Glass Beads	2	Low Fill, Drain	1 – 2	1 – 2	1.83 ± 0.29

Table 12. Filling scenarios: experimental radial extent of resuspension compared with modeled radial extent of resuspension. Shear stresses for modeled results obtained using the ANSYS® Fluent® CFD™ software.

Particle	Particle Diameter (mm)	Test Type	Modeled Radial Extent of Particle Resuspension from Edge of Inlet/Drain (cm)		Experimental Radial Extent of Particle Resuspension from Edge of Inlet/Drain (cm)
			Shields Model	Beheshti Model	
Silica Sand	0.053-0.104	Low Flow Fill	0-1	0-1	0.15 ± 0.05
Silica Sand	0.853-1.68	Low Flow Fill	0-1	0-1	0.22 ± 0.11
Silica Sand	0.053-0.104	High Flow Fill	0-1	0-1	0.15 ± 0.05
Silica Sand	0.853-1.68	High Flow Fill	0-1	0-1	0.30 ± 0.01
Glass Beads	1	Low Flow Fill	0-1	0-1	0.44 ± 0.12
Glass Beads	2	Low Flow Fill	0-1	0-1	0.30 ± 0.01
Glass Beads	1	High Flow Fill	0-1	0-1	0.50 ± 0.01
Glass Beads	2	High Flow Fill	0-1	0-1	0.30 ± 0.01

Because the visible radial extent of resuspension is based on where the largest particles remained after draining, nominal particle diameter used in the Shields and Beheshti prediction models was set at the 95th percentile. As expected, the largest particles are less likely to experience any motion due to the draining fluid; therefore particles in the 95th percentile would most likely be the observed particles during radial extent measurements.

The predicted radial extents of particle resuspension during draining using Solidworks™ and Fluent® software codes and the experimental data are shown in Figure 52– Figure 52. Both codes tended to over predict the radial extent of particle resuspension for silica sand. The non-spherical shape of the sand may have inhibited mobility and caused the radial extent of particle resuspension in the experiments to be less. The Solidworks™ model generally under predicted the extent of particle resuspension for glass beads during draining. During filling, both the simulations from Fluent® and the experiments show that the radial extent of particle resuspension is significantly less than during draining.
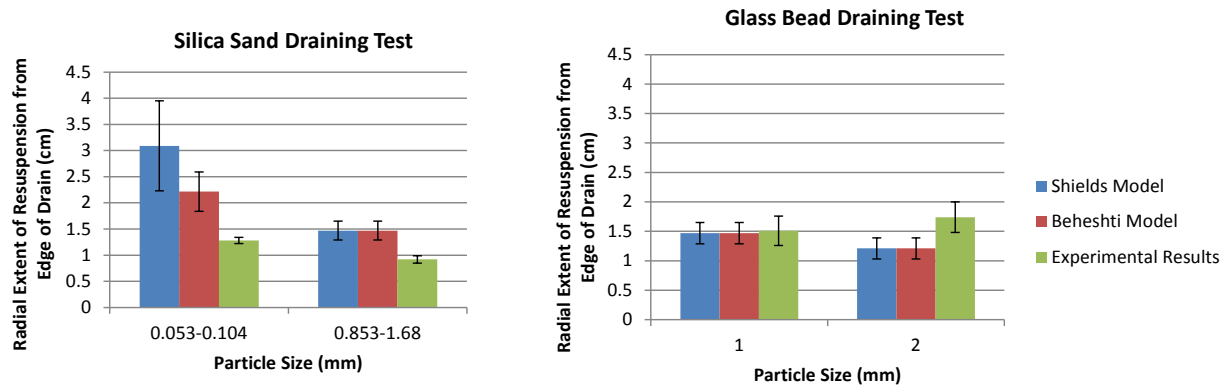
Figure 51. Draining scenarios: comparison of simulated (Solidworks™ software) and experimental average radial extents of particle resuspension. Left: silica sand. Right: glass beads. Error bars represent one standard deviation about the mean.
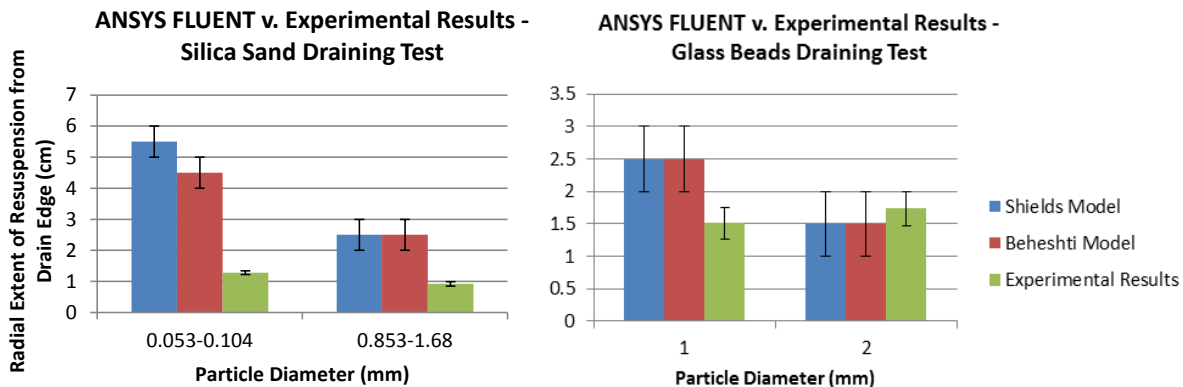

Figure 52. Draining scenarios: comparison of simulated (ANSYS Fluent®) and experimental average radial extents of particle resuspension. Left: silica sand. Right: glass beads. Error bars represent one standard deviation about the mean.

3.3. Impact of Raised Inlet/Outlet on Particle Resuspension

Testing also included an evaluation of an inlet/outlet line raised 1 cm (0.4 in) above the tank bottom to determine if the extension would reduce the amount of particle resuspension (see Figure 53).

Figure 53. Extended line installed above drain.

Table 13 and Table 14 show that the extended line mitigated the resuspension of particles during both filling and draining. No region of scoured particles was observed near the inlet/drain. Only the smallest of particles was resuspended and recovered during the silica sand drainage test, but the mass of particles resuspended was significantly less than for a pure draining test. The mass of silica sand resuspended with the extended line installed was about a tenth of the mass resuspended without the extended drain.

Table 13. Extended line draining results.

Particle	Particle Density (kg/m^3)	Particle Diameter (mm)	Particles Collected during Draining (% by mass)	Average Radial Extent of Resuspension from Drain Edge (cm)
Silica Sand	2650	0.053 – 0.104	0.55	0
Silica Sand	2650	0.853 – 1.68	0	0
Glass Beads	2450	2	0	0
Glass Beads	2450	1	0	0

Table 14. Extended line filling results.

Particle	Particle Density (kg/m^3)	Particle Diameter (mm)	Fill Rate (m^3/s)	Average Radial Extent of Resuspension from Drain Edge (cm)
Silica Sand	2650	0.053 – 0.104	1.94E-04	No visible extent
Silica Sand	2650	0.053 – 0.104	3.82E-04	No visible extent
Silica Sand	2650	0.853 – 1.68	1.96E-04	No visible extent
Silica Sand	2650	0.853 – 1.68	3.82E-04	No visible extent
Glass Beads	2450	1	1.94E-04	No visible extent
Glass Beads	2450	1	3.79E-04	No visible extent
Glass Beads	2450	2	1.92E-04	No visible extent
Glass Beads	2450	2	3.79E-04	No visible extent

4. Summary and Conclusions

This report has presented studies of particle resuspension and movement in water distribution storage tanks during filling and draining cycles. Two computational studies were performed: (1) an operational study of a 11,000 m^3 (3 million gallon) water tank was performed to determine when and where different sized particles were resuspended from the tank bottom and transported during filling and draining cycles at low and high flow rates, and (2) a parametric study to determine the impact of parameters such as particle size, flow rate, inlet/outlet diameter and location, and filling vs. draining on the shear stresses and potential for particle resuspension on the tank bottom. Testing was also performed with a small-scale water tank to investigate particle resuspension during filling and draining cycles with different particle sizes and densities (glass beads and silica sand). The test results were compared to simulations of the physical tests conducted in order to verify the modeling approach. Finally, the use of a raised inlet/outlet line was investigated to mitigate particle resuspension. Results of these investigations are summarized below.

4.1. Results of Operational Study

In the operational study, the resuspension and movement of different sized particles (0.01, 0.1, and 1 mm diameter) were simulated during subsequent filling and draining cycles in the tank. Two different flow rates were used based on representative minimum and maximum flow rates provided by the Albuquerque Water Authority. Key results of the numerical simulations were as follows:

- Particle resuspension from the tank bottom generally occurred immediately following the start of either the filling or draining processes

- Smaller particles were more susceptible to resuspension and entrainment

- Once entrained in the fluid flow, particles were typically carried further away from the inlet/outlet during the filling cycle, making them less susceptible to removal during draining

- Greater shear stress during draining led to more particle resuspension than during filling

- Recirculation zones near the inlet/outlet were observed

4.2. Results of Parametric Study

A parametric study was performed to determine the impact of particle size, flow rate, inlet/outlet diameter and location, and filling vs. draining on the shear stress and potential for particle resuspension on the tank bottom. Key findings were as follows:

- Particle size, flow rate, and inlet/outlet location were found to be important factors for particle resuspension
    - Smaller particles were more susceptible to resuspension, although the difference was less during draining than filling
    - Higher flow rates yielded greater resuspension
    - Inlet/outlets located near the side wall (vs. at the center of the tank) yielded greater resuspension
    - Draining yielded greater resuspension of particles than filling
- Particle resuspension was directly correlated to the amount of momentum flow, or jet effect, through the inlet/outlet. Reducing the flow rate or increasing the diameter of the inlet/outlet reduces the momentum flow and the potential for particle resuspension.
- Placing the inlet/outlet near the center of the tank rather than near the side wall reduced particle resuspension during filling.

4.3. Results of Mitigation Measures

In order to mitigate the potential for particle resuspension near the inlet/outlet line, a raised inlet/outlet was investigated. The hypothesis was that this would reduce the shear stresses near the inlet/outlet and reduce the potential for particle resuspension. The extension pipe configuration (with varying extension heights) was added to the 2D axisymmetric tank model that had been previously used in the operational study. Key results were as follows:

- During filling, a pipe height extending 6 inches (15 cm) above the center of the tank bottom substantially reduced the number of particles resuspended
- During draining, a pipe height extending 12 – 24 inches (30 – 61 cm) above the center of the tank bottom substantially reduced the number of particles drained from the tank

4.4. Results of Testing

Small-scale tests were performed to investigate particle resuspension during filling and draining in a 4-ft (1.2 m) diameter water-filled tank with a 0.8 in (2 cm) diameter inlet/outlet located in the center of the tank. Photos and videos were recorded before and after each filling and draining event to determine where particles were resuspended from the tank bottom. Tracer tests were also performed to characterize the flow patterns and velocity fields. Finally, mitigation measures were investigated by raising the pipe inlet, which was normally flush with the tank bottom, 1 cm (0.4 in) above the tank bottom. Key results were as follows:

- Measured and simulated velocities along tank bottom matched well up to about 5 cm from drain, including region where particles were resuspended

- Velocities along the tank bottom were very small away from the inlet (<1 cm/s), but increased exponentially within 2 – 3 cm from the inlet/outlet to above 10 cm/s

- Resuspension of particles was limited to within ~1 cm from the inlet/outlet during filling and draining cycles for the flow rates used in the study.

- Smaller particles yielded a greater radial extent of resuspension from the inlet/outlet during filling and draining cycles

- Less dense particles (glass beads) than the silica sand exhibited greater resuspension

- During the fill-drain-fill-drain cycle, fewer large particles were drained when compared to the drain-only scenario. This is likely because during the fill cycle, particles close to the inlet were resuspended and deposited further away. When the drain cycle commenced, there were fewer particles near the inlet to be drained. However, a greater fraction of the smaller particles were drained when compared to the drain-only scenario. A possible reason may be that the small particles remained entrained during filling and were subsequently drained, and the fill-drain-fill-drain sequence caused additional perturbations and shear stress that enable a greater amount of smaller particles to be drained.

- Model predictions of resuspension generally matched experimental data for glass beads, and generally over predicted the amount of resuspension for silica sand. The non-spherical shape of the sand may have reduced the amount of resuspension in the tests.

- Both modeling and experiments showed that a raised inlet reduced particle resuspension and removal during filling & draining
  - Minimum height to completely mitigate particle movement near the inlet/outlet was found to be about 3 -8% of the head of water
    - In the tests, an extension of 1 cm (0.39") mitigated particle movement with a maximum head of water of 30 cm (12")
    - In the models, an extension of ~0.38 m (1.3 ft) mitigated particle movement with a head of water of 4.9 m (16 ft)

References

[1]   Grayman, W.M., L.A. Rossman, C. Arnold, R.A. Deininger, C. Smith, J.F. Smith, and R. Schnipke, 1999, Water Quality Modeling of Distribution System Storage Facilities, American Water Works Association, Denver, CO.

[2]   Mahmood, F., J.G. Pimblett, N.O. Grace, and W.M. Grayman, 2005, Evaluation of water mixing characteristics in distribution system storage tanks, *Journal American Water Works Association*, **97**(3), p. 74-88.

[3]   Tian, X.D. and P.J.W. Roberts, 2008, Mixing in Water Storage Tanks. II: With Buoyancy Effects, *Journal of Environmental Engineering-ASCE*, **134**(12), p. 986-995.

[4]   Tian, X.D. and P.J.W. Roberts, 2008, Mixing in Water Storage Tanks. I: No Buoyancy Effects, *Journal of Environmental Engineering-ASCE*, **134**(12), p. 974-985.

[5]   Rossman, L.A. and W.M. Grayman, 1999, Scale-model studies of mixing in drinking water storage tanks, *Journal of Environmental Engineering-ASCE*, **125**(8), p. 755-761.

[6]   Roberts, P.J.W., X. Tian, F. Sotiropoulos, and M. Duer, 2005, Physical Modeling of Mixing in Water Storage Tanks, AWWA Research Foundation, Report #91112, Denver, CO.

[7]   Adamsson, A., V. Stovin, and L. Bergdahl, 2003, Bed shear stress boundary condition for storage tank sedimentation, *Journal of Environmental Engineering-ASCE*, **129**(7), p. 651-658.

[8]   Cheng, N.S. and Y.M. Chiew, 1999, Analysis of initiation of sediment suspension from bed load, *Journal of Hydraulic Engineering-ASCE*, **125**(8), p. 855-861.

[9]   Choi, S.U. and S. Kwak, 2000, *Probabilistic analysis of incipient motion of sediment particles*, in *in Proceedings of the 8th International Symposium on Stochastic Hydraulics ISSH2000*, Beijing, China, July 25 - 28, 2000.

[10]   Dey, S. and A. Papanicolaou, 2008, Sediment Threshold under Stream Flow: A State-of-the-Art Review, *KSCE Journal of Civil Engineering*, **12**(1), p. 45-60.

[11]   He, C., J. Marsalek, and Q. Rochfort, 2004, Numerical modelling of enhancing suspended solids removal in a CSO facility, *Water Quality Research Journal of Canada*, **39**(4), p. 457-465.

[12]   Stovin, V.R. and A.J. Saul, 1994, Sedimentation in Storage Tank Structures, *Water Science and Technology*, **29**(1-2), p. 363-372.

[13]   Stovin, V.R. and A.J. Saul, 1998, A computational fluid dynamics (CFD) particle tracking approach to efficiency prediction, *Water Science and Technology*, **37**(1), p. 285-293.

[14]   Stovin, V.R. and A.J. Saul, 2000, Computational fluid dynamics and the design of sewage storage chambers, *Journal of the Chartered Institution of Water and Environmental Management*, **14**(2), p. 103-110.

[15]   Vanoni, V.A., 1975, Factors Determining Bed Forms of Alluvial Streams, *Journal of the Hydraulics Division-ASCE*, **101**(11), p. 1435-1440.

[16]   Delleur, J.W., 2003, Hydraulics of sediment movement in urban drainage systems, *Journal of Hydraulic Engineering-ASCE*, **129**(4), p. 251-252.

[17]   U.S. Environmental Protection Agency, 2009, Community Water System Survey. Volume II: Detailed Tables and Survey Methodology, EPA/815/R-09/002, Office of Water.

[18]   Mays, L., 2001, *Water Distribution Systems Handbook*, Larry Mays (Editor), McGraw-Hill, New York.

[19]   Lamfers, J., 2011, Kansas Water System Contaminated due to Birds Accessing Storage Tank, *Kansas Lifeline*, p. 38-41, November 2011.

[20]   U.S. Environmental Protection Agency. *Finished Water Storage Facilities*. 2002 August 15, 2002 [cited 2015 March 3]; Available from: http://www.epa.gov/ogwdw/disinfection/tcr/pdfs/whitepaper_tcr_storage.pdf.

[21]   Grayman, W.M., L.A. Rossman, R.A. Deininger, J.F. Smith, and R. Schnipke, 1999, Water Quality Modeling of Distribution System Storage Facilities, AWWARF.

[22]   Kirmeyer, G.J., L. Kirby, B.M. Murphy, N. P.F., M. K., and L. J.L., 1999, Maintaining Water Quality in Finished Water Storage Facilities, AWWARF.

[23]   Angulo, F.J., S. Tippen, D.J. Sharp, B.J. Payne, C. Collier, J.E. Hill, T.J. Barrett, R.M. Clark, E.E. Geldreich, H.D. Donnell, and D.L. Swerdlow, 1997, A community waterborne outbreak of salmonellosis and the effectiveness of a boil water order, *American Journal of Public Health*, **87**(4), p. 580-584.

[24]   Safe Drinking Water Program (SDWP). *Waterborne Salmonella Outbreak in Alamosa, Colorado, March and April 2008: Outbreak Identification, Response, and Investigation. Water Quality Control Division. Colorado Department of Public Health and Environment, Denver, CO.* November 2009 [cited 2015 March 9]; Available from: https://www.colorado.gov/pacific/sites/default/files/WQ-DW-Publications-Alamosa-Outbreak-Investigation-Report.pdf

[25]   Craun, G.F., J.M. Brunkard, J.S. Yoder, and V.A. Roberts, 2010, Causes of Outbreaks Associated with Drinking Water in the United States from 1971 to 2006, *Clinical Microbiology Reviews*, **23**(3), p. 507-528.

[26]   Centers for Disease Control (CDC), 2013, Surveillance for Waterborne Disease Outbreaks Associated with Drinking Water and Other Nonrecreational Water — United States, 2009–2010, *MMWR*, **62**(35), p. 714-720.

[27]   U.S. Environmental Protection Agency. *Adherence of Chemical, Biological, and Radiological Contaminants to Sediments Found in Water Storage Tanks*. EPA/600/S-14/224 2014 [cited 2015 Mardch 9]; Available from: http://cfpub.epa.gov/si/si_public_file_download.cfm?p_download_id=521345.

[28]   U.S. Environmental Protection Agency, 2015, Report on Physical and Chemical Properties of Drinking Water Storage Tank Sediments, in preparation.

[29]   Lu, J., I. Struewing, S. Yelton, and A. N., 2015, Molecular Survey of Occurrence and Quantity of Legionalla spp., Mycobacterium spp., Pseudomonas aeruginosa and Amoeba Hosts in Municipal Drinking Water Storage Tanks, *Journal of Applied Microbiology (in press)*.

[30]   Wu, J.H. and S.F. You, 2011, Validation of FLUENT Type Simulation of Heat Pump Water Tank Containing PCM, *2011 3rd World Congress in Applied Computing, Computer Science, and Computer Engineering (Acc 2011), Vol 3*, **3**, p. 321-329.

[31]   Patel, T., L. Gill, and M.G. Faram, 2011, Grit Removal from Wastewater Using Secondary Currents in Open-Channel Flow around Bends, *Journal of Environmental Engineering-Asce*, **137**(11), p. 1026-1039.

[32]   Dautova, L.S., I. Milanovic, and K.J. Hammad, 2012, *CFD Study of the Effect of Jet Placement on Flow Patterns Inside a Jet Stirred Tank*, in *2012 ASEE Northeast Section Conference*, University of Massachusetts Lowell, April 27 - 28, 2012.

[33]   Beheshti, A.A. and B. Ataie-Ashtiani, 2008, Analysis of threshold and incipient conditions for sediment movement, *Coastal Engineering*, **55**(5), p. 423-430.

[34]   Delleur, J.W., 2001, New results and research needs on sediment movement in urban drainage, *Journal of Water Resources Planning and Management-ASCE*, **127**(3), p. 186-193.

[35]   Hager, W.H. and G. Oliveto, 2001, Simplified shields condition for sediment transport inception, *Hydraulics of Rivers Water Works and Machinery, Vol II, Theme D, Proceedings*, p. 264-269.

[36]   Mantz, P.A., 1977, Incipient Transport of Fine Grains and Flakes by Fluids - Extended Shields Diagram, *Journal of the Hydraulics Division-ASCE*, **103**(6), p. 601-615.

[37]   Motamedi, A., H. Afzalimehr, and V.P. Singh, 2010, Evaluation of a Novel Approach to Determine the Critical Shields Stress, *Journal of Hydrologic Engineering*, **15**(11), p. 892-900.

[38]   Huber, W.C. and R.E. Dickinson, 1988, Storm Water Management Model, Version 4: User's Manual, EPA/600/3-88/001a, Environmtnal Research Laboratory, U.S. Environmental Protection Agency, Athens, GA.

[39]   Morsi, S.A. and Alexande.Aj, 1972, Investigation of Particle Trajectories in 2-Phase Flow Systems, *Journal of Fluid Mechanics*, **55**(Sep26), p. 193-&.

[40]   Cushman-Roisin, B., 2013, *Environmental Fluid Mechanics*, John Wiley & Sons, Inc., New York.

[41]   McNaughton, K.J. and C.G. Sinclair, 1966, Submerged Jets in Short Cylindrical Flow Vessels, *Journal of Fluid Mechanics*, **25**(2), p. 367-375.

[42]   Dautova, L.S., I. Milanovic, and K.J. Hammad, Year, *CFD Study of the Effect of Jet Placement on Flow Patterns Inside a Jet Stirred Tank*, in *2012 ASEE Northeast Section Conference*, University of Massachusetts Lowell, April 27-28, 2012.

Appendix A: Hydraulic Model Evaluation

Turbulence models are necessary to capture the chaotic flow patterns caused by the inlet jet when pumping water into the tank. This appendix evaluates different turbulence models available for multiphase flow in the Fluent® software. Comparisons to experiments with water jets were used to evaluate the conditions representative of water being injected into a tank. Water jets have been studied and classified based on their Reynolds number in several reports [40, 41]. A fully turbulent jet is considered to have a Reynolds number of greater than 3,000 in the inlet. The Reynolds numbers for the inflow in this study are all greater than 3,000.

Two options for modeling turbulence in the Fluent® software exist:

1. k-ω SST: This model solves the Reynolds-Averaged Navier-Stokes (RANS) equations using an isotropic eddy viscosity value to solve for the Reynolds stress values. This model is capable of solving turbulence equations in the near-wall region as well as in the free-stream region necessary in this problem.

2. Scale-Adaptive Simulation: This model solves the unsteady-RANS equations which accounts for fluctuations in the turbulent flow as the equations progress. This model utilizes the Reynolds stress model which individually solves all of the Reynolds stress values for the transport equations without using the isotropic eddy viscosity value used in the RANS equations. This model can be more accurate in solving for small turbulent eddies and may be appropriate for this type of modeling.
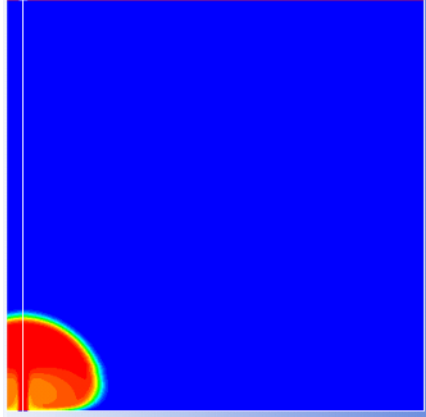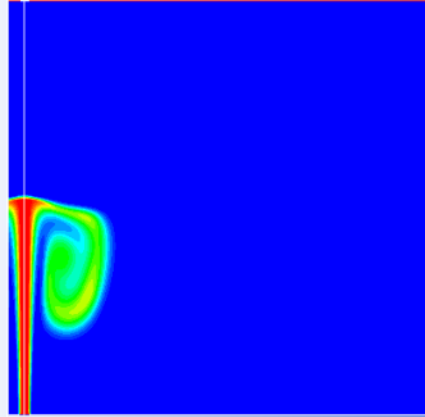
The solutions from these two turbulence models were compared with experimental tank mixing images given in Roberts et al. [4, 6] in which the geometric tank configuration (GC02) matched those of the current study. Simulations were performed assuming two-dimensional axisymmetry using the k-ω SST and Scale-Adaptive Simulation models to determine which turbulence model would be best suited for the computational studies conducted in this report. The modeling conditions for this comparison were as follows:

- Mixture multiphase solution model (to evaluate mixing behavior in the Fluent® software)
- Three phase mixture: air, water, and tracer (water)
    - Tracer was injected into the tank with a volume fraction of 1 with a velocity of 2.33 m/s (fully turbulent jet)
- 50,000 grid elements

Both the k-ω SST and scale adaptive turbulence models qualitatively captured the tracer mixing patterns within the tank (Table 15 and Figure 54). It was seen that the simulated flow patterns followed the general movement of the tracer concentrations in Roberts et al. [6]. The tracer concentrations were not matched completely, probably due to unknown diffusion parameters and not being able to accurately capture the small turbulent eddies forming in the jet region. However, those factors are not expected to significantly impact analysis of particle resuspension in terms of the general advective flow patterns and simulated shear stress along the bottom of the tank. It is not necessary to capture the tracer diffusive mixing and concentrations, allowing for the use of the simpler VOF multiphase model. In addition, because the advective flow patterns were similar

between the two turbulence models, small turbulent eddies (modeled in the scale-adaptive simulation) are neglected in favor of using the simpler k-ω SST model. While turbulent eddies are expected near the inlet jet during filling of a tank, they are not expected to be significant during draining of the water tanks. Further support of the k-ω SST model comes from Dautova et al. [42]. They studied the impacts of a submerged jet in water on an impingement plate. They compare the k-ω SST model to a Reynolds Stress model as well and determined that the k-ω SST model provided more accurate answers when compared to experimental data.

Table 15. Comparison of tracer concentrations as a function of time during injection into a water-filled tank using two different turbulence models.

Time (s)	k-w SST Turbulence Model	Scale Adaptive Turbulence Model
4		

Time (s)	k-w SST Turbulence Model	Scale Adaptive Turbulence Model
27		
41		

Time (s)	k-w SST Turbulence Model	Scale Adaptive Turbulence Model
57		
71		

Time (s)	k-w SST Turbulence Model	Scale Adaptive Turbulence Model
144		
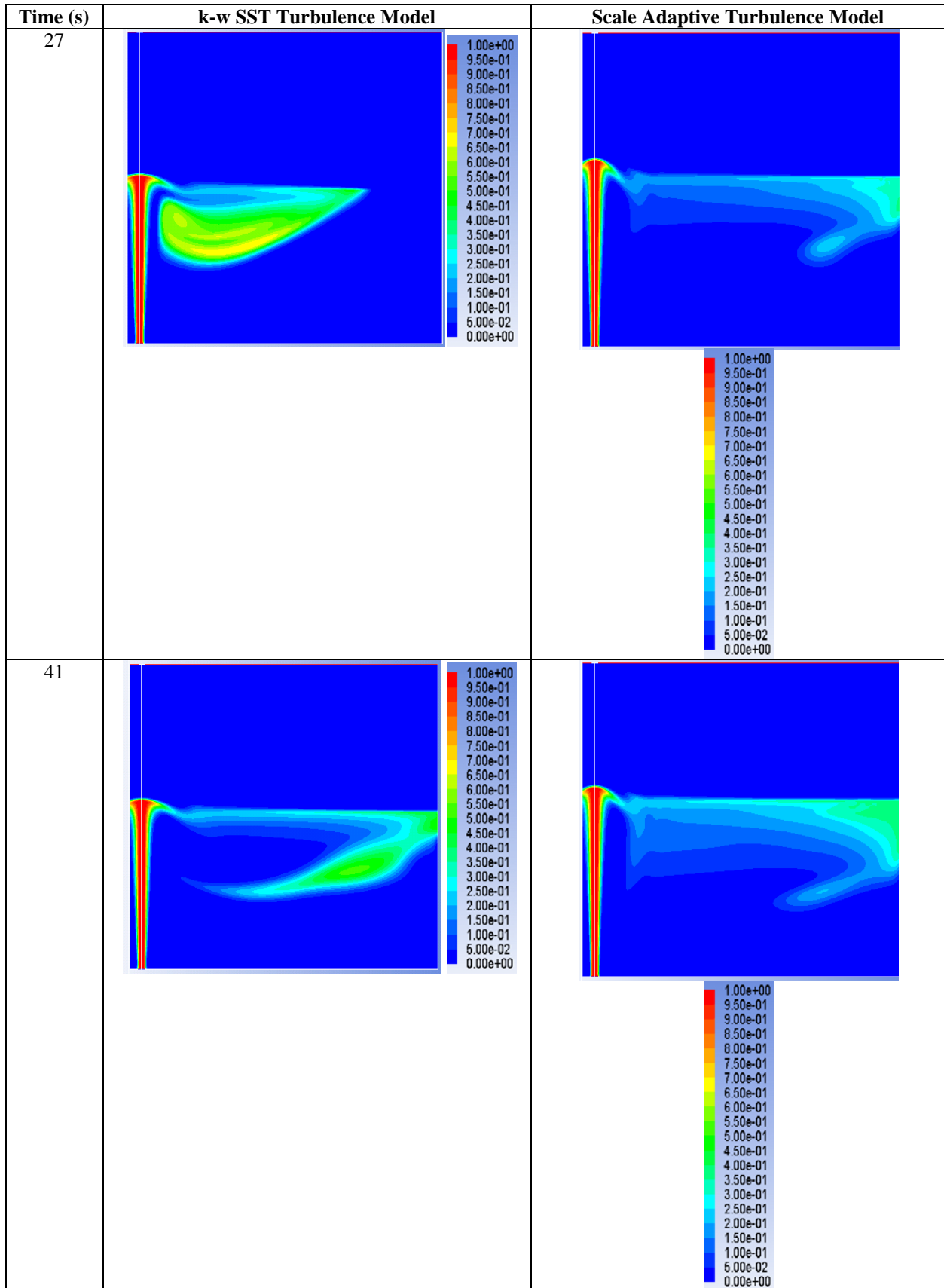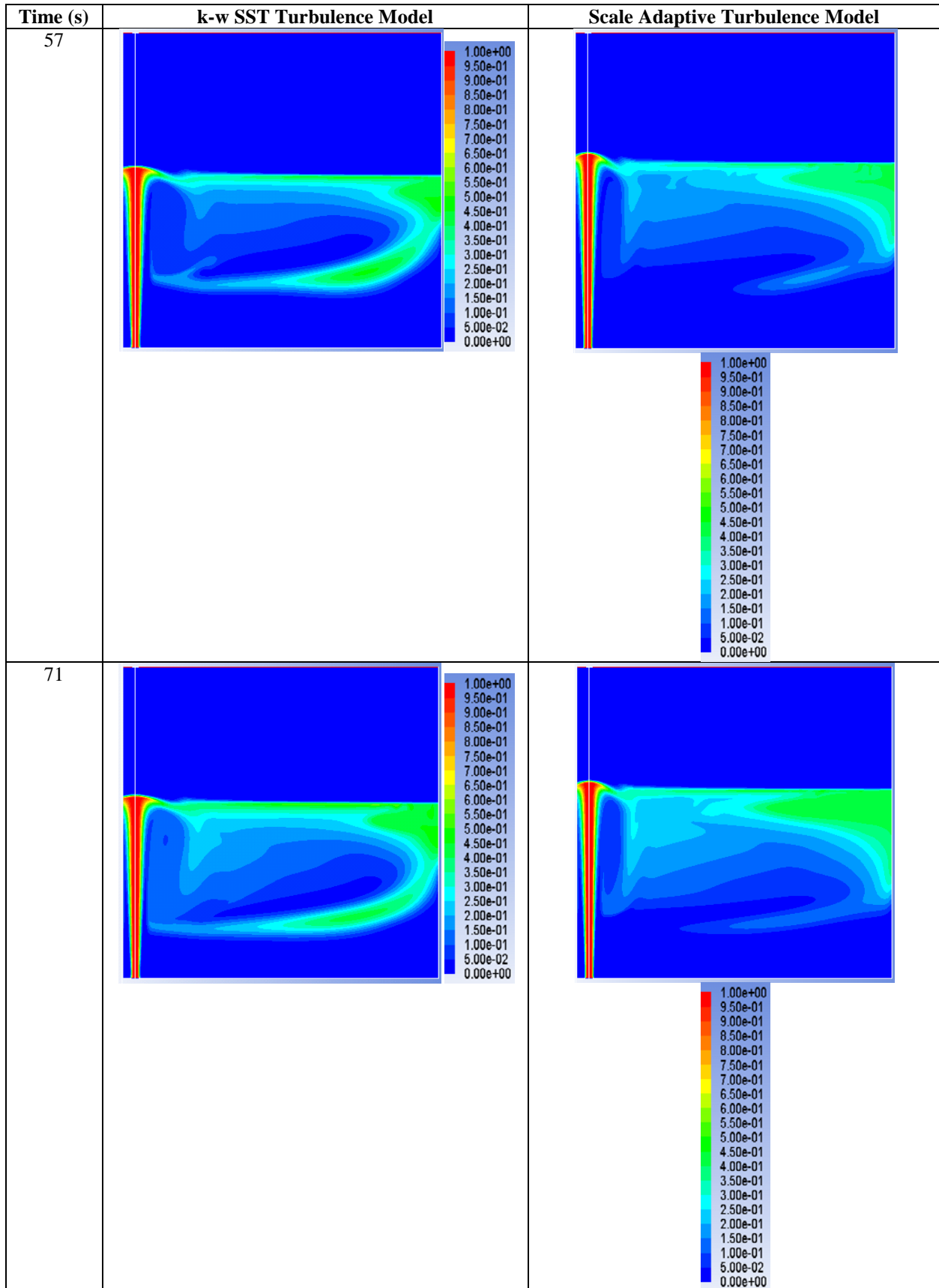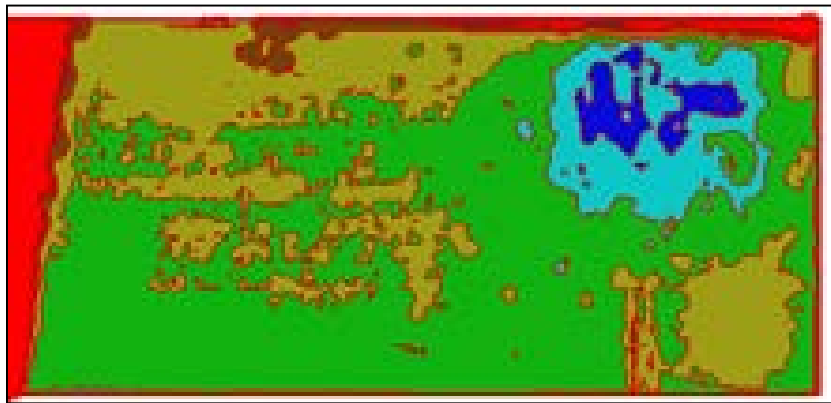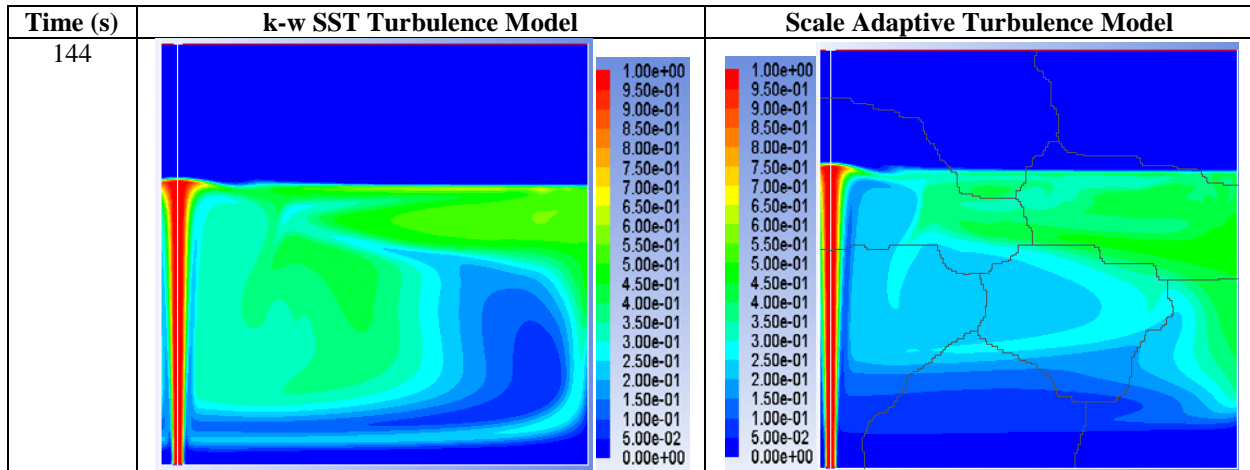
Figure 54. Tracer concentrations from Roberts et al. experiment ([6], Fig. 3.9) with 2.16 m/s inflow jet on left (red is concentration, blue is low concentration).

To further evaluate the turbulence models, a CFD model with a submerged jet in a cylindrical container was compared to an existing CFD/experimental verification study. Replicating this study with the same type of jet flow and turbulence model (k-ω SST) gives confidence that the CFD results can predict jet behavior in a submerged liquid within a cylindrical tank.

Results from Dautova et al. [42] were recreated using the k-ω SST model. The geometry was replicated for the center line location. The solution was transient with the k-ω SST turbulence model included. The jet flow enters the tank through a pipe, impinges on the bottom of the tank and then the flow develops within the tank. The model has complex flow features due to the jet impingement thus giving confidence that the CFD model can predict complex jet flow behavior. The results were compared to those obtained in the Dautova report. Dautova was able reproduce the behavior of experimental work in the CFD calculations (Figure 55).
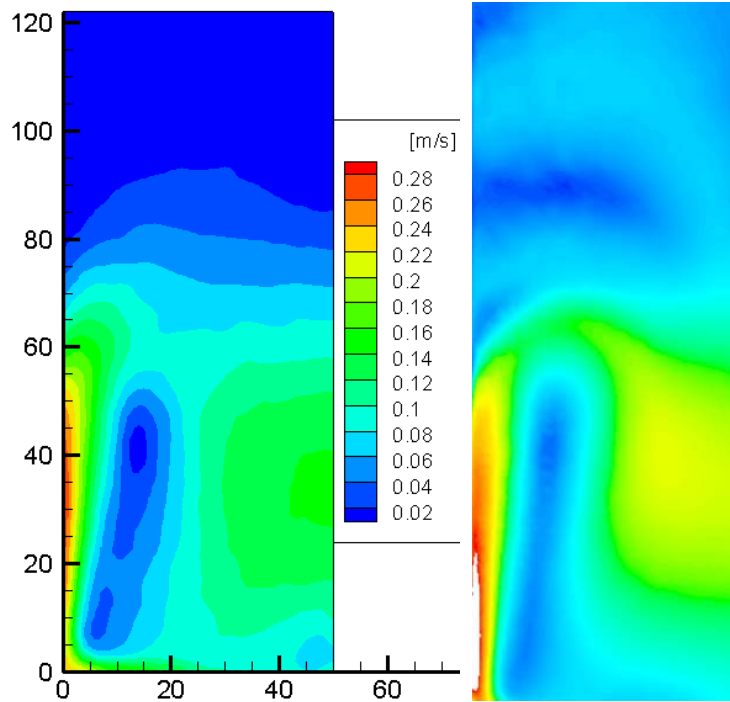
Figure 55. Experimental (left) and simulated (right) contours of velocity magnitude in a jet-stirred mixing tank (from Fig. 7 in [42]).

The jet profile in the CFD tank studies can also be compared to general jet information provided in [40]. It is reported that turbulent jets submerged in a quiescent fluid have the same jet opening angle regardless of velocity and diameter of line. This universal jet opening angle is 11.8⁰ (Figure 56). The jet opening angle for the CFD studies is ~12⁰. This value is found from looking at the jet velocity profile in Figure 57 and Figure 58 and applying the appropriate trigonometric equations, see equation below.

$$\theta = \tan^{-1}\frac{w}{h}$$

Where θ is the jet opening angle, w (1.04 m) is the half width of the jet velocity profile, and h (4.7 m) is the height where the jet profile is taken (note that this height is measured from the x value [5*(diameter of line)/2] since the initial jet radius is not zero).

The CFD jet opening angle is close to the universal jet opening angle reported in [40] for turbulent, submerged jets. This gives confidence that the CFD model is predicting the jet profile overall shape without inclusion of small turbulent eddies.
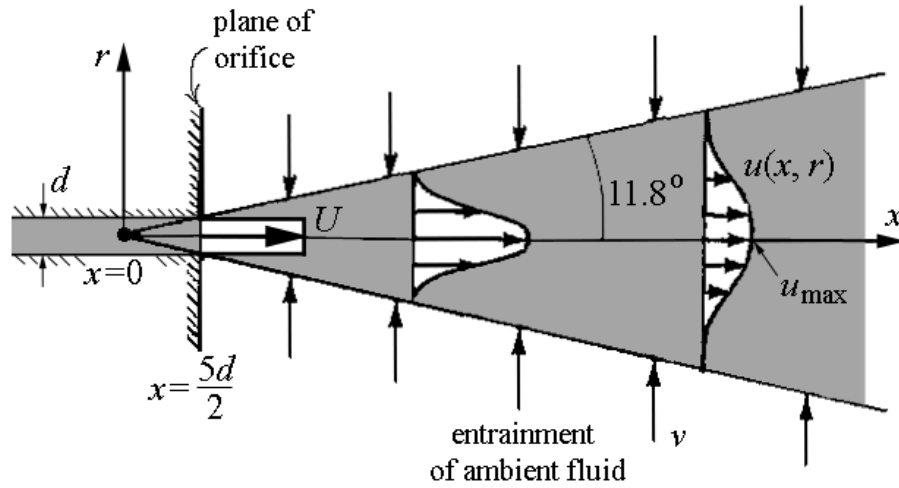
Figure 56. Schematic of jet penetration into quiescent fluid [40], the jet opening angle of 11.8° is universal regardless of inlet velocity and line diameter
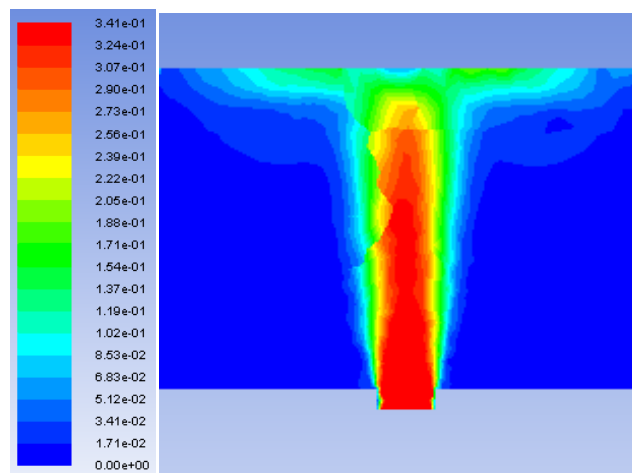
Figure 57. 3D CFD jet velocity (m/s) in center line tank with inlet velocity of 0.33 m/s
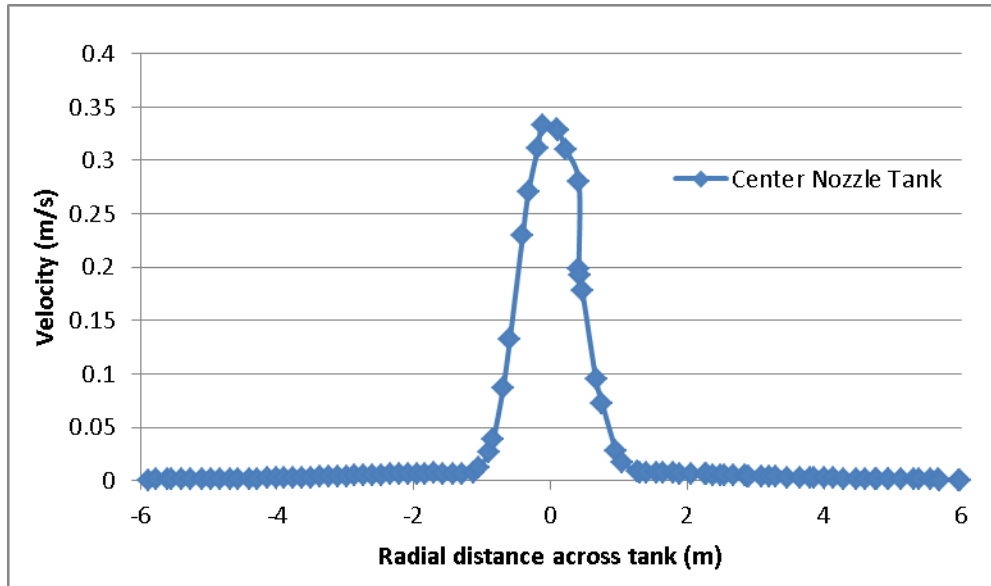
Figure 58. Jet velocity (m/s) profile at quarter height of tank along radial distance of tank for 0.33 m/s jet.

The Volume of Fluid (VOF) method and Mixture method were two main candidates for the multiphase modeling required in this study. However, since tracer mixing is not important to particle resuspension, the Mixture method is not required. The VOF method tracks the sharp interface between phases. The interface in this study was the region where the air and water meet. The jet can penetrate into the air region and the solver will track this water intrusion on the air region. This model also solves for the flow within the water region of the tank. This multiphase model was used for both tank filling and draining scenarios.

Initially, it was hypothesized that a two-phase (air, water) model would not be required after a certain water head level. At some point the jet will stop penetrating the air region and dissipate before reaching the air-water interface for inflow boundary conditions. However, after running comparison simulations, it was concluded that the free surface plays an important role in the flow patterns within the tank. During filling the jet penetrates the free surface for the tank sizes considered. A single phase solution would not be plausible for the tank filling scenario. A two-phase transient solution was used for all tank filling scenarios.

The shear stress profiles along the bottom of a center line tank for a steady single phase vs. transient two-phase draining solution are shown in Figure 59. Results show that for regions near the drain, the simulated shear stresses are similar between the two models. Away from the drain, the simulated shear stresses deviate between the different models. During draining, as the free surface starts to drop the water at the free surface develops both axial and radial velocity components causing recirculation zones to form. A single phase draining simulation does not capture this physical process. However, for the purposes of simulating particle resuspension during draining, a steady single-phase model, which is much more computationally efficient than than the transient two-phase model, may be appropriate. A steady single-phase Solidworks^{TM} model was used to simulate particle resuspension in the small-scale tests, and comparisons were shown to be good (see Section 3.3).

81
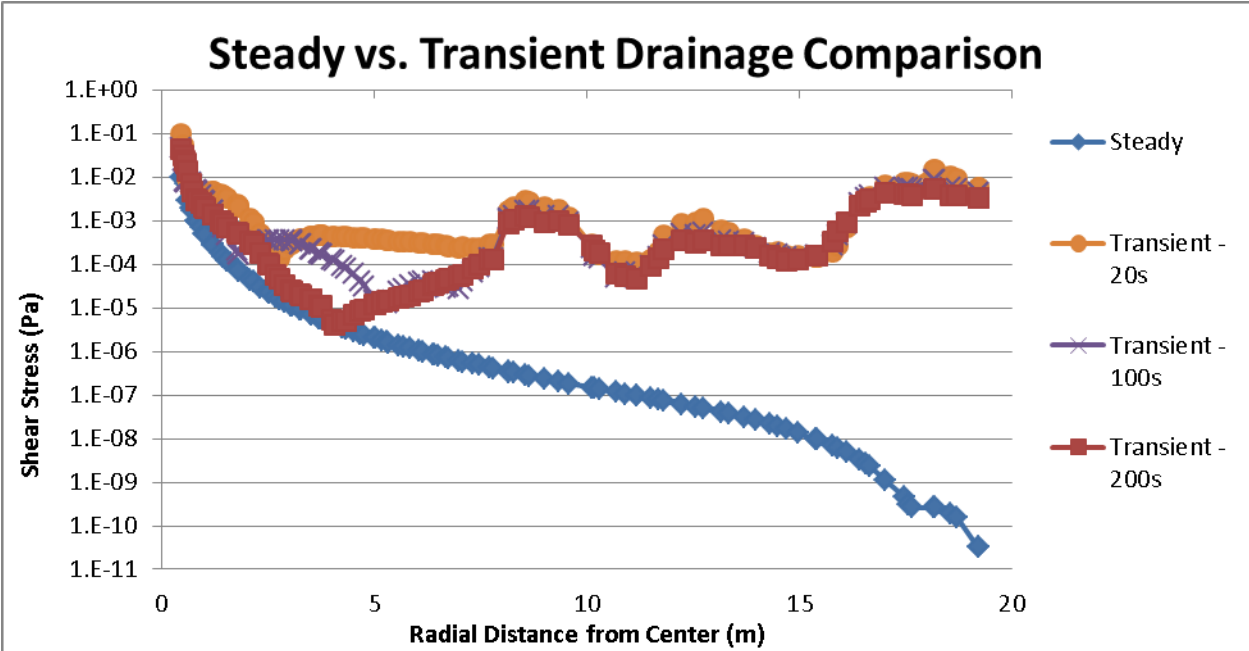
Figure 59. Shear stress profiles along bottom of tank with center line : comparison of steady-state single-phase drainage solution compared to transient two-phase drainage solution.

Appendix B: Particle Size Distribution

A representative particle size distribution was provided by the Colorado Tower in Columbus, Ohio [28], where a sample of sediment particles was sieved and weighed (see Figure 60). The total weight of all particles was 72.202 g. Table 16 and Figure 61 provide data collected on the mass fractions and size distributions. The mass fractions of each particle diameter bin were converted to number fractions based on the following procedure in order to determine an appropriate particle size distribution to be used in the CFD models.

The total mass of each bin was calculated by multiplying the total mass of all particles by the mass fraction of the bin.

$$m_i = m_{tot} \times m_{f,i}$$
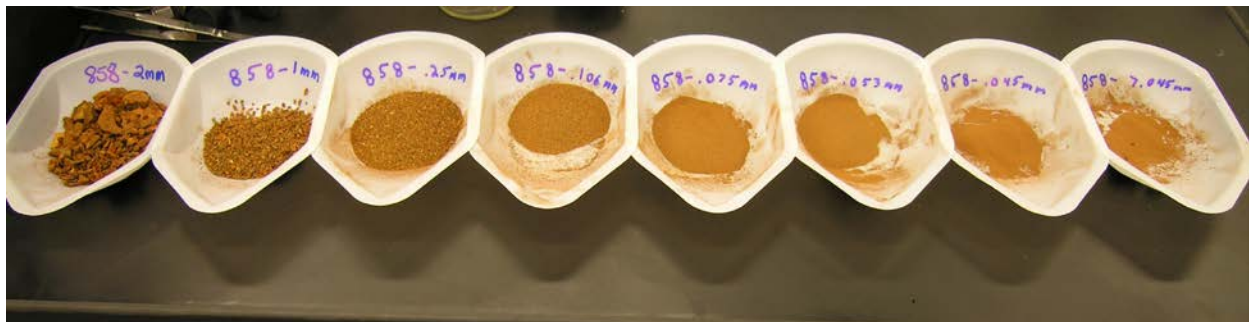
Figure 60. Sediment particles from the Colorado Tower, Columbus, Ohio. The sample was sieved and weighed to develop a sediment weight distribution.

Table 16. Diameter range and mass fraction of each particle bin.

Bin Number	1	2	3	4	5	6	7	8
Particle Diameter (mm)	>2	1-2	.25-1	.106-.25	.75-.106	.53-.75	.45-.53	<.45
Mass Fraction	.5279	.1372	.1657	.856	.277	.255	.171	.132
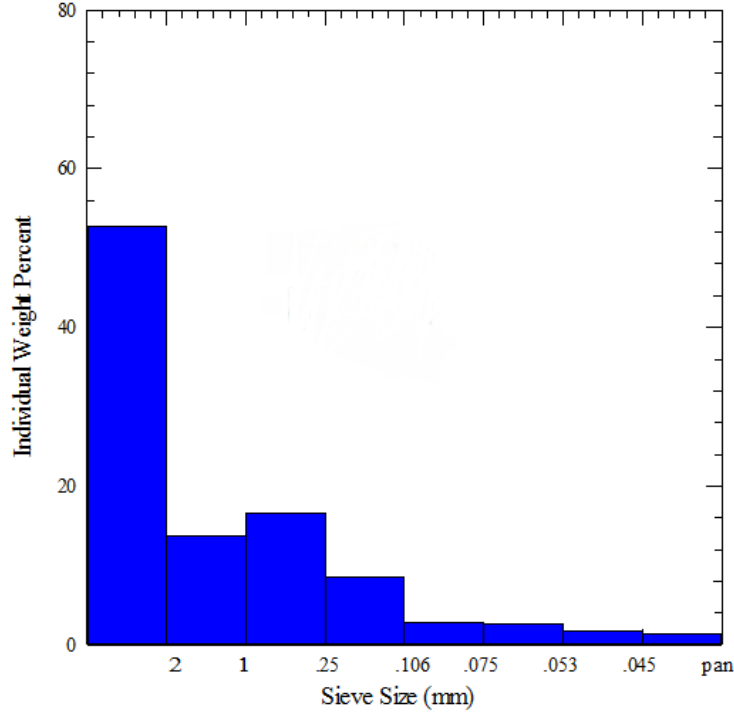
Figure 61. Histogram of mass fraction against particle diameter.

A representative diameter for each bin was then determined by a mass-weighted average of the maximum and minimum diameters of the bin. The representative diameters of the smallest and largest bins were calculated based on the ranges of the closest bins in size:

$$m_{max,2\text{-}7} = \rho \frac{4}{3} \pi \left(\frac{d_{max,2\text{-}7}}{2}\right)^3, \quad m_{min,2\text{-}7} = \rho \frac{4}{3} \pi \left(\frac{d_{min,2\text{-}7}}{2}\right)^3 \tag{12}$$

$$d_{rep,2\text{-}7} = \frac{d_{max,2\text{-}7}(m_{max,2\text{-}7}) + d_{min,2\text{-}7}(m_{min,2\text{-}7})}{m_{max,2\text{-}7} + m_{min,2\text{-}7}} \tag{13}$$

$$d_{rep,1} = d_{min,1} + \left(d_{max,2} - d_{min,2}\right) \tag{14}$$

$$d_{rep,8} = d_{min,7} - \left(d_{max,7} - d_{min,7}\right) \tag{15}$$

The number of particles in each bin was determined by dividing the mass of each bin by a representative unit mass:

$$m_{rep,i} = \rho \frac{4}{3} \pi \left(\frac{d_{rep,i}}{2}\right)^3 \tag{16}$$

$$N_i = \frac{m_i}{m_{rep,i}} \tag{17}$$

The number of particles in each bin was divided by the total number of particles to yield the number fraction of each bin:

$$N_{tot} = \sum_{i=1}^{8} N_i \tag{18}$$

$$N_{f,i} = \frac{N_i}{N_{tot}} \tag{19}$$

The resulting number fractions are shown in Table 17.

Table 17. Particle diameter range, mass fraction, and number fraction of each bin.

Bin Number	1	2	3	4	5	6	7	8
Particle Diameter (mm)	>2	1-2	.25-1	.106-.25	.075-.106	.053-.075	.045-.053	<.045
Mass Fraction	.5279	.1372	.1657	.856	.277	.255	.171	.132
Number Fraction	3.83e-5	3.99e-5	3.36e-4	.0122	.0579	.1504	.2686	.5106

Very few large particles made up the total number of particles in the sample; however, they contributed greatly to the total mass simply because each large particle is orders of magnitude heavier than the smaller particles.

The complementary cumulative distribution function (CCDF) displayed in Figure 62 describes the probability of occurrence of a particle with a diameter greater than or equal to a specific value on the x-axis. The x-values of each data point represent the minimum diameter of the corresponding bin (except for the smallest bin); the y-values represent the cumulative number fraction of the corresponding bin and of all larger bins. For instance, the rightmost data point indicates that approximately fifty percent of the particles in a sample will have diameters greater than 45 microns. The data points plotted on this CCDF are shown in Table **18**.

Table 18. Probability of occurrence of a particle with a diameter greater than or equal to the specified diameter. The displayed diameters are the endpoints of each bin (Table 16).

Particle Diameter (mm)	2	1	0.25	0.106	0.075	0.053	0.045
Probability of Occurrence	3.83e-5	7.82e-5	4.14e-4	0.0126	0.0704	0.2208	0.4894
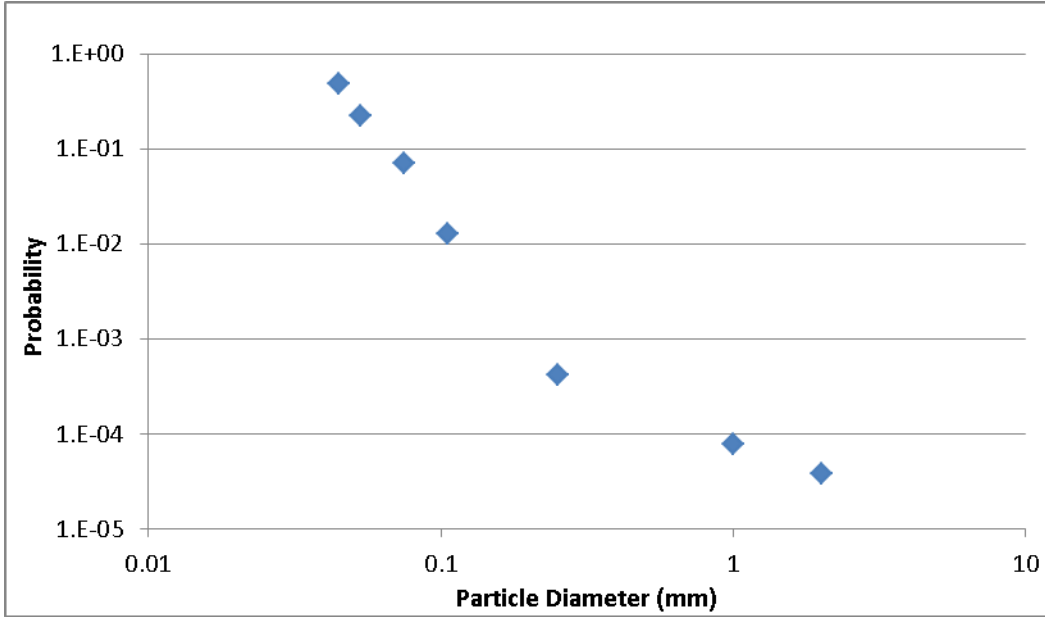
Figure 62. Complementary cumulative distribution function of particle diameter based on number fraction.

Implementing the Colorado Tower particle distribution in a CFD model would require a considerable number of particles to simulate even a few large particles for the operational study. Therefore, an injection of 6,000 particles consisting of equal numbers of 1-mm, 100-micron, and 10-micron diameter particles was used instead. Each division of particles was distributed across the bottom face of the tank in the same locations, resulting in 2,000 different initial positions and 3 different-sized particles at each position. The initial particle positions were scaled towards the tank center since the particles further away from the inlet/outlet line were less likely to experience resuspension and were thus of less interest. The positions were determined by the following equation:

$$R = \frac{n^a}{1000} + 0.3048 \tag{20}$$

Where

$$a = \frac{\log[1000(19.2024 - .3048) - 1]}{\log 2000}$$

R is the radial distance of the particle from the tank center (mm), and *n* is the particle index (1-2000). For *n* = 1, *R* = 0.306 m, and for *n* = 2000, *R* = 19.2 m. Note that the bottom wall spans a radial distance of 0.3048 meters to 19.2024 m. This scaled distribution allowed for a characteristic representation of particle suspension and trajectories for a wide range of particle sizes. Figure 63 shows the initial distribution of particles along the tank bottom. The density of the particles was assumed to be 2650 kg/m^3 (silica sand).

86
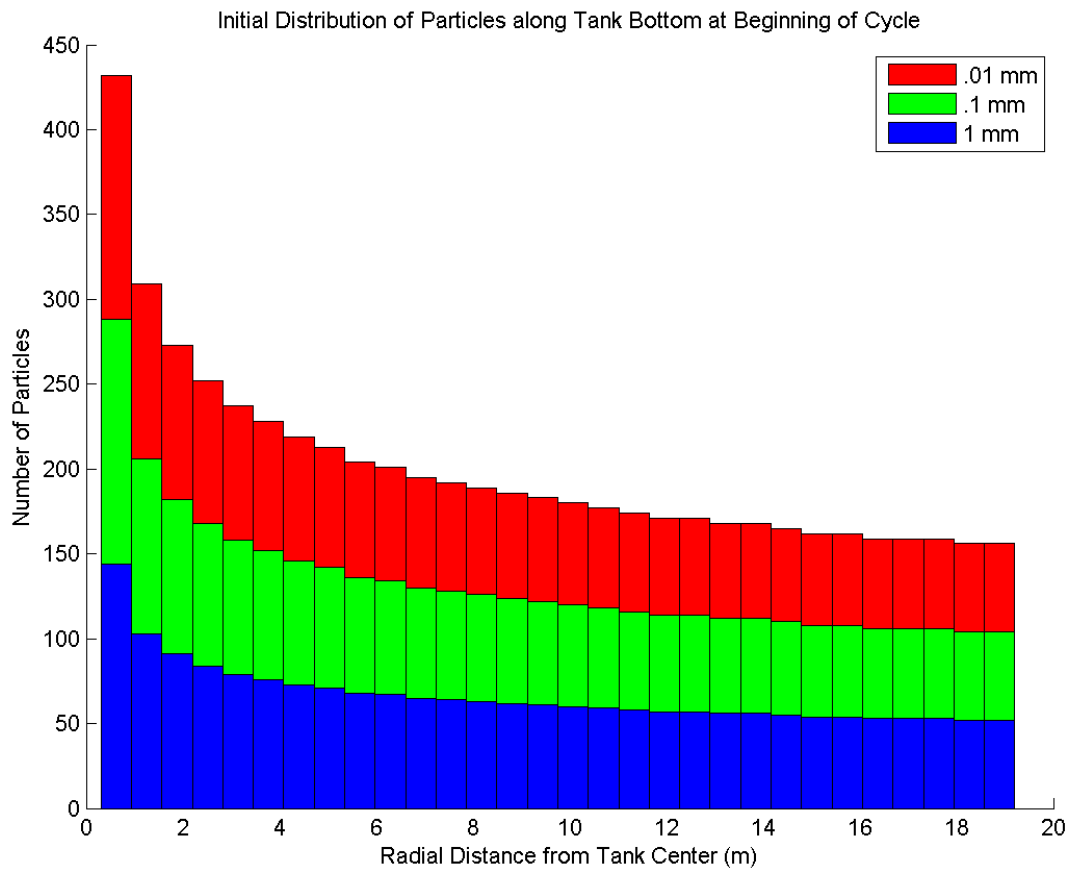
Figure 63. Bar graph displaying initial distribution of particles along bottom wall.

Appendix C: Surface Tension Model for Particles at the Air-Water Interface

Background

The operational study of particle movement (Section 2.3) is designed to determine the general positions along the bottom of water storage tanks at which sediment particles are most likely to be deposited or resuspended into the fluid flow. The trajectories of the resuspended particles are then tracked until they are re-deposited. However, using the initial model, some of these particles were observed to pass above the water surface into the air region (Figure 64). The Fluent® software does not by default include forces due to surface tension at the air-water interface. Therefore, a surface tension model was created and implemented by writing a user-defined function (UDF).
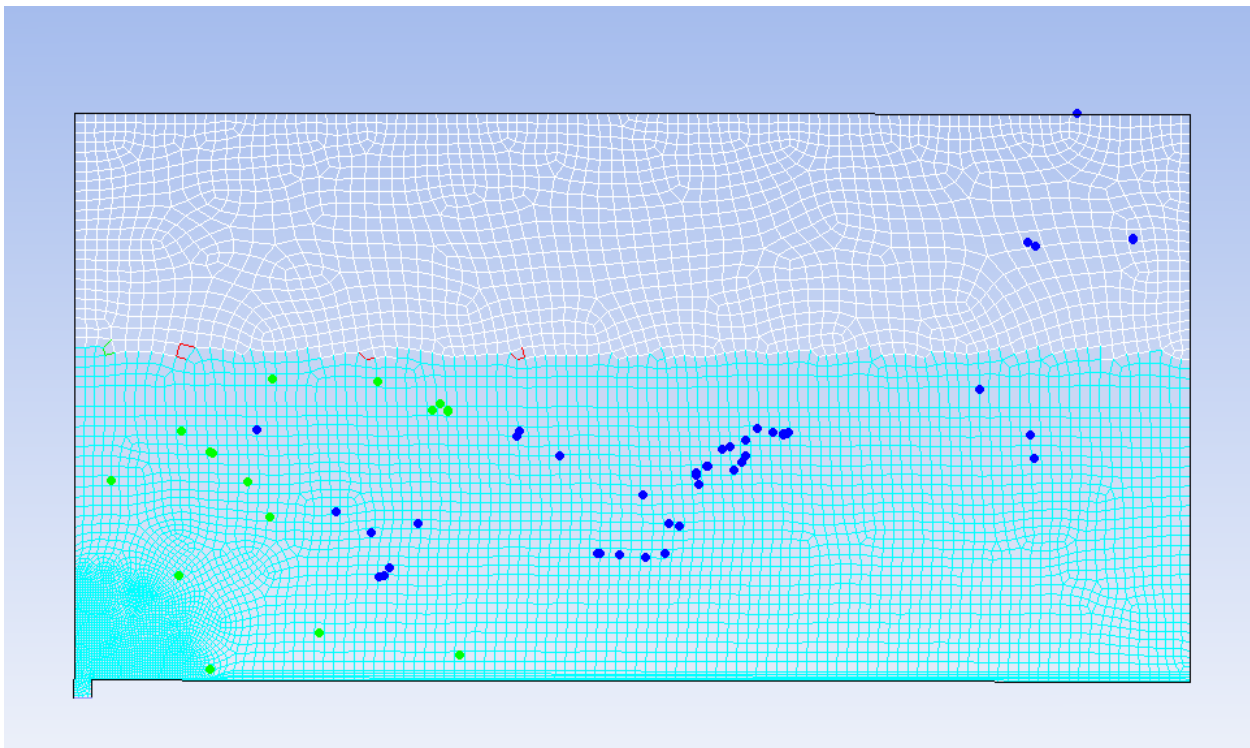
Figure 64. Snapshot of model displaying particles suspended above the water surface. Blue cells indicate water phase; white cells indicate air phase. Blue dots represent 10-micron-diameter particles; green dots represent 100-micron-diameter particles.

Implementation

Figure 65 shows a schematic of the surface tension forces acting on a spherical particle at the water/air interface. The UDF is defined by a macro that loops through all particles in the domain at every particle time step. For each particle in the domain, the UDF instructs the Fluent® software to find the cell in which the particle is located and determine the air volume fraction of the cell (see Figure 66). If the air volume fraction is 0, indicating that the cell contains only water, then no additional force is applied to the particle; if the air volume fraction is greater than

0, then the particle undergoes a downward force due to surface tension ($F_{s,y}$). The magnitude of the force is calculated as described below.
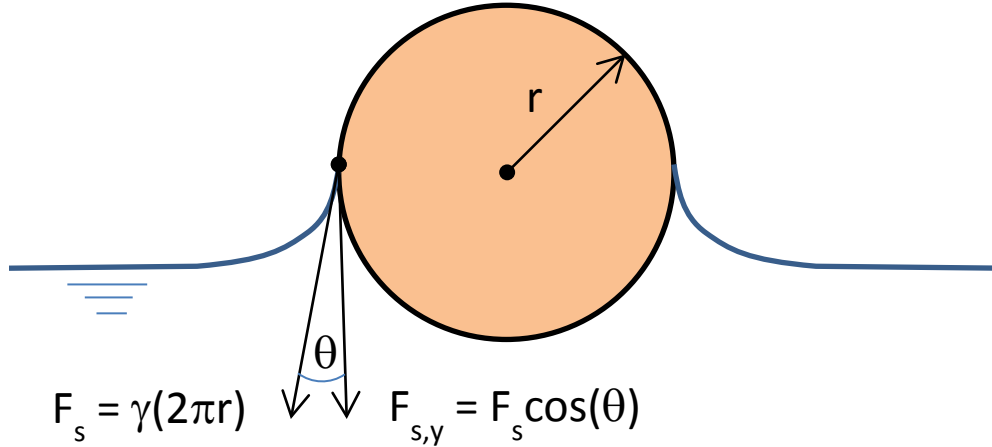
Figure 65. Schematic of surface tension forces on spherical particle at water/air interface.

where

γ *Surface tension of water at 20 °C (0.073 N/m)*
F_s *Force exerted by surface tension on the particle (N)*
$F_{s,y}$ *Downward force exerted by surface tension on the particle (N)*
r *Radius of the particle (m)*
P *Perimeter of particle (m)*
θ *Contact angle between liquid and particle with respect to downward direction*

The surface tension, γ, is defined as a force per unit length. Thus, the maximum force exerted by surface tension on the particle is equal to the surface tension times the perimeter of the particle, *P*:

$$F_s = \gamma\,(2\pi r) \tag{21}$$

The downward component of the surface tension force is obtained by multiplying the surface tension force by the cosine of the contact angle shown in Figure 65:

$$F_{s,y} = F_s \cos(\theta) = \gamma\,(2\pi r)\cos(\theta) \tag{22}$$

Assuming the contact angle equals zero ($\theta = 0$), the maximum downward component of the surface tension force is as follows:

$$F_{s,y} = F_s \cos(\theta) = \gamma\,(2\pi r) \tag{23}$$

This model has been implemented in a user-defined function in the Fluent® software and has successfully prevented particles from leaving the water phase during the operational simulations.
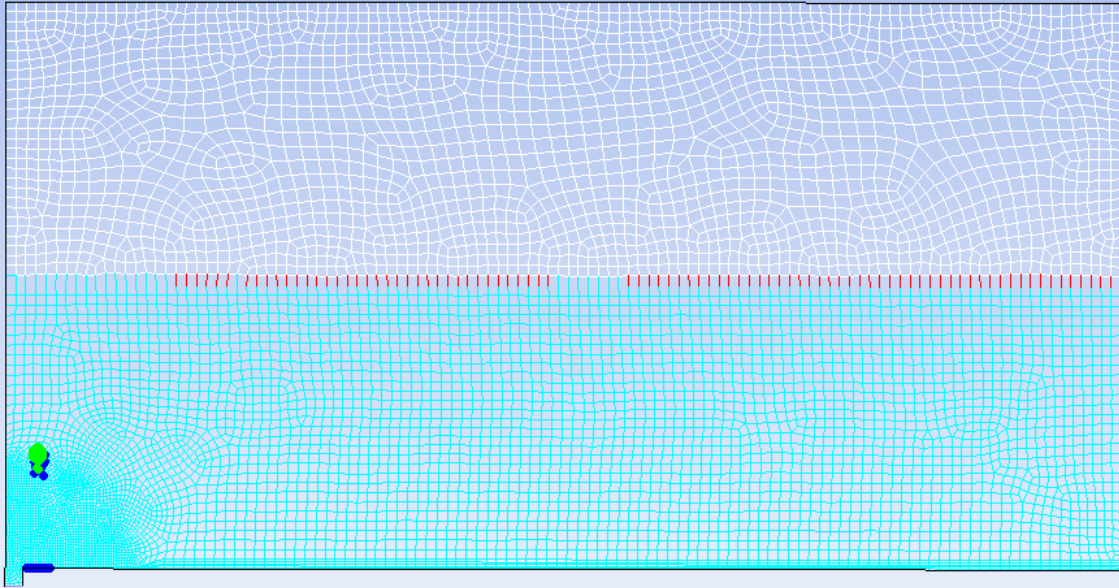
Figure 66. Contour map of air volume fraction illustrating that cells at the air-water interface are not strictly water or strictly air. The red cells indicate an intermediate air volume fraction between 0 and 1.

Appendix D: Justification for Using a 2D Axisymmetric Model

Initially, the operational study employed a 3D model with reflection symmetry, as in the parametric study. However, preliminary testing revealed that using a 3D model would require substantial computation time to provide an accurate representation of the particle trajectories for sufficient flow time. Therefore, a 2D axisymmetric model was proposed instead due to the significantly less computational memory required. The tank size, tank configuration, and inflow rate used in this section are the same as for the operational study (Table 19). Two metrics were used to compare the 2D and 3D models: wall shear stress on the tank bottom (see Figure 67) and velocity pathlines (see Figure 68 and Figure 69).

The wall shear stress curves of both models show the greatest inconsistencies in two major regions: around 5-10 meters away from the line and very close to the line. Five to ten meters away from the line, the shear stresses predicted by both models failed to initiate movement of any of the simulated particles, so the discrepancy between models can be neglected. Very close to the inlet/outlet line (radial distance less than ~2 – 3 meters), the discrepancy is considerably less.

The velocity pathlines are largely similar except in the region far away from the inlet/outlet and outside the recirculation zone. However, preliminary testing revealed that particles do not travel past the recirculation zone; therefore, the particle trajectories in both models should match well. The 2D model was thus employed for the operational study, with a time step of .002 s to allow the Fluent® software to finely capture fluid flow from mesh cell to mesh cell.

Table 19. Tank model and flow rate used in the 2D and 3D comparison. These values were used in the actual operational study as well.

Parameter	Tank Diameter m (ft)	Tank Height m (ft)	Line Diameter m (in)	Inlet Flow Rate (m/s)	Line Placement
Value	38.4 m (126 ft)	9.8 m (32 ft)	0.61 m (24 in)	0.631	Center
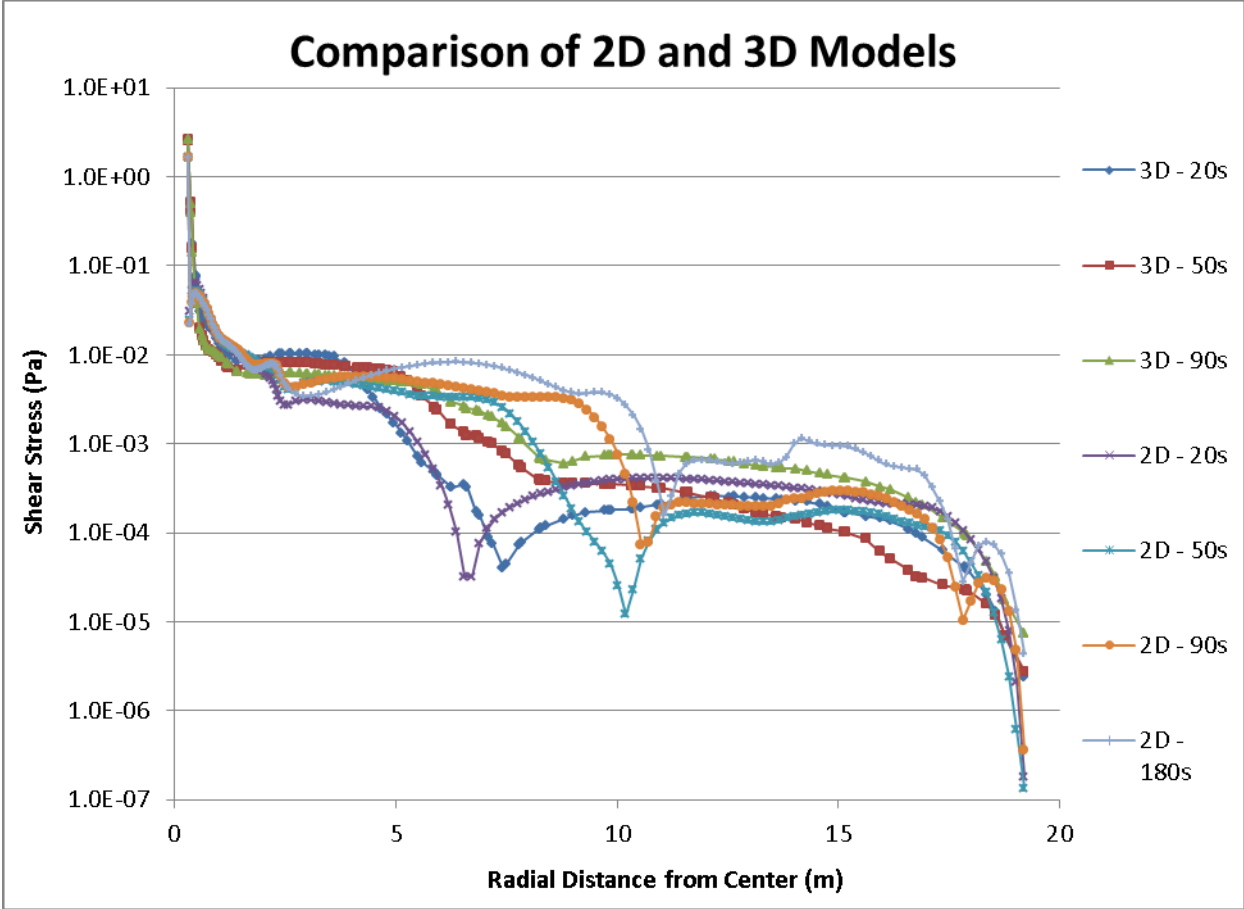
Figure 67. Comparison of shear stresses on tank bottom between a 2D and 3D model.
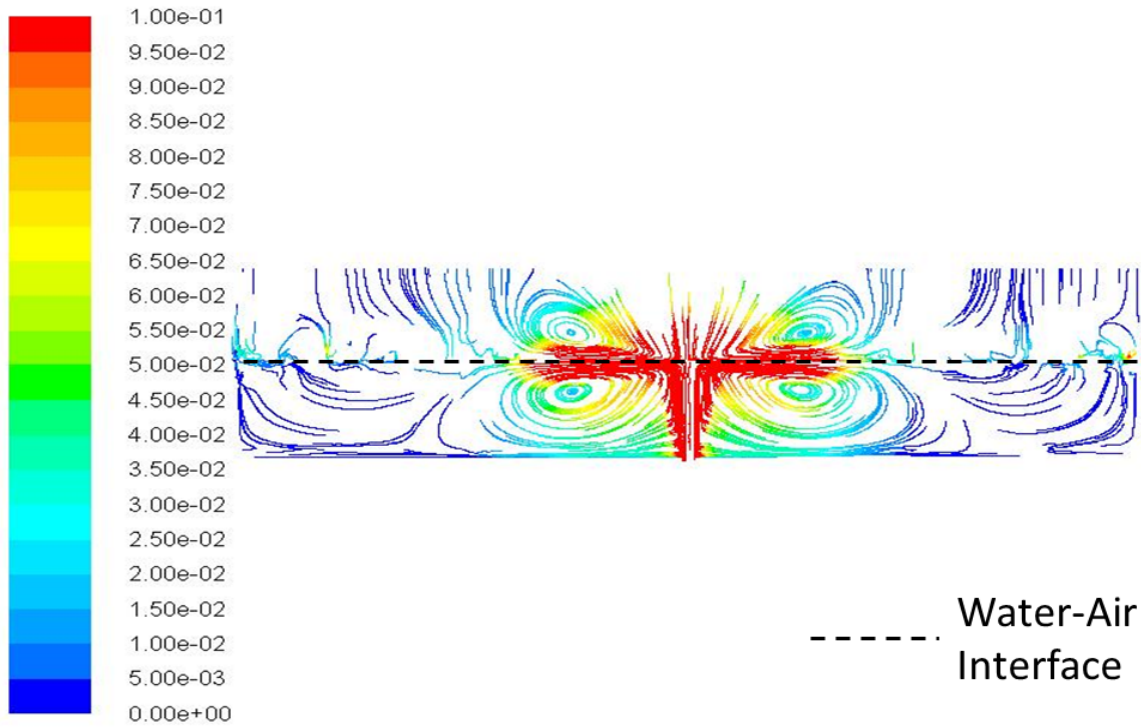
Pathlines Colored by Velocity Magnitude (mixture) (m/s) (Time=9.0000e+01)

Figure 68. Velocity pathlines at 90 seconds for 3D Model

Pathlines Colored by Velocity Magnitude (mixture) (m/s) (Time=9.0000e+01)
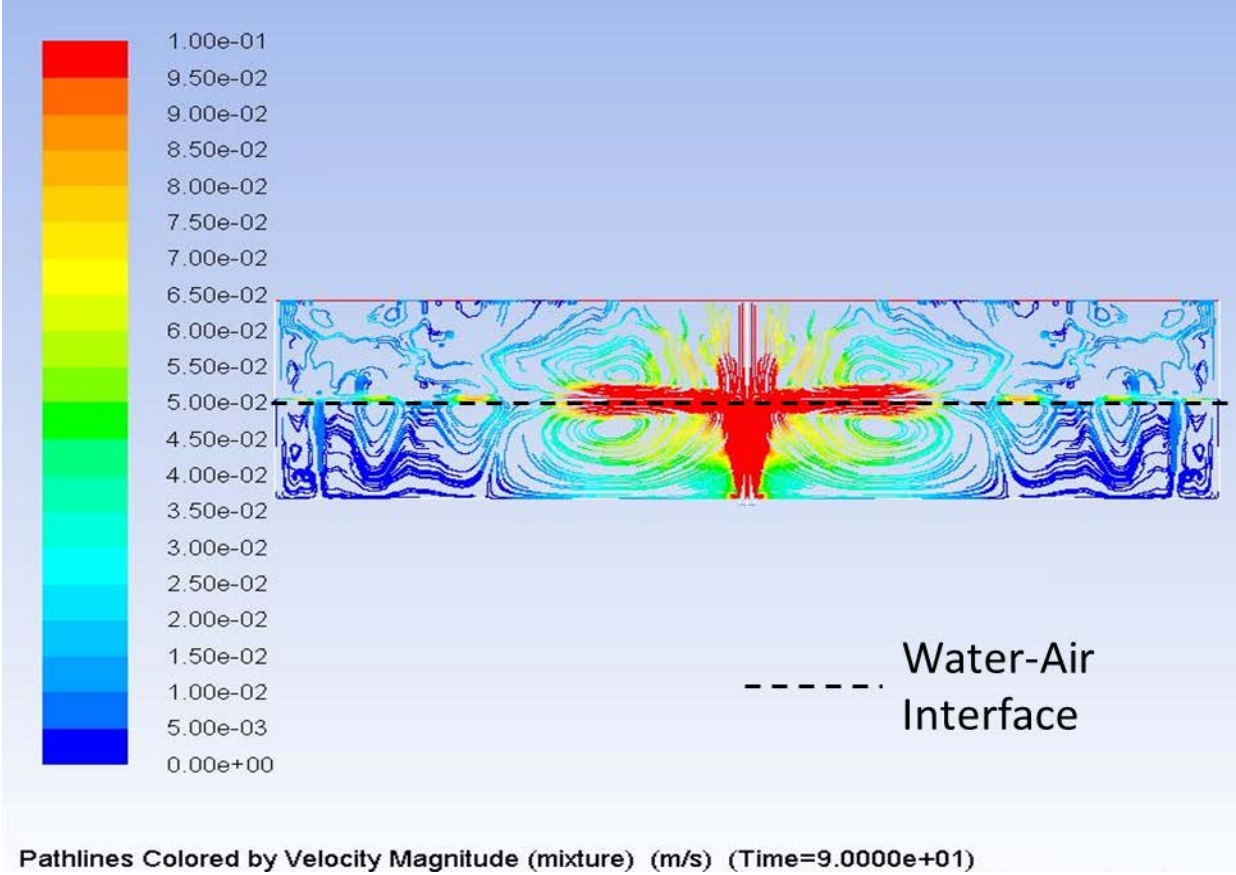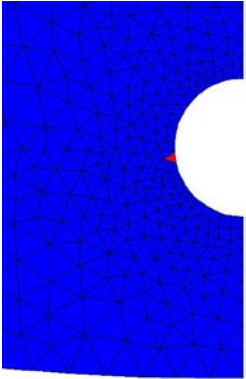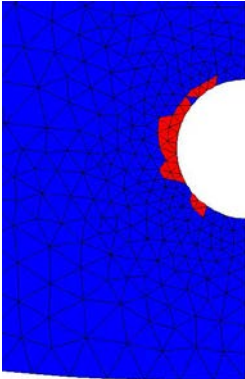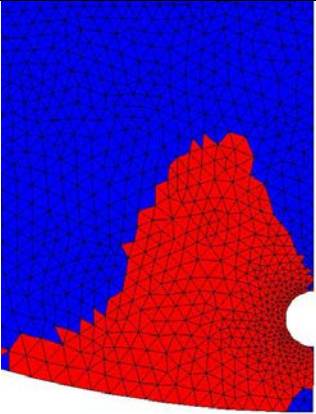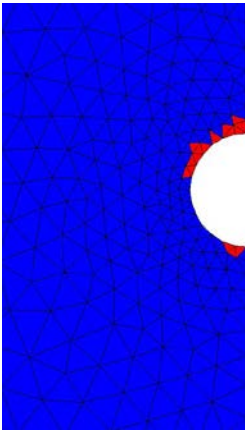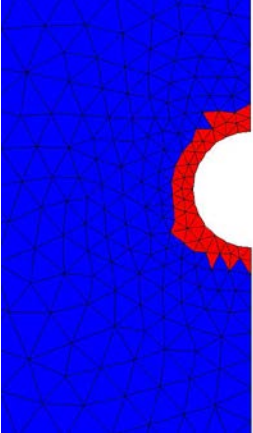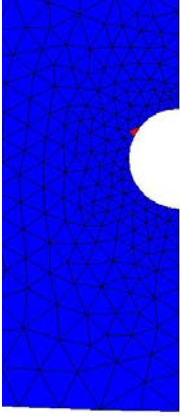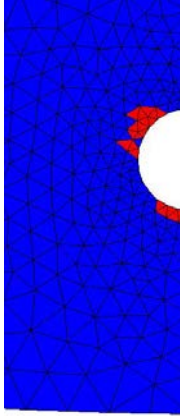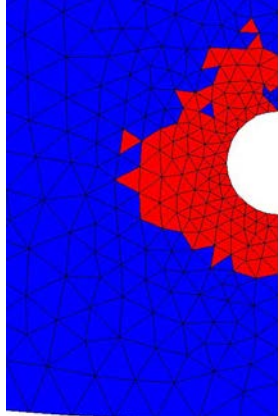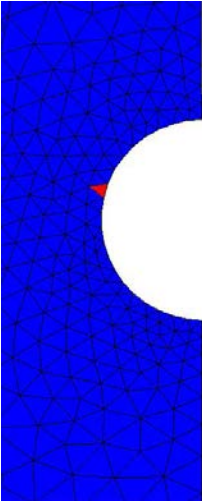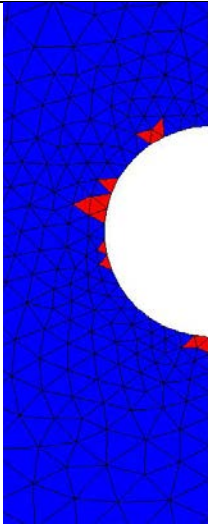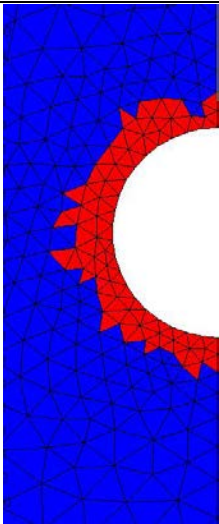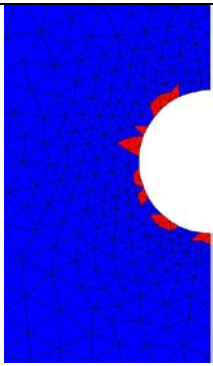
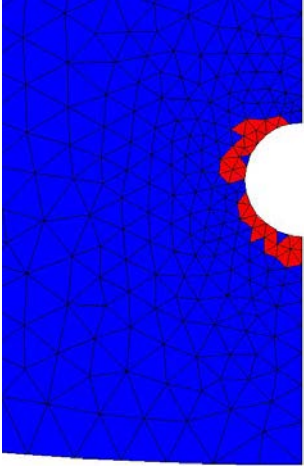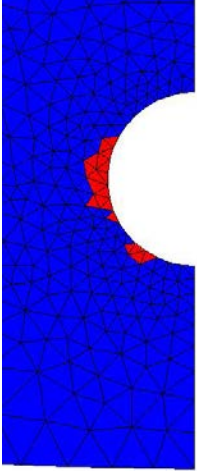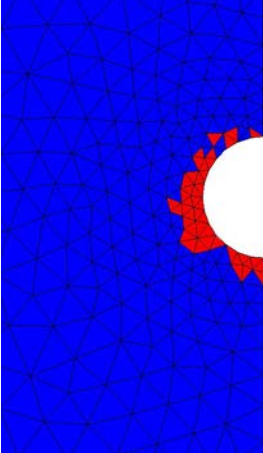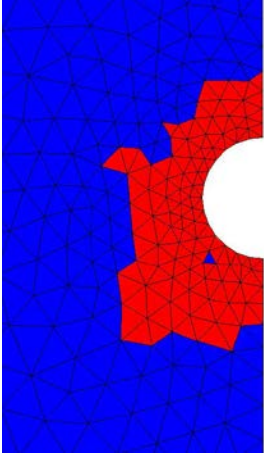**Figure 69. Velocity pathlines at 90 seconds for 2D Model**
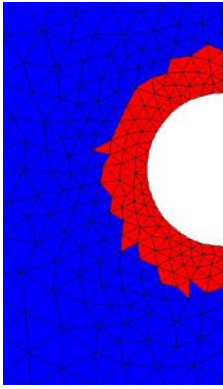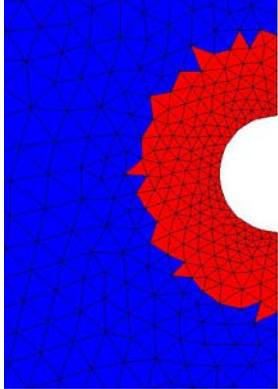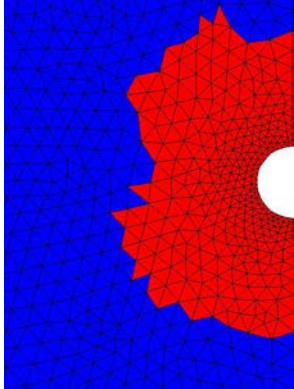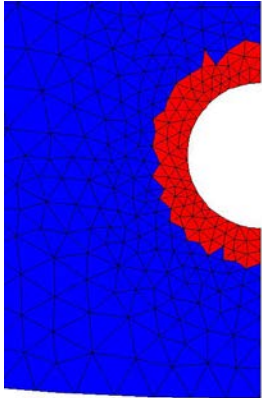
Appendix E: Additional Results from Parametric Analysis
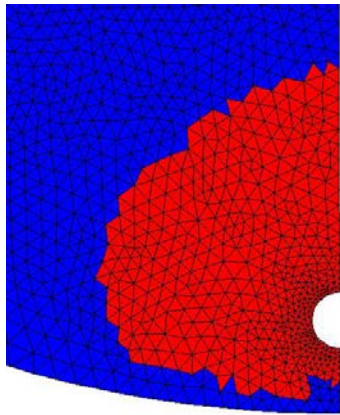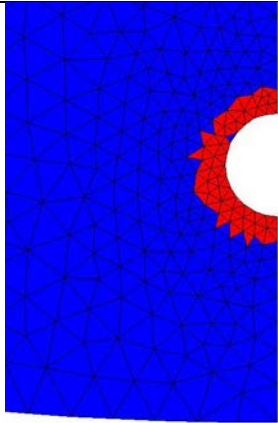
Table 20 presents a summary of the simulated regions along the bottom of the tank wall that were susceptible to particle resuspension (shown in red) according to the Beheshti model assuming a particle density of 2650 kg/m^3.   If the simulated shear stress along the bottom resulted in a Beheshti movability number that was greater than the critical movability number, indicating a potential for particle resuspension, the cell was colored red. The different cases shown in Table 20 correspond to the parametric studies discussed in Section 2.4.
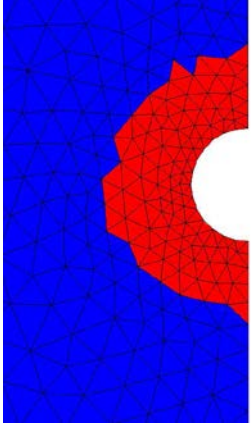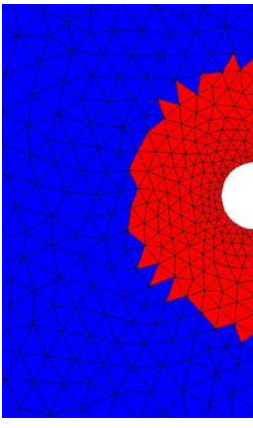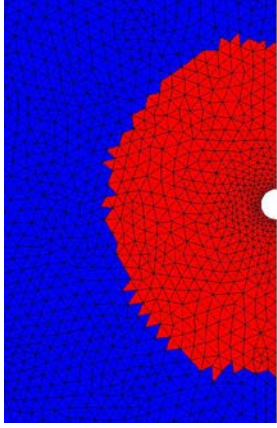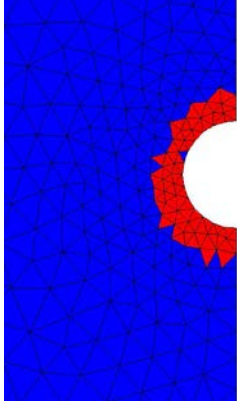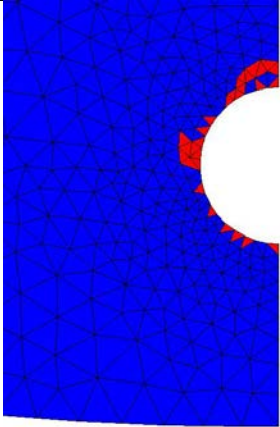
Table 20. Summary of simulated regions susceptible to particle resuspension (shown in red) based on bottom-wall shear stress for the different parametric cases (Table 4)
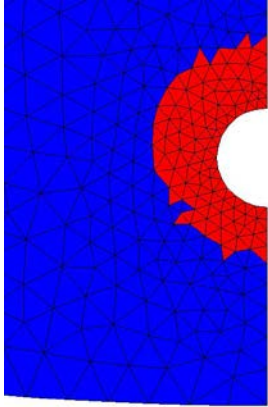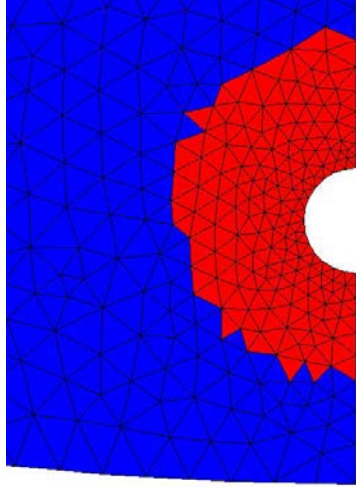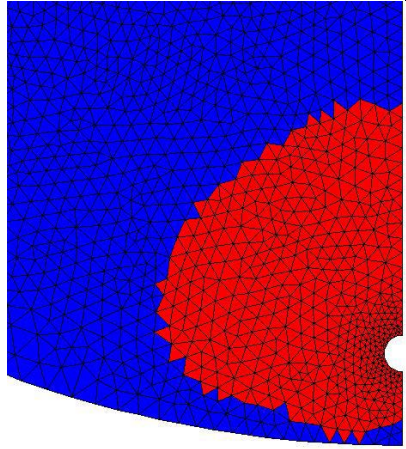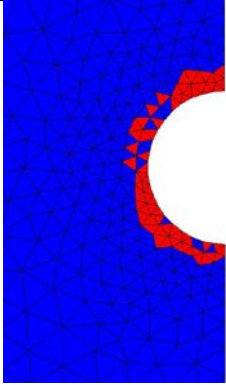
Case	Area susceptible to resuspension in red (1 mm particle size)	Area susceptible to resuspension in red (0.1 mm particle size)	Area susceptible to resuspension in red (0.01 mm particle size)
Filling 1 High flow Large diameter inlet Near wall			
Filling 2 Low flow Small diameter inlet Center	**None**		

Case	Area susceptible to resuspension in red (1 mm particle size)	Area susceptible to resuspension in red (0.1 mm particle size)	Area susceptible to resuspension in red (0.01 mm particle size)
Filling **3** High flow Small diameter inlet Near wall			
Filling **4** High flow Large diameter inlet Center			
Filling **5** Low flow Large diameter inlet Center	**None**	**None**	

Case	Area susceptible to resuspension in red (1 mm particle size)	Area susceptible to resuspension in red (0.1 mm particle size)	Area susceptible to resuspension in red (0.01 mm particle size)
Filling **6** Low flow Small diameter inlet Near wall	**None**	**None**	
Filling **7** Low flow Large diameter inlet Near wall	**None**	**None**	
Filling **8** High flow Small diameter inlet Center	**None**		

Case	Area susceptible to resuspension in red (1 mm particle size)	Area susceptible to resuspension in red (0.1 mm particle size)	Area susceptible to resuspension in red (0.01 mm particle size)
Draining **1** High flow Large diameter inlet Center			
Draining **2** High flow Large diameter inlet Near wall			
Draining **3** Low flow Small diameter inlet Near wall	**None**	**None**	

Case	Area susceptible to resuspension in red (1 mm particle size)	Area susceptible to resuspension in red (0.1 mm particle size)	Area susceptible to resuspension in red (0.01 mm particle size)
Draining 4 High flow Small diameter inlet Center			
Draining 5 Low flow Small diameter inlet Center	**None**	**None**	
Draining 6 Low flow Large diameter inlet Near wall	**None**	**None**	

Case	Area susceptible to resuspension in red (1 mm particle size)	Area susceptible to resuspension in red (0.1 mm particle size)	Area susceptible to resuspension in red (0.01 mm particle size)
Draining **7** High flow Small diameter inlet Near wall			
Draining **8** Low flow Large diameter inlet Center	**None**	**None**	

SCIENCE

EPA
United States
Environmental Protection
Agency

Office of Research and Development (8101R)
Washington, DC 20460

Official Business
Penalty for Private Use
$300